A Study of Extracellular Vesicles as Carriers of Neurotrophic Signals During Sympathetic Neuronal Circuit Development

Ashley Jane Mason

B.S. Neurobiology, University of California, Irvine

A dissertation presented to the Graduate Faculty of the University of Virginia in Candidacy for the Degree of Doctor of Philosophy

Neuroscience Graduate Program

University of Virginia

April 2023

Table of Contents

Acknowledgements

First, I would like to thank my mentors. To Dr. Bettina Winckler thank you for your leadership, compassion, and kindness during my tenure in your lab especially during a global pandemic. Thank you for celebrating and fostering my scrupulous attention to the minutiae of my project and our shared passion for experimental controls. Your support, guidance and scientific rigor was indispensable to my training. To Dr. Christopher Deppmann thank you for your generous support, feedback, and resources. Thank you for receiving me into your lab. Thank you to Dr. Austin Keeler for your expertise and technical help on my project, and for your empathy, and friendship. Special thanks to my committee members Drs. Scott Zeitlin, Xiaowei Lu, Jung-Bum Shin, and Anna Cliffe whose feedback, insight and scientific expertise made my research better. Thank you to my collaborators, Drs. Uta Erdbruegger and Luca Musante for providing resources, equipment, expertise, and enthusiasm to my work on EVs.

I would like to thank all members, past and present of the Winckler lab: Dr. Chan Choo Yap, Laura Digilio, Lloyd McMahon, Dr. Christopher Bott, Ryan Mulligan, Jonathon Sewell, and Isaiah Swann. Thank you to Chan Choo for your scientific expertise and for listening to and caring about me. Laura, thank you so much for your technical help, mouse support, and for always checking in on me. Ryan, thanks for being a great lab bench mate and friend. It has been a pleasure doing research alongside you and sharing the same dark sense of humor and music taste.

I would like to thank all members, past and present, of the Deppmann lab for your support and help over the years. Big thanks to Farah Kabir, for her help on my project. Shayla Vradenburgh, Sarah Hunter-Chang, Katya Stepanova, Sushanth Kumar, Dr. Amrita Pathak, Dr. Tony Spano and Dr. Brandon Podyma thanks for all the long talks, support, laughter, and care over the years.

I would like to thank my funding sources and fellowships: NIH/NIGMS 2T32GM007055-44 and NIH/NINDS F31NS126020. Thank you also to the vivarium staff Brian, Kelly, Day, AJ and Dodzi who made this work all possible.

I would like to thank all of my friends, both near and far that have supported me throughout the years. Special thanks to my NGP cohort: Ben, Thaddeus, Shayla, Courtney, Sarah, Maureen, Anastasia, and Zach. Gustavo and Raegan it was a joy spending time with you. Philip, our dinners, and shared outlook on life brought me so much joy. Holly, thanks for all of our long chats and our shared philosophy on the empowerment of women. Xavier thanks for always making me laugh. To Lauren and Morgan, thanks for walking through life with me and carrying me through this PhD.

Lastly, thank you to my family. Thank you to my parents, and Jolene and Al for their guidance, support, and faith in me throughout all these years. To my mom and Al, thanks for your devoted love, endless encouragement and for always picking me back up again. To my dad and Jolene thank you for your unyielding support and inspiration as my scientific role models. Thank you to my grandparents, in-laws, aunts, uncles, and

siblings for listening to me ramble on about science. Special thanks to my sister and lifelong best friend for always being there and completely understanding me.

To my life partner, Karl, thank you for your unwavering belief in me and my dreams. You are my biggest supporter and champion of all that I do. Thank you for always seeing me and giving me unconditional love. We made it! Thanks for taking care of me through this PhD by feeding me, waiting for me, listening to me, holding me, and boosting me. Thanks for reading every draft of my work, for troubleshooting my experiments, and talking science with me. You make me a better person and scientist and I love growing with you.

Chapter I. Development of the Peripheral Nervous System: NGF and TrkA Trafficking and Signaling.

Parts of this chapter were submitted as an area paper entitled “ Extracellular Vesicles as Potential Carriers of Neurotrophin Signals” in partial fulfillment of the requirements for my advancement to candidacy.

I. Introduction and Central Question

How do neurons achieve the synaptic specificity that is required for proper wiring of a functional circuit? In the central nervous system this is a difficult question to tackle due to the overwhelming number of permutations possible within the circuit, but the hierarchical linearity of the sympathetic peripheral nervous system (PNS) lends itself as a model circuit by which to study this question. During the development of the sympathetic PNS, neurons are initially overproduced and are subsequently pared down through neuronal death. The decision of which neuron dies, and which neuron survives is determined through complex survival signaling that is mediated by neurotrophins and their receptors. Neurotrophic signaling by nerve growth factor (NGF) and its receptor, TrkA, is critical to PNS circuit formation by promoting neuronal survival and target innervation. Neurotrophic signals must traffic long distances from the axon terminal back to their site of action in the soma and even into dendrites where they regulate pre- and postsynaptic connectivity. Superior cervical ganglion (SCG) neurons from the developing sympathetic nervous system have been used to investigate long distance NGF signaling. NGF signaling relies on internalization of the NGF-TrkA receptor complex in the axon terminal into a signaling endosome (SE). This SE is then retrogradely trafficked to the soma to induce signaling cascades which upregulate survival, growth and postsynaptic maturation in the postganglionic neuron, either directly via local signaling or indirectly through transcriptional changes.

The discovery of NGF led to the proposal of the Neurotrophic Factor Hypothesis that states that **during development neurons are overproduced and compete for limited amounts of neurotrophic factor to survive**[1]. A critical component of this

hypothesis is that neurotrophic survival signaling is extremely localized to each neuron, as neighboring neurons can easily die off. This observation led to the idea of target matching. **Target matching states that the target field sets the number of innervating neurons which in turn sets the number of innervating neurons upstream throughout the circuit.** In context, this means limiting amounts of NGF in the peripheral target (i.e., salivary gland) sets the number of surviving postganglionic neurons in the SCG. This then sets the number of surviving preganglionic neurons in the spinal cord that can innervate the postganglionic neurons in the SCG. How does the postganglionic neuron relay survival signals to its upstream preganglionic neuron? The mechanism underlying this retrograde trans-synaptic transfer is unknown and is the focus of my research. To start to address this mechanism, I hypothesized that the NGF/TrkA complex retrogradely traffics to the soma, is secreted as an extracellular vesicle (EV), and then signals in a paracrine manner to the preganglionic neuron. My research focused on the discovery of a novel pathway for TrkA trafficking as neurotrophic EVs. We thus postulate the existence of neurotrophic EVs.

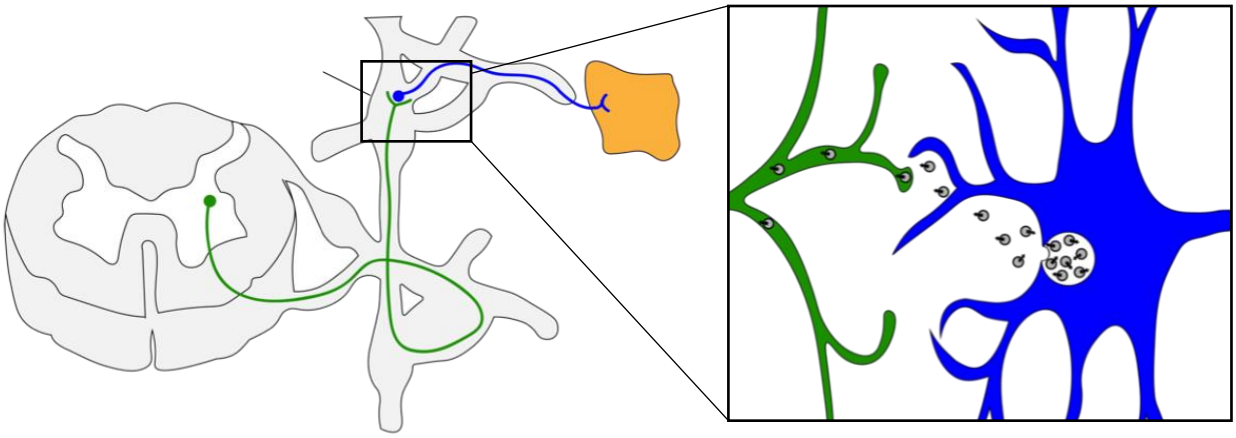

Figure 1. Diagram of the sympathetic nervous system circuit and the proposed role of extracellular vesicles in survival signaling. The preganglionic sympathetic neurons (green) of the spinal cord innervate the postganglionic neurons (blue) in the SCG. The postganglionic neurons innervate their target organ (orange) and transfer survival signals possibly mediated by NGF from the post to the preganglionic neurons. The mechanism behind this transfer is partially mediated by extracellular vesicles *in vitro*.

II. Background of Peripheral Nervous System Development

How does the Nervous System Develop?

The nervous system is one of the most complex organ systems in the body and its development is thus extraordinarily important. Miswiring of neurons during development can lead to both physical and mental disorders. To address the question of how the nervous system develops, I am going to focus on the sympathetic peripheral nervous system. This system is advantageous to study as the hierarchal order of neurons is simpler than in the CNS as peripheral neurons are well mapped to specific target organs in a linear fashion. In this system the somata of neurons reside outside the central nervous system in clusters called ganglia and the somata of their upstream presynaptic partners reside in the spinal cord. I will refer to the ganglionic neurons

whose cell bodies reside in the superior cervical ganglion (SCG) as the postganglionic neurons (blue in Figure 1). In contrast, the presynaptic neurons in the spinal cord are known as the preganglionic neurons (green in Figure 1).

During development, more neurons are produced than are ultimately needed in the mature circuit. An initial period of proliferation and migration is followed by a period of competition for survival and maturation until the circuit is complete. Importantly, the decision to survive or die is regulated by soluble trophic factors, the most famous of which is nerve growth factor, NGF. NGF was discovered by Rita Levi Montalcini and purified by Stanley Cohen in the 1950's. Preceding this, Levi-Montalcini conducted a series of mouse sarcoma transplantation and limb extirpation experiments in developing chick embryos. In these experiments Levi-Montalcini observed hyperinnervation of organs that had been exposed to the tumors. Further experiments showed that secretion of a soluble factor (later identified as NGF) emanating from a mouse sarcoma promoted the survival of sensory and sympathetic neurons and increased neuronal outgrowth [2–6].

However, before neurons can respond to a soluble trophic factor, they must first grow axons to reach this survival factor. The axons of postganglionic neurons are guided to their final targets by responding to a series of guidance cues. Axon guidance is a delicately coordinated process by which axons move along the blood vessels by responding to gradients of cues such as Endothelin 3, Artemin, NT3, VEGF-A and Semaphorin3A that are secreted by vascular smooth muscle and neighboring tissues and cells [7–9]. Knockout of these guidance cues or their receptors results in deficits in neuronal migration leading to the reduced size and mislocalization of the SCG and

postganglionic neurons [10,11]. Axons continue to pathfind along the vasculature until they defasciculate to innervate their final targets. The mechanisms behind how different populations of axons know when to defasciculate as to not overshoot their target or to innervate while other axon fibers continue pathfinding is still relatively unknown[12–14].

Once the axons reach their final targets they respond to a neurotrophin that enables target innervation of sympathetic neurons, nerve growth factor [2,6]. After the mouse sarcoma transplantation experiments, Levi-Montalcini and Stanley Cohen set out to isolate the soluble factor that promoted sensory and sympathetic neuron survival [2–6]. Through a series of fortuitous experiments and observations using snake venom, they determined that NGF was the soluble factor that was secreted from salivary glands and it was thus subsequently purified [2–6]. The discovery of NGF resulted in the formation of the Neurotrophic Factor Hypothesis that proposed that neurons were overproduced during development and therefore they must compete with one another for limited amounts of neurotrophic factor in order to survive[1]. This neurotrophic factor is provided by the target organs (i.e., salivary gland, eye) that the axons of these neurons innervate. Therefore, a critical component of this hypothesis is that neurons need a mechanism by which survival signaling that is initiated in the axon terminal can be propagated to the soma to upregulate survival signaling in the nucleus.

III. Background of the NGF-TrkA Signaling Endosome

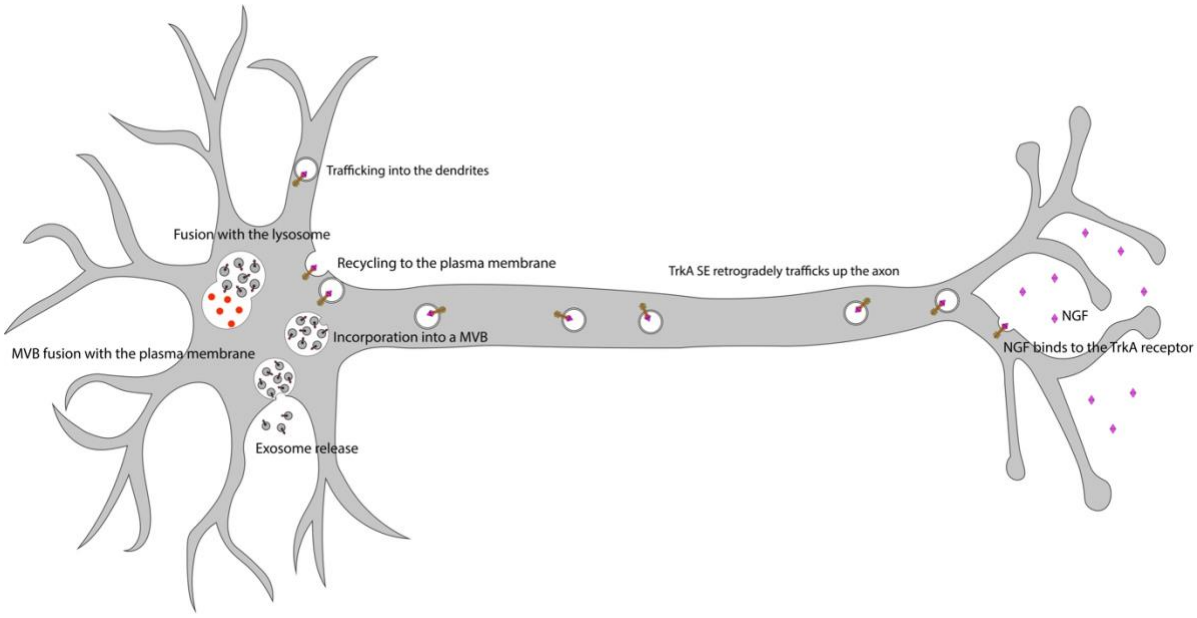

Figure 2. Local and retrograde neurotrophic signaling. NGF binds to the TrkA receptor in the distal axon and is internalized as a signaling endosome. Locally, it can signal to increase axon branching. The signaling endosome can also be retrogradely trafficked to the soma to initiate survival signaling in the nucleus. It can also traffic into the dendrites to support synaptic maturation, or it can fuse with the lysosome and be degraded. My work posits a new date which is secretion as extracellular vesicles depicted as exosomes here.

How does NGF-TrkA signal?

NGF binds with picomolar affinity (K_d = 10^{-10} to 10^{-11} M) to the TrkA receptor and with less affinity (K_d = 10^{-9} M) to the neurotrophin receptor p75 (p75NTR) [15,16]. Upon ligand binding, TrkA dimerizes and subsequently transautophosphorylates tyrosine residues located on its intracellular domain thus initiating a kinase cascade on the downstream effector signaling pathways: Ras/MAPK, P13K and PLCɣ [17,18]. TrkA is a member of the receptor tyrosine kinase (RTK) superfamily and is highly expressed during development (expression peaks at E12.5 to E14.5) in the dorsal root and sympathetic ganglia and is subsequently downregulated into adulthood [19]. This shift in

expression allows for high specificity and sensitivity to NGF during development when neuronal competition and target matching is necessary for proper circuit formation. This age-dependent reliance on NGF is most notable in knockout (-/-) mouse phenotypes that show significantly poor survival outcomes postnatally. Most $TrkA^{-/-}$ mice die at birth as they lack the sensory feedback to suckle. Those that survive have smaller SCGs that contain irreversibly pyknotic neurons representing apoptotic cell death at postnatal day 10 (P10) [20]. Furthermore, $NGF^{-/-}$ mice struggle to survive postnatally and show a significant reduction in SCG size until its eventual disappearance (as evidence by its visual absence during dissection) by P14[20]. These homozygous knockout phenotypes show that NGF and TrkA signaling is not only necessary, but also sufficient for development and survival of the sympathetic nervous system.

Local neurotrophin signaling in the axon

First, the NGF-TrkA receptor signals locally in the distal axon to promote axonal outgrowth and branching. *In vitro* evidence that NGF is required for distal axon development was demonstrated by growing sympathetic neurons in three compartment devices known as Campenot chambers[21]. These chambers allowed for separation of the axons from the cell bodies allowing investigation into NGF's effects on different neuronal compartments. Application of NGF to the distal axon chamber caused outgrowth of neurites from the soma chamber into the axon chamber; however, removal of NGF in the distal axon chamber would cause the axons to degenerate regardless of NGF presence or absence in the cell body chamber, thereby demonstrating that NGF signals locally to promote axonal branching [21]. Later experiments showed that axonal

outgrowth is dependent on PI3K and Ras-MAPK signaling that is initiated by NGF-TrkA signaling from both the surface and internalized receptors [22,23]. NGF-TrkA signaling through PI3K causes local inhibition of GSK-3β thus stimulating microtubule assembly for cytoskeletal rearrangement necessary for axonal growth [23,24]. Lastly, NGF-TrkA signaling serves as its own positive feedback mechanism for promoting axonal growth by increasing TrkA receptor endocytosis through calcineurin mediated dephosphorylation of dynamin1, the GTPase responsible for pinching off the plasma membrane after endocytosis [25].

Retrograde neurotrophin trafficking to the soma

An important mechanism for signal termination is through the downregulation and degradation of a receptor through endocytosis. However, given the highly polarized nature of neurons, NGF-TrkA signaling at the axon terminal must persist and traverse a few millimeters to the soma to induce transcriptional upregulation of survival genes. A long-standing debate in the field was the mechanism behind the retrograde translocation of the NGF-TrkA signal from the distal axon to the soma and the signaling competency of the receptor during this translocation[26,27]. It is now known that the activated TrkA receptor is internalized via macropinocytosis [28], caveolin-dependent endocytosis [29] or clathrin-mediated endocytosis [22]. Upon endocytosis, NGF remains bound to TrkA forming a receptor complex that enters the canonical endocytic pathway while maintaining its phosphorylated state and thus signaling competency. At this stage, the internalized ligand receptor complex is known as a signaling endosome (SE). This SE can signal locally in the distal axon and/or undergo retrograde transport to the soma

and into the dendrites[22,28,30]. Due to the uniform plus-end out polarity of microtubules in axons, in order to move retrogradely, the SE must hook onto the minus-end directed molecular motor, dynein. To do this, SEs associate with the small G proteins in the Rab family, which cycle through a GTP-bound and GDP-bound state and attach to the endosomal membrane through a prenyl anchor on their C- terminus[31,32]. Activated GTP-bound Rabs can recruit downstream effectors to carry out a variety of processes including membrane trafficking, tethering, exocytosis, maturation, and sorting through the formation of functional microdomains on endosomes[31]. Canonically, newly internalized cargo from the plasma membrane associates with early endosomal traffickers such as Rab5 and early endosomal antigen 1 (EEA1). Cargo can then be recycled back to the plasma membrane either through fast recycling mediated by Rab4 or slow recycling mediated by Rab11. As the endosome matures it can form what is known as a late endosome or multivesicular body (MVB) that is destined for degradation. These late endocytic organelles are associated with Rab7 and ultimately fuse with the lysosome. Rabs can be considered endosomal traffickers as they have the ability to recruit different effectors and adaptor molecules of molecular motors that allow the endosomes to move. Because the maturation process of an endosome is governed by sequential action and exchange of Rabs, they can be used as molecular markers of different types of endosomes.

What "molecular markers" define the retrogradely trafficked signaling endosome?

The precise identity and morphology of the TrkA SE is still debated due to the constant flux (both temporally and spatially) of Rab interconversion. For example, Rab5 is classically associated with the early endosome therefore it would be expected to associate with newly internalized NGF-TrkA receptors in the axon terminals[33]. However, Rab5 has also been found in the axons of hippocampal neurons and colocalized with NGF and ERK in the soma and axons of DRG neurons[34]. Intriguingly, immunoelectron micrographs (IEM) have shown the TrkA-containing SE associated with Rab5+ MVBs [35]. This is quite unusual as MVBs are generally considered to be endosomally mature compartments that are destined for degradation. Therefore, it is striking that MVBs would colocalize with an early endosomal Rab in such a morphologically mature compartment. These data suggest that Rab5 might be the Rab associated with retrograde transport of the SE. However, another study looking at the effects of different neurotrophins on TrkA SE transport provides evidence to refute this notion. In this study, activation of TrkA by either neurotrophin-3 (NT3) or NGF was sufficient to induce endocytosis and colocalization with Rab5; however, the NT3 endosome was not capable of retrograde transport possibly indicating that conversion from Rab5 is necessary to be transport-competent[11]. Due to NT3's low binding affinity for TrkA it readily dissociates in the slightly acidified environment of the early endosome thus reducing its signaling capacity and potential to recruit other Rab effectors necessary for transport[11]. Additionally, evidence from live imaging of TrkB in motor neurons shows that GFP-Rab5 was associated primarily with stationary or short range movement in axons, whereas overexpression of the dominant negative (DN) Rab5 abolished all

retrograde traffic; indicating that the Rab5 compartment is not long distance retrograde transport-competent[36].

There is also data supporting a role for Rab7 in the retrograde transport of SEs. The same study implicating Rab5 in short range transport also showed that Rab7 was necessary for fast axonal transport[36]. Rab7 has been shown to be required for TrkA SE transport in PC12 cells as expression of a DN Rab7 resulted in potentiation of NGF signaling on axonal outgrowth possibly due to altering the flux (localization and duration) of the signaling endosome in a specific neuronal compartment [37]. Importantly, SEs bound to Rab7 become transport competent as Rab7 can bind to its downstream effector, RILP, which functions to recruit the molecular motor dynein. Evidence for a role of RILP in retrograde transport of SEs has been presented[38,39], but the experiments were not optimally controlled. In the case of the Epidermal Growth Factor Receptor (EGFR) endosome, phosphorylation of Rab7 predominately recruits the RILP effector thus facilitating dynein-dynactin binding and retrograde transport [39]. Overexpression of the dynamitin subunit caused dynactin to unhook from cargo and this was used to show the necessity of retrograde transport for survival signaling[40]. Furthermore, TrkA has been shown colocalized with dynein motor proteins *in vivo* in the rat sciatic nerve [41]. Lastly, siRNA knockdown of Rab7 resulted in the accumulation of Rab5+ TrkA SEs, suggesting Rab5 conversion to Rab7 is necessary for the progressive fate decisions of the SE [42].

What compartment defines the retrogradely trafficked signaling endosome? Evidence for the multivesicular body in neurotrophin trafficking

Despite MVBs originally being discovered in neurons, much of the pioneering work was carried out on non-neuronal cells. MVBs are endosomal compartments that are morphologically defined by the inclusion of internal vesicles called intraluminal vesicles (ILVs). MVBs have been found most commonly in the dendrites and somata of peripheral and central neurons[43]. Their role in axons has been much harder to parse apart as they are less commonly localized there; however, they have been suggested to be the transport-competent organelle for the NGF-TrkA SE. Early studies utilizing immunogold EM in PC12 cells showed Pincher, a pinocytic chaperone, in Rab5+ MVBs indicating that Pincher-mediated endocytosis resulted in the formation of multivesicular bodies [35]. Further studies confirmed that Pincher-mediated macroendocytosis results in Trk associated MVBs[44]. However, it was still unknown whether a MVB was the retrogradely trafficked SE or if the SE became a MVB after arriving in the soma. Electron micrographs of rat sympathetic neurons fed at their distal axons with radiolabeled NGF showed dense accumulations in MVBs and lysosomes in the cell body at both 1 hour and 8 hours post NGF pulse indicating fast axonal transport of NGF and biogenesis of MVBs [45]. Cooling studies conducted on mouse saphenous nerves attempting to slow down axonal transport showed evidence of MVB organelles being retrogradely trafficked in the axons[46]. Additionally, ligation experiments on the rat sciatic nerve showed accumulation of phosphorylated Trk+ MVBs just distal to the ligation site 24 hours after injury[41]. Interestingly, no MVBs were seen upstream of the ligation site indicating that retrogradely trafficked MVBs arriving from the distal axon were being halted at the site of ligation[41]. This evidence from the late 20th century led to the proposal of several models for the retrograde transport of SEs as MVBs. Model 1

suggested that the internalized Trk receptors enter the endosomal pathway and through subsequent sorting eventually get sequestered and retrogradely trafficked to the soma where they mature into MVBs en route[47]. Model 2 proposed that the formation of MVBs was a result of TrkA receptor sorting through invaginations into a SE MVB that then gets targeted for transport to the soma [47]. Another hypothesis lent support to Model 2 by suggesting that a SE MVB would preserve the integrity of the TrkA receptor signaling scaffold and its 2nd messengers inside an ILV during transport[48]. Thus, the prevailing idea was that SEs were trafficked as MVBs. However, once it reached the soma, how the Trk receptor-initiated survival signaling while sequestered in an ILV was and still is unknown.

Despite the prevailing hypotheses at the time there were several groups that doubted MVBs as the transport competent SE. Several studies reported that neurotrophins do not retrogradely traffic in MVBs and that MVB presence in the axon is likely caused by aberrant or dystrophic stimuli such as delayed fixation methodology or injury-induced MVB formation in the case of ligation studies[49,50]. Analysis of MVBs in axons by IEM 7.5 hours after injection of brain derived neurotrophic factor (BDNF) or glia cell-derived neurotrophic factor (GDNF) in rat hypoglossal nerves showed no neurotrophin+ MVBs [50]. While it is difficult to reconcile these results with the aforementioned studies it is worth noting that timing is critically important in catching MVB trafficking and analysis should be done in the first few hours not just at 7.5 hours.

Recently, a thorough analysis was conducted examining the role of MVBs as the retrogradely trafficked SE[38]. This paper by Ye et al., first characterized the ultrastructural features of SEs *in vitro* using SCG neurons derived from a mouse

transgenic line which expresses a FLAG epitope on the TrkA receptor. Using microfluidic devices to compartmentalize the neurons into an axon chamber and soma chamber, they fed gold conjugated anti-Flag antibody to the distal axon (DA) chamber and then fixed the culture for EM analysis at different time points[38]. Early endosomes were identified as single vesicles (SV) whereas the majority of the gold label was detected on the limiting membrane and ILVs of MVBs in both the soma and proximal axons[38]. Using transfected EGFP-Rab5 or EGFP-Rab7 they found that the majority of the anti-FLAG TrkA receptor endosomes that colocalized with Rab5 in the DA were stationary or moved short distances whereas the majority of retrogradely trafficked SEs were Rab7+[38]. To confirm that the retrogradely trafficked SEs were indeed dependent on Rab7, they performed a conditional knockout of Rab7 *in vivo* during early development which resulted in atrophic SCGs[38]. *In vitro*, shRNA knockdown of Rab7 abolished retrograde TrkA signaling[38]. To examine specificity, they used a human Rab7 construct that is resistant to the shRNA and a mouse Rab7 construct that is sensitive to the shRNA. In the presence of the shRNA the human Rab7 was able to rescue the retrograde TrkA transport and survival signaling[38]. Through this work, they confirmed the prior studies showing that Rab7 is necessary for transport of the SE, but interestingly they also confirm the studies indicating that SEs are MVBs. However, the question still remains: are TrkA receptors on the ILVS of MVBs capable of signaling? They found that retrogradely trafficked TrkA MVBs were signaling-competent through IEM staining against P-TrkA Y785 and P-TrkA Y490. Furthermore, the CD63+ FLAG-TrkA endosomes avoided colocalization with LAMP1 suggesting that these signaling MVBs are degradation resistant[38]. In contrast, non-signaling cargoes such as the

transferrin receptor and BSA segregated into distinct MVBs from the TrkA MVBs and they associated with lysosomes within two hours[38].

To examine the maturation of MVBs after DA NGF feeding, the microtubule depolymerization agent nocodazole was used to halt retrograde transport 25 mins after distal application of NGF and anti-FLAG antibody. EM analysis indicated that the main species of endosomes in which TrkA was localized in axons included MVBs, single vesicles, and lysosomes. In the MVB, the majority of TrkA receptors were found on in ILVs compared to the limiting membrane and FLAG topology showed that 80% of the FLAG epitope was on the outer leaflet of the ILV as expected. If the MVB is the transport-competent SE and its purpose is to sequester the signaling scaffold and 2nd messengers away from phosphatases or degradation during transport as suggested by Weible et al., then what is the mechanism that allows for these signals to be detected by the cytosol once the SE arrives in the soma[48]? Ye et al. suggests that the MVB is signaling-competent as demonstrated through IEM showing P-TrkA as well as the TrkA effector PLCγ incorporated into both the limiting and ILV membranes of MVBs[38]. They suggest that once the MVB reaches the soma the ILVs undergo back fusion with the limiting membrane to generate single vesicles. Again, using the retrograde transport block, they found that the number of single vesicles in the soma increased after 5 hours although association with lysosomes remained low during the first 8 hours after the transport block. Additionally, the single vesicles were not associated with the early endosomal marker, Rab5 allowing the authors to conclude that this pool of single vesicles was derived from MVBs. While they suggest back fusion of the ILVs with the

limiting membrane as the source of the single vesicles they present no mechanism or evidence for this hypothesis[38].

Fate of the Multivesicular Body Signaling Endosome: Recycled, Degraded or Secreted

Alternatively, this mysterious pool of single vesicles could be derived from recycling endosomes known as post-transcytotic signaling endosomes (PTSE). Previous work from the Deppmann and Winckler labs have shown that retrogradely transported signaling endosomes can reinsert the TrkA receptor into the plasma membrane of the soma and then be re-endocytosed into a “less mature” signaling endosome known as a PTSE[51,52]. This was first described by Suo et al. who identified a novel role for the actin binding protein, Coronin 1. Coronin 1 is able to stabilize the retrogradely trafficked SEs and mediate their recycling to the plasma membrane rather than routing them to the lysosome for degradation[51]. Utilizing microfluidic devices and the aforementioned Anti-FLAG + NGF feeding assay they found that retrogradely trafficked TrkA colocalized with coronin 1 and Rab11 and peaked in the soma 6 hours after DA feeding. Importantly, the SEs avoided degradation by the lysosome for more than 24 hours, however the evidence would be more compelling if they blocked lysosomal degradation and still saw no accumulation of the TrkA SE[51]. In contrast, in Coronin 1 knockout animals, SE fusion with the lysosome occurred within 2.5 hours after anti-FLAG feeding in the DA and Rab11 did not associate with the SE in the cell body[51].

This study raises speculation into what is happening to this disappearing pool of SEs around 8 hours if they aren't being degraded by lysosomes? Firstly, the population of SEs could be undergoing degradation as proper controls to inhibit lysosomal function were not used. A second explanation is that these SEs were being counted in the soma and therefore the SEs that were being trafficked into the dendrites would not be counted. A third explanation is that these SEs could be undergoing exocytosis either through MVB fusion with the plasma membrane releasing signaling EVs or through re-inserted receptors budding off of the plasma membrane as microvesicles. Lastly, these cells could utilize a combination of these mechanisms: trafficking of the signaling endosomes into the dendrites to promote postsynaptic density formation and then exocytosis as EVs to promote presynaptic terminal maturation and survival of the upstream preganglionic neuron.

IV. Introduction to Extracellular Vesicles

Extracellular vesicle (EV) is the general term used to describe lipid bilayer enclosed particles that are secreted by cells and range in size from 30 to 10,000 nm in diameter. Originally, only specific cells types, such as dendritic cells and cancer cells, were thought to secrete these extracellular vesicles; however, it is now well established that all cells can release EVs and they have been identified in all taxonomic domains and kingdoms (Plantae, Animalia, Protista, and Fungi)[53–56]. Exosomes are a subset of EVs that range in size from 30-150 nm and originate from the multivesicular body (MVB). The multivesicular body is a late endosome characterized by small vesicular

inclusions known as intraluminal vesicles (ILVs) that form from the inward budding of the limiting membrane of the organelle. Exosomes were first described in the 1980's as the particle or mechanism by which maturing reticulocytes shed their transferrin receptors in both rats and sheep[57,58]. These papers showed through electron micrographs (EM) that gold-labeled transferrin is internalized into the intraluminal vesicles (ILVs) of MVBs that subsequently fuse to the plasma membrane to shed their cargo. Importantly, no receptor-ligand dissociation occurred in the low pH environments of the MVB, leading to exocytosis of the intact transferrin-receptor complex [57,58]. Later the ILVs released by this fusion of the MVB to the plasma membrane were termed exosomes [59]. Since this first description the areas of biogenesis, secretion, uptake, cargo and function of these EVs have been of intense interest, and I will describe the past and current research on each of these areas.

V. Preganglionic neuron survival is dependent on NGF signaling

Dendritic development of postganglionic neurons

Retrograde neurotrophin signaling has long been shown to be necessary for synaptic maturation. Target-derived NGF not only increases survival of the sympathetic postganglionic neuron, but also signals for survival in the upstream preganglionic neurons. Early work in the 1980s focused on describing the influence of preganglionic innervation on dendritic outgrowth in the postganglionic neuron[60–63]. While we now know that both the presynaptic and postsynaptic cells innervate their targets and undergo dendritic branching independently of one another they require intercommunication for

the formation of synapses and survival signaling[64,65]. This was shown in a series of experiments in the developing rat sympathetic nervous system that qualitatively and quantitatively described the number of neurons, axons and dendrites over different ages. Most postganglionic dendritic growth occurs postnatally, independently of preganglionic innervation, and continues into adulthood. Dendritic branching begins at E14 and increases over 400% in the first 4 weeks after birth in both the number of primary dendrites and the complexity of the dendrites[60]. Denervated ganglia, caused by cutting of the sympathetic cervical trunk, showed the same increase in the size and complexity of dendrites compared to the controls; however, there was a 90% reduction in the number of synapses by electron micrograph analysis at 4 weeks post denervation[60]. This experiment shows that the development of both the preganglionic axons and the postganglionic dendrites occurs independently until synapse formation requires communication between the two sets of neurons.

Survival and axonal innervation of preganglionic neurons depends on NGF

As previously mentioned, only 50% of both the postganglionic and preganglionic neurons that are born survive via NGF signaling into adulthood; however, the preganglionic neuronal death occurs after the postganglionic neuronal death which occurs at P14-21[66]. This was shown electrophysiologically in the developing hamster through whole cell patch clamp recordings[62]. An electrode patched onto an SCG neuron was used to record excitatory postsynaptic potentials (EPSP), which serve as a measurement of the number and strength of synaptic inputs received by the neuron, over different developmental ages. In early development, the size of the EPSPs was

much larger indicating that many (~14) preganglionic axons innervated a single SCG postganglionic neuron[62]. Later in development, fewer axons (~7) innervated a single SCG neuron[62]. This was also shown morphologically, through EM analysis of both the cervical sympathetic trunk (preganglionic axons) or the SCG (synapses) in rats treated with NGF or saline for up to 10 days[67]. In the SCG at P0 there were 0.4 synapses per neuron (normalized to the number of neuronal nuclei) in the saline group compared to 0.6 in the NGF-treated group[67]. At P10, the number of synapses increased from 1.3 in the saline group to 2.6 in the NGF treated group indicating that exogenous NGF boosts the number of surviving neurons and thus synapse number[67]. The number of preganglionic axons in the cervical sympathetic trunk (CST) normally drops from 13,000 axons at birth to 7,700 axons at P10[67]. In comparison, exogenous NGF increased that number from 21,000 at birth to 37,000 by P10, whereas denervation of the CST to the SCG decreased the number of remaining preganglionic neurons to 10% of the original[67]. Lastly, another group showed that subcutaneous injections of NGF into neonatal rats showed an increase in dendritic arborization and complexity [68]. While these experiments not only corroborate the findings of Hamburger and Montalcini in the developing chick limb bud, they also show that the preganglionic neurons, which do not express TrkA receptors or have access to soluble NGF increase their survival in response to exogenous NGF. While these experiments were important in identifying the influence of excess NGF on the development of these neuron populations, they did not exactly identify the postganglionic neuron as the source of this NGF-mediated synaptic maturation, dendritic arborization and preganglionic survival. My hypothesis is that

extracellular vesicles are responsible for this preganglionic survival and synaptic specificity.

VI. Intersection between Extracellular Vesicles and Signaling Endosomes

Neurotrophin trafficking into the dendrites

Target-derived NGF is indeed necessary for both pre and postganglionic synaptic specialization providing more evidence for the plausibility of retrograde-transsynaptic transfer of survival signaling. In $NGF^{-/-}$ mice, synaptic specializations on the postganglionic neuron are significantly reduced as demonstrated by the lack of the postsynaptic density (PSD) markers, MAGUK and Shank[64]. It was shown that retrogradely transported SEs enter dendrites. In fact, it is the retrogradely trafficked NGF-TrkA SEs that are responsible for this dendritic PSD formation and maturation[64]. Interestingly, this dendritic pool of SEs moves bidirectionally and exhibits more frequent pauses and oscillatory movements compared to axonal SEs suggesting that they can be pausing below putative synapses and signaling locally to form the PSD[65]. Indeed phosphorylated TrkA can be found *in vivo* in the dendrites of SCGs throughout development and inhibition of TrkA kinase activity results in a decrease of both pre and postsynaptic specializations[65]. Lastly, dendritic SEs have been shown to be molecularly diverse associating with both Rab7 and Rab11[52]. Furthermore, dendritic SEs can promote their lifespan by undergoing post-transcytotic signaling endocytosis (Fig. 2) into an early endosome marked by EEA1[52]. Interestingly, SEs are also able to undergo putative fission and fusion events suggesting that the sorting and recycling fates of a SE

are dynamic. One study reports live imaging of large SE that seems to give rise to several smaller SEs[52]. These aforementioned studies indicate that SEs not only traffic into, and signal within the dendrites, but that they are necessary for the formation of synapses. However, these studies fail to address the morphology of these signaling endosomes. The precise morphology of these dendritic signaling endosomes might shed light on their capacity to signal extracellularly thus addressing the question of how the upstream preganglionic neuron receives survival signaling and makes a one-to-one connection with the surviving postganglionic neuron. For example, SEs reinserted into the plasma membrane might be able to bud off of the plasma membrane as a microvesicle. If the SEs were shown to be Rab11+ MVBs that traffic into the dendrites that would give more plausibility to an exosome-mediated form of synaptic communication.

Intercellular communication via neurotrophic extracellular vesicles

While I have presented evidence for TrkA SEs existing as MVBs, what evidence is there for retrograde transsynaptic transfer of neurotrophins? Answers to this question, rely on excellent research done on viral retrograde trans neuronal transfer. In neuroscience, viral machinery has been exploited to study the synaptic inputs and circuitry of a particular neuronal pathway. Rabies virus in particular spreads trans-synaptically, preferentially in the retrograde direction[69]. This observation led to the identification of the rabies virus glycoprotein-G as responsible for the transsynaptic retrograde transport and internalization of rabies into presynaptic neurons[70,71]. Furthermore, viruses are able to accumulate inside and utilize MVBs for intracellular

transport and to escape degradation. Similarly bacteria such as anthrax lethal toxin is comprised of a protective antigen (PA) and a lethal factor (LF) that is preferentially packaged into ILVs[72]. The low pH of the ILV supports PA's insertion into the ILV membrane thus allowing channel formation and translocation of LF into ILVs where they can persist long term. Once triggered the toxin can then subsequently back fuse and release into the cytosol or be released as exosomes[72]. Additionally, West Nile Virus has been found inside vesicular structures in close vicinity to the axodendritic spines of both pre and postsynaptic neurons of the spinal cord of rhesus monkeys[73]. Although viruses serve as the classical model for retrograde transsynaptic transfer is there any evidence for retrograde neurotrophin transsynaptic transfer?

One study followed the localization of radiolabeled tetanus toxin, tetanus fragment, NGF, cholera toxin, or WGA in SCG neuronal bodies after peripheral injection[74,75]. WGA, cholera, tetanus and NGF all showed robust labeling in the sympathetic postganglionic cell bodies and dendrites; however, only tetanus toxin labeled the preganglionic neuron with scarce labeling by WGA[74]. In the cases of transsynaptic transfer no staining remained in the synaptic cleft or extracellular space indicating immediate uptake[74,75]. While it appears that NGF was not trans-neuronally transferred other neurotrophins such as BDNF and GDNF have been shown to undergo transsynaptic transcytosis. This was seen in rat hypoglossal neonatal neurons using autoradiographic electron microscopy. Radiolabeled GDNF and BDNF highly accumulated in dendritic MVBs whereas FGF did not[50]. Furthermore, transcytosis of GDNF and BDNF into the presynaptic terminal took 15 hours whereas tetanus toxin bypassed MVBs and more quickly traversed the synapse[76]. This is significant because it

suggests that tetanus toxin and possibly viruses' traverse synapses by different and quicker mechanisms compared to neurotrophins. It also suggests that signaling cargoes, such as neurotrophins, are shuttled towards different fates (i.e., degradation or recycling) compared to non-signaling cargoes, such as toxins. Lastly, 40-65% of BDNF or GDNF containing MVBs were within 400nm of a PSD and radioactive grains were found outside dendritic MVBs within 60nm of the limiting membrane. In contrast radioactive grains from perinuclear MVBs were localized inside the MVBs within 120-180nm from the limiting membrane [76]. This suggests that these neurotrophin 'grains' might have undergone fission or exocytotic release events either from the MVB limiting membrane or with the plasma membrane. Additionally, the presence of these putative neurotrophin grains might correspond with the single vesicles (SV) reported by Ye et al. However, immune or radioactive EM labeling does not lend to the temporal resolution necessary for capturing these rare events and these grains might represent background signal.

Table 1

Cell Type	Cargo	Presynaptic Presence	Postsynaptic Presence	Time to transsynaptic transfer	Organelle	Reference
Rat Hypoglossal Nerve	Rabies Virus	Yes	Yes	2.0-2.5 days post infection	not known	Ugolini 1995
Retinal pigmented epithelial (RPE1) cells (in vitro)	Anthrax Toxin	Transfer of toxin from RPE1 cells cocultured with Chinese Hamster Ovary cells		2 hrs. to 4.0 days	MVB	Abrami 2013
Rhesus macaque intrathalamically	West Nile Virus	Yes	Yes	7 days post infection	MVB	Maximova 2016
Rat anterior eye chamber or submandibular gland	Tetanus toxin	Yes	Yes	14 hrs. to 1 day post injection	MVB	Schwab 1977

Rat anterior eye chamber or submandibular gland	NGF	No	Yes	14 hrs. to 1 day post injection	MVB	Schwab 1977
Rat anterior eye chamber or submandibular gland	Tetanus toxin	Yes	Yes	14 hrs. post injection	MVB	Schwab 1979
Rat anterior eye chamber or submandibular gland	Tetanus toxin fragment	Yes	Yes	14 hrs. post injection	MVB	Schwab 1979
Rat anterior eye chamber or submandibular gland	NGF	low amount	Yes	14 hrs. post injection	MVB	Schwab 1979
Rat anterior eye chamber or submandibular gland	Wheat germ agglutinin	low amount	Yes	14 hrs. post injection	MVB	Schwab 1979
Rat anterior eye chamber or submandibular gland	Phyto haemagglutinin	low amount	Yes	14 hrs. post injection	not known	Schwab 1979
Rat anterior eye chamber or submandibular gland	Ricin	low amount	Yes	14 hrs. post injection	not known	Schwab 1979
Rat anterior eye chamber or submandibular gland	Cholera toxin	very low amount	Yes	14 hrs. post injection	not known	Schwab 1979
Rat tongue	Tetanus toxin	Yes	Yes	8 or 15 hrs. post injection	MVB	Rind 2005
Rat tongue	GDNF	Yes	Yes	8 or 15 hrs. post injection	MVB	Rind 2005
Rat tongue	BDNF	Yes	Yes	8 or 15 hrs. post injection	MVB	Rind 2005

VII. Conclusion

NGF signaling is critical for the proper wiring of the sympathetic neuronal circuit. The TrkA SE is required for the survival of both postganglionic and preganglionic neurons. Confoundingly, preganglionic neurons do not express the TrkA receptor, nor do they have access to NGF. However, the trafficking of the TrkA SE supports the conclusion that TrkA can be trafficked to the post synaptic density of the synapse

between pre- and postganglionic neurons. Furthermore, the TrkA SE is well-poised to be secreted as EVs as it can diversify into a MVB or be recycled to the plasma membrane of postganglionic neurons. Additionally, the literature further supports the notion that neurotrophic factors as well as other viral proteins colocalize with MVBs and are subsequently secreted and taken up by upstream presynaptic neurons. Further understanding of the mechanism and regulation of the TrkA SE and its fate are critical to understanding the proper wiring of sympathetic circuits during development.

Chapter II. Emerging Roles of Neuronal Extracellular Vesicles at the Synapse

This chapter is published as “Emerging Roles of Neuronal Extracellular Vesicles at the Synapse.” Ashley J. Mason, Christopher Deppmann and Bettina Winckler. *Neuroscientist.* (2023).

Abstract

Extracellular vesicles (EVs) are secreted from most if not all cell types and implicated in short and long distance signaling throughout the body. EVs are also secreted from neurons and represent an emergent neuronal communication platform. Understanding the functional implications of EV signaling to recipient neurons and glia requires understanding the cell biology involved in EV biogenesis, cargo loading, secretion, uptake, and signal transduction in the recipient cell. Here we review these major questions of EV biology, while highlighting recent new insights and examples within the nervous system such as modulating synaptic function or morphogenesis in recipient neurons.

I. Introduction to Extracellular Vesicles

After much initial skepticism, extracellular vesicles (EVs) are now widely recognized as a novel form of intercellular communication. They hold tremendous promise as diagnostic and therapeutic tools, but the field faces several barriers to progress including: **1)** determining how certain cargos are selected for inclusion into EVs, **2)** if and how EV secretion is regulated, and **3)** if and how uptake and signaling in the target cell is selective. In this review, we will first give a brief overview of EV biogenesis, cargo loading, secretion, and uptake with particular emphasis on the newest research. Secondly, we will discuss the accumulating evidence for functional roles for neuronally-derived EVs with an emphasis on synaptic function.

EV is the general term used to describe lipid bilayer enclosed particles that are secreted by cells and range in size from 30 to 10,000 nm in diameter. Originally, only specific cell types were thought to release EVs. However, with the advancement of new

techniques and years of work to overcome skepticism, it is now well established that all cells can release EVs and that they are physiologically produced and functionally relevant[53–56]. The field has developed strict guidelines for how to characterize EVs[77]. Techniques such as biochemical isolation followed by proteomics (Western blot, mass spectrometry), nanoparticle tracking analysis, single-particle interferometric reflectance imaging sensing, and electron microscopy in combination are used to validate EVs. Inroads have also been made in the gentle dissociation of tissues in order to study EVs *in vivo* derived from the extracellular space with the first credible isolation of EVs from brain tissue described a few years ago[78]. While EV is the umbrella term for all vesicles secreted from a cell, there are many different types of EVs that are delineated based on their biogenic origin, size, or role. The main subdivision of EVs is based on biogenic origin: ectosomes (e.g., microvesicles, exophers, apoptotic bodies, migrasomes, etc.) bud off from the plasma membrane (Fig. 1A) while exosomes are derived from intraluminal vesicles (ILVs) via fusion of endosomes (such as multivesicular bodies) (Fig. 1E). The multivesicular body (MVB) forms from early and late endosomes by inward budding of the limiting membrane (Fig. 1C) to form small vesicular inclusions known as intraluminal vesicles (ILVs)[57,58]. When MVBs fuse with the plasma membrane, the ILVs are secreted (Fig. 1E). Secreted ILVs are referred to as exosomes (Fig. 1E). Historically, MVBs were viewed as cellular waste-transporting compartments that were either sent for degradation (Fig. 1F) or secreted to release cellular waste with exosomes being considered trash. However, in the last couple of decades, MVBs have come to be appreciated as long-lived signaling competent organelles with multiple fates. No current method cleanly isolates these specific subpopulations from heterogeneous sources

such as during isolation from cell culture conditioned media or from the brain extracellular space. Generally, exosomes are of smaller size whereas ectosomes have a wide range of sizes. Differential centrifugation can thus partially separate larger EVs (presumptive ectosomes) from smaller EVs (exosomes and small ectosomes). Additionally, ectosomes and exosomes are virtually indistinguishable from each other from a mechanistic perspective because they share overlapping biogenic machinery and therefore no specific marker exists to separate them based on molecular composition.

Regardless of biogenic origin, EVs from the extracellular space contain a range of biomolecules (DNA, RNA, proteins) that would ordinarily be recycled into metabolic pathways if they fluxed through the degradative pathway. In fact, neuronal EVs can regulate synaptic plasticity, neurodegenerative pathogenic spread, and neuronal proliferation by delivering regulatory payloads. EVs derived from other nervous system cell types including astrocytes, microglia, oligodendrocytes, Schwann cells and blood-brain barrier tissue also serve functions within the nervous system. Non-neuron derived EVs as well as EV roles in neurodegenerative diseases have been the subject of several excellent reviews[79–81] and will not be the focus of this review.

II. Biogenesis

How are EVs generated inside cells, and can their generation and release be regulated? In this section we will review the mechanisms by which ectosomes bud from cells and by which cargos are included in MVBs prior to secretion in exosomes.

Ectosome Biogenesis

Ectosomes are EVs that bud out from the surface of the plasma membrane (Fig. 1A). First, cargo must be sequestered and targeted to be enriched in microdomains along the plasma membrane[82]. The microdomains, consisting of asymmetric lipid leaflet distribution coordinated by enzymes that can move lipids from one leaflet to the other, i.e. flippases and floppases, serve as nucleation points for ectosome formation[83]. Additionally, the Endosomal Sorting Complex Required for Transport (ESCRT) proteins function in cargo sequestration and assist in the membrane deformation and scission necessary for ectosome shedding[83,84]. Lastly, cytoskeletal dynamics and cortical actin deformation are important for ectosome generation with Rho GTPases regulating these vesicle and cytoskeletal processes[85,86] (Fig. 1A).

Exosome Biogenesis

MVBs are endosomes that are formed by the inward budding of the limiting membrane, resulting in the formation of multiple, small vesicles within a larger vesicle[87]. When the limiting membrane of the MVB fuses to the plasma membrane, small vesicles called ILVs are released into the extracellular space as exosomes[57,59,88] (Fig. 1E). Similar to ectosomes, exosomes can carry a wide range of cargos, including protein, RNA, miRNA, and signaling proteins[88].

ESCRT-dependent MVB biogenesis

The biogenesis of some, but not all ectosomes and exosomes occurs via the ESCRT pathway (Fig. 1A,C). Here we briefly summarize and highlight new research which is also covered in detail in several excellent reviews[89,90]. The formation of ILVs to generate MVBs is classically viewed as a pathway that sequesters cargo fated for degradation (e.g., ubiquitinated proteins). Therefore, the first step in biogenesis is the

recognition and clustering of ubiquitinated proteins by ESCRT0[91]. ESCRTI and II are responsible for the invagination and formation of membrane buds and for recruitment of ESCRTIII to the bud neck of the membrane to initiate scission[91,92]. After scission, dissociation of the ESCRT protein complex is driven by the AAA-ATPase, Vps4 (Fig. 1C). Several studies show that the knockdown or depletion of any of these four main ESCRT proteins and their adaptors can affect the size, morphology, and number of ILVs and thus ultimately the number of exosomes that are secreted by the cell[92,93]. Although this biogenic machinery appears to be redundant, a critical question remains as to what machinery determines cargo selection. Recent work lends clues towards answering this question. Certain ESCRT proteins and their adaptors such as tsg101, ALIX and CHMP4 can regulate the loading of specific cargos into ILVs thereby generating different subtypes of EVs[94–96]. Increasingly this cargo sorting has been shown to occur early on in the endosomal pathway (i.e., occurring on early endosomes)[94–96]. Lastly, lipids can also direct the recruitment of ESCRT proteins. For example, the FYVE domain of Hrs, an ESCRT0 subunit, binds with high specificity to PI(3)P thus recruiting the ESCRT0 complex to the early endosome[97]. We will discuss more of the role of lipids in MVB biogenesis below.

ESCRT-independent, lipid-dependent mechanisms of MVB biogenesis:

In addition to ESCRT, there are also less well-defined ESCRT-independent pathways for ILV formation. It is now clear that lipids play critical and often instructive roles in EV biology. Lipid composition not only influences MVB biogenesis and cargo loading but can also delineate secretory versus degradative MVBs. Much remains to be learned about the roles of lipids in regulating EV biogenesis processes, and the

challenges to cleanly manipulate single lipid species experimentally are substantial. The diversity of lipids on the endosome and endosomal compartments gives rise to more fluid and more lipid raft-like microdomains which can impact the fate, function, sorting and biogenesis of maturing endosomal compartments with lipid dynamics playing a large role in endosomal membrane deformation[98]. Here we will discuss several lipids, including ceramide, sphingomyelin, lysobisphosphatidic acid and cholesterol, and their roles in EV biogenesis (including ILV formation, cargo selection, and secretion).

One important lipid involved in ESCRT-independent ILV formation is **ceramide**. The exact mechanism behind ceramide-modulated ILV formation is unknown; however, it is proposed that the cone-like structure of ceramide supports the negative membrane curvature necessary for inward budding[99] (Fig. 1C). Ceramide is generated from the conversion of **sphingomyelin** into ceramide by the enzyme neutral sphingomyelinase 2 (nSMase2). Activity of nSMase2 is dependent on the fluidity of the membrane and the presence of sphingomyelin-enriched, lipid-ordered microdomains[100,101]. Interestingly, the lipid composition and activity of nSMase2 on the limiting membrane of MVBs can determine the fate of the compartment either for secretion or degradation. Blocking nSMase2 activity induces accumulation and assembly of the V-ATPase complex on the sphingomyelin-enriched lipid microdomains on the limiting membrane of MVBs[101] forming active V-ATPase pumps that drive lumen acidification thus routing the MVB from a secretory towards a degradation pathway[102] (Fig. 1D). This delineating decision between secretory MVBs and degradative MVBs will be discussed below but is also influenced by lipid composition of the MVB limiting membrane.

In addition to nSMase2-mediated generation of ceramide on MVBs, ceramide can also be transported to the MVB by the ceramide transfer protein, CERT, where it can stimulate ILV biogenesis in the presence of palmitate[103]. CERT usually transports ceramide at ER-Golgi membrane contact sites (MCS); however, CERT has been shown to localize to ER-MVB MCS by binding to the tether VAP-A where it mediates formation of RNA containing ILVs and eventually EVs[104]. CERT can also directly bind to tsg101 and mediate ESCRT-dependent ILV formation. Interestingly, inhibition of ceramide synthesis by blocking nSMase2 does not block CERT-tsg101 interactions and EV biogenesis, suggesting that EV formation by nSMase ceramide conversion is an alternative pathway to ceramide-independent CERT-ESCRT mediated EV biogenesis[95]. Lastly, knocking out CERT reduces the number of released EVs without impacting the size and number of MVBs[103] suggesting that ceramide might also be important for EV secretion as well as MVB biogenesis. These studies highlight how the cell has many pathways and redundancies to accomplish MVB biogenesis and that different subtypes of EVs arise from different biogenic pathways. Future studies examining cargo or ILV subtypes will further elucidate the role of specific proteins or lipids in ILV biogenesis.

Another unusual lipid, known as **lysobisphosphatidic acid (LBPA)** or **bis(monoacylglycerol)phosphate (BMP),** has been shown to be enriched in ILVs derived from ESCRT-independent mechanisms[105]. LBPA's structure includes a phosphatidic acid head group surrounded by two glycerol chains with a cis double carbon bond in the middle of each acyl chain causing it to introduce a wedge-shape conformation in the bilayer membrane[106]. LBPA is synthesized from phosphatidylglycerol and cardiolipin originating in the mitochondria and transported to

the late endosome via the ER or by autophagosomes[107,108]. LPBA is enriched on the ILVs of late MVB endosomes,[109] but is surprisingly not found on exosomes[110,111] unless the endolysosomal system has been perturbed[112].

If LBPA is not secreted, then what precisely is its role on the ILVs of late endosome? A potential role might be in the formation of ILVs and sorting of cargos out of the late MVB, a process called back-fusion. Back-fusion refers to the reversal of ILV budding into the MVB interior by having ILVs fuse back with the limiting membrane of the MVB. Back-fusion is often invoked as a potential regulatory node to control the exposure of signaling-competent receptor cytoplasmic tails to the cytoplasm. ILV formation would terminate signaling whereas back-fusion would reactivate signaling. Similarly, ILV formation could remove other receptors from the limiting membrane to change effector cascades and back-fusion would allow access again. The evidence that back-fusion can occur is difficult to obtain and only a few papers have carefully tried to show back-fusion experimentally. LBPA is a candidate lipid that might promote back-fusion. In the low pH (<5) of the late endosome, LPBA becomes highly fusogenic and this property may serve as the mechanism behind back-fusion[113]. This LBPA-enriched ILV fusogenic propensity is decreased at pH 6.0 and is completely abolished at pH 6.5[113] suggesting that this acidic protonation of LBPA in the late endosome might also enable lipid and protein translocation through kiss and run fusion events of LBPA-enriched ILVs and the limiting membrane of the MVB[114]. These kiss and run back-fusion events, dependent on LBPA, are utilized by viral capsids when escaping the late endosome[115]. Thus, the fusogenicity of LBPA-enriched ILVs could represent a final sorting or signaling opportunity for proteins present on the ILV membrane. Surprisingly,

a study looking at back-fusion of ILV cargo to the limiting MVB membrane showed that pharmacologically increasing LBPA on ILVs resulted in a retention of a canonical EV tetraspanin cargo, CD63[116]. Why an EV cargo did not undergo back-fusion when LBPA levels were increased suggests that maybe only certain EV cargos can undergo back-fusion and that lipid concentration heavily influences the fate of MVBs and of ILVs.

LPBA enrichment in ILVs also controls the accumulation and distribution of cholesterol transport through the endolysosomal system. **Cholesterol**, along with sphingomyelin, localizes to the ILVs of early MVBs and is purported to be enriched in secreted MVBs[117]. Recent work has shown that CD63 directs cholesterol by sorting it to ILVs and exosomes[118]. In contrast, LBPA shows up most heavily in the ILVs of late MVBs[119]. However, application of an anti-LBPA antibody causes rapid accumulation of cholesterol in late endosomes indicating that LBPA influences the localization of cholesterol and therefore might play a role in the sorting and recycling dynamics of maturing MVBs[120]. Lateralized enriched distinct lipid domains might thus contribute to sorting different cargos into distinct ILVs, ultimately generating distinct exosomes.

In conclusion, it is not understood how the decision to create EVs via MVB secretion or ectosome budding is regulated, but one could envision that cargo selection and presence of receptors or lipids on these different EV subpopulations could be very different. Illuminating the biogenic origin of different EVs is thus important to fully explore the diagnostic and therapeutic potential of EVs in the future.

Regulating trafficking of MVBs for secretion or degradation: evidence in neurons

The decision to degrade or secrete cargo is influenced by a variety of factors including the type of cargo, cell state, signaling capacity, synaptic plasticity, and development. What drives the trafficking of MVBs towards secretion versus degradation in neurons has been relatively understudied because it is technically difficult to molecularly define endolysosomal compartment flux as it exists as a continuum. One group used the trafficking and spread of cellular prion protein (PrP^C) to study the decision between degradation versus secretion[121]. PrP^C has been shown to be secreted in EVs but can also be routed to the lysosome for degradation. In this study, the cargo adaptor, muskelin was identified as a coordinator of PrP^C transport to the lysosome for degradation over release. Knockout of muskelin, reduced the trafficking of PrP^C to the lysosome and increased the concentration of PrP^C on the neuronal surface and in secreted EVs (Fig. 1D). Conversely, routing of MVBs toward secretion in mouse hippocampal neurons is influenced by the scaffolding protein, KIBRA[122]. KIBRA regulates AMPA receptor trafficking during synaptic plasticity, but also stabilizes Rab27a preventing it from ubiquitination and thus degradation. Rab27a association with MVBs is important for MVB docking with the plasma membrane for subsequent fusion. Loss of KIBRA, and thus, loss of Rab27a decreases the number of EVs with a subsequent increase in the number of MVBs and ILVs per MVB (Fig. 1E). Do mutants in these genes affect only one cargo or all cargos? Open questions regarding cargo-mediated recruitment of trafficking adaptors to MVBs remain, but defects in these genes might explain pathogenic spread within the brain.

Novel EV formation in neurons: lessons from viruses

Inter-neuronal communication via EVs is a novel pathway by which cells communicate. As discussed in this review, EVs are generally formed by budding out from the plasma membrane or from the endosomal system. Recently, in both fly and mouse models, it was shown that viral-like structures can bud out from the plasma membrane as EVs[123,124]. This novel EV biogenic pathway came from the discovery that the immediate early gene Arc contains structural elements of the retroviral Gag proteins and can self-assemble into viral-like capsid structures. Upon synaptic plasticity-like stimuli, Arc (dArc in *Drosophila*) mRNA is translocated to the dendrites in an activity-dependent manner where it is locally translated. Arc protein oligomers can then self-assemble into capsids that bind Arc RNA and subsequently bud off from the plasma membrane as EVs. Recipient neurons or the muscle in the *Drosophila* model, bind and internalize these Arc capsid EVs, that subsequently disassemble and allow for translation of their RNA cargos. These studies demonstrate a novel pathway by which neurons utilize a conserved viral mechanism to transfer RNA cargos. It is suspected that budding out from the plasma membrane as an EV enriches the appropriate surface receptors to the EV to mediate targeting and uptake. In addition, a coat of extracellular proteins, apolipoproteins, and immunoglobulins (“EV corona”) can associate with the outside of the EV to surround it and function in part to mediate targeting to and uptake by the recipient neuron[125].

III. EV cargo loading in neurons

Cargos along the endosomal pathway are sorted into EVs

While it is well established that all cells release EVs, their composition can vary widely with cell type and growth conditions raising many questions about the molecular

logic underlying which cargos get loaded into EVs, especially in neurons. In order to answer this question in neurons, the *Drosophila* neuromuscular junction (NMJ) has proven to be a powerful model system to study the secretion and cargo sorting that occurs at the presynaptic terminal. In addition to canonical neurotransmitter release, the presynaptic terminal also releases EVs containing cargoes such as tetraspanins, synaptotagmin-4 (Syt-4), neuroglian (Nrg), amyloid precursor protein (APP) and evenness interrupted (Evi)[126–128]. In this system, secretion can be clearly visualized in the whole tissue since secreted cargos are trapped in the extrasynaptic space and apposing muscle cells. In contrast, in cultured mammalian neurons, it is difficult to track EVs post-secretion since they are released into the medium and can no longer be visualized by microscopy.

Using this system, recent studies in the *Drosophila* NMJ examined how inclusion of EV cargos into secreted EVs was affected by interfering with either retromer (Vps35), a protein complex involved in sorting and retrieving cargos from the endolysosomal system to the plasma membrane, or Rab11, a small GTPase regulating many recycling pathways. Rab11 and Vps35 played opposing roles in the decision to sort EV cargos into either EV-generating MVBs or degradation-fated MVBs. These results suggest that early and/or recycling endosomes can include different cargos into distinct MVBs that are ultimately either secreted or degraded[127]. Surprisingly, Drosophila mutants in presynaptic endocytic machinery further perturb the EV cargo pathway, suggesting multitasking roles for endocytic proteins past the control of endocytosis per se[128]. More work will elucidate how the cell decides which cargos are destined for secretion or just locally maintained in the presynaptic terminal[127,128]. Since presynaptic terminals are

highly specialized and can activate bulk endocytic pathways after high stimulation, it remains to be seen to what degree the machinery responsible for regulation of cargo sorting and EV secretion in the NMJ is also responsible in other locations in neurons.

Canonical EV markers, such as the tetraspanins CD9, CD63 and specifically CD81 might have a role in cargo sorting in neuronally-derived EVs as well. In cultured mouse hippocampal neurons, endogenous expression of CD81 localizes to the axon and axon terminals where it packages synaptobrevin-2 (Syb2) into EVs and modulates their release[129]. CD81 knockdown neurons were still able to secrete EVS, but they did not contain detectable levels of Syb2 suggesting that CD81 is critical for the correct packaging of Syb2 into EVs [129]. Lastly, sonic hedgehog (Shh) in mouse embryonic brains was shown to be secreted on a specific subtype of EV generated by CHMP4 and containing the proteins Rab18, tyrosine-protein kinase receptor UFO (AXL), and transmembrane emp24 domain-containing protein 10 (TMED10) and CD81 but not CD63[94]. Strong evidence thus suggests that the synaptic vesicle recycling pathway, endosomal sorting pathways, and endocytic machinery all play a role in sorting exosome cargo, but there are still many unanswered questions about the precise mechanisms that control the selection, binding, and incorporation of exosome cargo into MVBs for release, as well as how these processes are regulated in different regions of neurons.

IV. Secretion

EV secretion can occur from the plasma membrane (ectosomes) or from an endosomal origin (exosomes); however, many of the key molecular players are used in both pathways. Excellent reviews regarding mechanisms of secretion and ways to

inhibit release can be found here[130] and here[131]. Below, we briefly summarize some of the molecular players involved in EV secretion including Rab GTPases and the SNARE complex.

Rab GTPases orchestrate MVB routing to the plasma membrane

Several groups have performed RNAi screens to identify Rabs involved in the process of EV release[132,133]. Rab27a and Rab27b regulate EV secretion as well as MVB positioning and docking at the plasma membrane[132,133]. Using mass spectrometry, Rab35 was also identified as an EV secretion effector that acts similarly to Rab27 by controlling the docking of endosomes to the plasma membrane in an oligodendroglia precursor cell line[134,135]. Knockdown studies of Rab11 also resulted in decreased release of EVs containing the Drosophila Wnt ligand, Wg. In this system, Rab11 and MVBs were localized to the active zone of synaptic boutons and in some instances in close contact with the plasma membrane[136]. Given their critical role in endosomal maturation and trafficking, it is perhaps not surprising that this family of membrane effectors would also play a role in MVB routing and EV secretion. As with other examples of Rab function, the context of cargo, cell type, and cell state seem to work in concert with particular Rabs to determine EV release.

SNAREs execute the fusion of MVBs with the plasma membrane

The soluble NSF attachment proteins receptor (SNARE) complex family consists of at least 60 proteins whose essential roles are mediating membrane fusion. The core SNARE complex consists of syntaxin and SNAP proteins which reside on the plasma membrane and synaptobrevin (VAMP) which is localized to the vesicular membrane[137]. Each SNARE protein contains a SNARE motif which allows formation of a coiled-coil

structure (four-helix SNAREpin) to bring the two membranes into close apposition to one another to facilitate fusion[138]. A particular SNARE pairing is thought to be required for allowing specific fusion events. Since MVBs can potentially fuse with either the plasma membrane or lysosomes, different vSNAREs are presumably required on the MVB to direct fusion to the correct target membrane. How different vSNAREs are trafficked to and partitioned into MVBs to control subsequent fusion potential is largely unknown[139]. However, VAMP7 and SNAP23 have specifically been shown to mediate exosome secretion [139]. VAMP7 is widely expressed in the rat brain localizing to vesicles in both dendrites and axons alongside CD63 [140].

While the SNAREs are canonically known for synaptic vesicle fusion in neurotransmitter release, they facilitate many membrane fusogenic events in the cell including MVB exocytosis from the cell[137,141]. This last role has been of increasing interest to EV researchers as a therapeutic target for controlling release of EVs associated with cancer and neurodegenerative pathologies. SNARE proteins have been implicated in EV release and their subsequent knockdown has reduced EV secretion. For example, knockdown of syntaxin1a decreased EV release of the Wg carrier, Evi, from perisynaptic and/or synaptic regions in Drosophila[136]. Similarly, SNAP23 has been shown to promote the fusion of MVBs with the plasma membrane in HeLa cells. Knockdown of SNAP23 using siRNA reduced fusion of CD63 containing MVBs with the plasma membrane [142]. Since SNARE complexes are ubiquitous and necessary for other cell homeostatic fusion events, interpretation of these studies remains difficult as it is challenging to obtain precise perturbation of just the SNARE control of exocytotic EV release.

Secretion of EVs in neurons

Neurons release EVs at a baseline rate but can also secrete more EVs in response to certain stimuli, such as an action potential or the exogenous application of potassium chloride (KCl). Studies have demonstrated that both AMPA and NMDA receptor activation can stimulate EV release in both young (7 DIV) and old (15 DIV) cortical cultures[143,144]. It has been shown that these EVs originate from MVBs through the detection of the C terminal fragment of tetanus toxin, which accumulates in ILVs and resultant EVs. Additionally, electron micrographs of stimulated cortical neurons demonstrate fusion-like events between MVBs and the plasma membrane, suggesting EV release. These findings indicate that EVs may play a role in modulating neuronal excitability and function. EVs have also been implicated in the pathogenic spread of neurological pathologies. Whether EV release is increased because of neurological diseases or disorders depends somewhat on the cargo being released. For example, α-synuclein release in EVs is increased when autophagy pathways fail, and higher levels of exosomes have been found in the brains of people with Down Syndrome[145,146]. Further information regarding pathogenic spread via EVs derived from neuronal and non-neuronal brain cells has been covered in several excellent reviews[79,147–151]. Currently, efforts are ongoing to bioengineer EV nanoparticles to deliver therapeutic cargo especially in the context of prion diseases[151–153]. Additionally, efforts to inhibit EV release to lessen pathogenic spread remains challenging as the tools to specifically inhibit only pathogenic EVs are not in place[79].

V. Uptake

EVs signal to their recipients through surface binding or internalization.

EVs have been shown to be internalized through a variety of mechanisms including but not limited to phagocytosis and endocytosis (Fig. 2A-F). The cell-specific spatial and temporal regulation of EV uptake is essential to understanding the signaling capacity and functionality of EVs. Despite its high importance, EV targeting, uptake and cargo accessibility remain some of the least characterized mechanisms in the field. Characterizing EV uptake has been one of the more difficult mechanisms to answer as their small size and lack of a specific marker makes it difficult to track and visualize EVs both *in vivo* and *in vitro*. Additionally, the propensity to internalize EVs appears to be cell type specific as phagocytic cells take up EVs more readily than non-phagocytic cells. Given that all cells produce EVs there is vast heterogeneity in EV cargoes and surface proteins which might influence the targeting and mechanism of uptake by the recipient cell. More detailed reviews regarding visualization of EV tracking and uptake *in vivo* can be found here[154] and here[155]. Lastly, understanding how EV cargo becomes accessible to the cytosol of the recipient cell, given that internalized EVs will be bound within another vesicle, remains an open question (Fig. 2G,H). Experimental inroads into understanding this question are currently being conducted and some researchers have shown that EVs can deliver cargo to specific locales within the cell (i.e. nucleus, mitochondria), although the majority of EV cargo in the study was retained within the endosomal pathway after internalization[156].

VI. EV function in neurons

In this section, we will explore the specific role of EVs in neurons. Some of the key questions we will address include what types of cargos are packaged and released

in EVs, how cargo selection is regulated, how EVs deliver their cargos to recipient cells, and what the functional consequences are of EV-mediated cargo transfer.

At the synapse: EVs function in neuromodulation

EVs released from neurons and other brain resident glial cells serve as a communication platform by which the excitability or synaptic activity of a network can be tuned. One study showed, both *in vivo* and *in vitro*, that CD63+ EVs derived from the somatodendritic domain of cortical neurons transfers the microRNA, miR-124-3p to astrocytes[157]. Internalization of miR-124-3p by astrocytes ultimately increases translation of the glutamate transporter 1 (glt1) mRNA thus increasing glutamate transporter protein levels. While the study does not directly investigate the impact of increased glutamate transporter protein in astrocytes, it is possible that increased GLT1 might play a role in modulating neurotransmission duration by taking up excess glutamate from the tripartite synaptic cleft. Since the EVs were secreted from the somatodendritic domain it is possible that the postsynaptic neuron releases EVs to downregulate the excitatory neurotransmission it receives over time. This study also demonstrates EVs can influence transcriptional changes in recipient cells suggesting that EV cargo can influence the transcript and protein expression in recipient cells.

Another study shows that neuronal EVs can influence inhibitory neurotransmission as well[129]. In mouse hippocampal cultures, a subset of secreted EVs contained the SNARE protein synaptobrevin 2 (syb2), which is responsible for synaptic vesicle fusion during neurotransmission. Incubation of Syb2-containing EVs with recipient hippocampal neurons resulted in an increase in the frequency of miniature inhibitory postsynaptic currents (mIPSC), but not miniature excitatory postsynaptic

currents (mEPSC) suggesting that Syb2 EVs modulate inhibitory, but not excitatory neurotransmission. The Syb2 protein transferred in EVs was shown to be actively incorporated into the recycling pool of synaptic vesicles in the recipient neurons using a syb2-pHluorin tagged protein. Interestingly, release of these Syb2 EVs was not activity-dependent, but instead relied on the tetraspanin CD81 (Fig. 3B). Which type of hippocampal neurons the Syb2 EVs were targeted to and why the cells would want to increase spontaneous inhibitory network activity remain open questions.

Lastly, synaptotagmin-4 (Syt-4) containing EVs released from Drosophila motor neurons regulate the formation of presynaptic boutons through retrograde signaling[126]. Calcium influx after high frequency stimulation at the NMJ, triggers postsynaptic vesicle fusion mediated by the calcium sensor, synaptotagmin-4. Fusion of these vesicles releases a signal that acts retrogradely on the presynaptic motor neurons to promote presynaptic growth through cAMP mediated cytoskeletal remodeling[158]. Korkut and colleagues demonstrate that Syt4 is most likely transferred trans-synaptically from presynaptic motor neurons to muscles in EVs. Using *syt4* null mutants and expressing Syt-4 exclusively in motor neurons was sufficient to rescue Syt-4 expression in both the motor neurons and muscle cells[126]. This study demonstrates how EVs from donor neurons can tune their own neuronal excitability and plasticity through communication with their postsynaptic partners. It is a great example of donor EV cargo being functionally incorporated into recipient cells and then in turn modulating the donor neuron to change its firing capacity or potential through the formation of presynaptic boutons.

EVs in neural development and proliferation

Some of the more interesting, but confounding cargos of neuronal EVs include trophic factors, morphogens, and guidance cues. In contrast to activity-dependent release, the regulation guiding the release of trophic neuronal EVs is not as well understood. Regulation of release as well as uptake specificity is especially important when considering the spatial and temporal effects these trophic factors, guidance cues and morphogens have on their recipient cell and the implications for the development of that circuit or tissue patterning. Neuronal EVs can influence neuronal circuit development by increasing neurogenesis and proliferation in the granule cell layer of the mouse dentate gyrus[159]. Furthermore, in mouse embryos the morphogen, sonic hedgehog (Shh) is secreted in EVs where it increases the number of neuronal progenitors. Loss of Shh+ EVs had dramatic impacts on brain development leading to an underdeveloped brain size[94]. Neurons can also tune cargos secreted in EVs during development. EVs derived from 3 DIV cortical cultures express HDAC2, a histone deacetylase that transcriptionally represses spine development[160]. As the neurons matured (15 DIV), they released fewer HDAC2 EVs to encourage spine growth. This effect could be reversed by the addition of 3 DIV EVs to 15 DIV cultures thus reducing spine number (Fig. 3C). In the developing *Drosophila* NMJ, the Wnt-1 ortholog, Wingless (Wg) is trafficked from the Golgi to the plasma membrane bound to a multipass transmembrane protein, evenness interrupted (Evi). This interaction is required for Wnt secretion on EVs[136,161,162]. Evi null mutants cannot secrete Wg and as a result the NMJ exhibited more ghost boutons (putative synaptic sites that lack active zones) suggesting a defect in synapse formation[161] (Fig. 3A).

In addition to morphogens, ligands and/or their receptors can be secreted on EVs. Ephrin ligands binding to their Eph receptors are important in establishing borders, delineating circuit boundaries and mediating axon repulsion during development. Although the canonical signaling modality between Ephrins and Eph receptors occurs through cell-to-cell contact, EVs have also been shown to contain full length Eph[163]. Importantly, these Eph^{pos} EVs could induce growth cone collapse when incubated with cortical mouse neurons or motor neuron explants. These intriguing data open more questions into the specificity, localization, and concentration of these EphB-containing EVs. To inform proper axonal guidance, Eph-containing EVs need to be trafficked to the correct location and exist in high enough concentration to have a functional output on cell migration.

Two other examples of ligand-receptor complexes being secreted on EVs includes the low affinity neurotrophin receptor p75 (p75NTR) and the tropomyosin receptor kinase A (TrkA). p75NTR signaling mediates apoptosis and survival signaling in sensory and sympathetic neurons. Interestingly, Escudero and colleagues discovered that the full length p75NTR receptor is secreted from sympathetic neurons on EVs following depolarizing stimuli[164]. This study did not investigate the functional role of these p75NTR^{pos} EVs, but the neurons selectively sorted them for secretion into CD63+ MVBs or Rab11 recycling endosomes rather than routing them to the lysosome for degradation (Fig. 4B)[164].

Lastly, our own work shows that TrkA derived from the distal axon of primary sympathetic neurons can be secreted in EVs[165]. The neurotrophin receptor, TrkA, binds nerve growth factor (NGF) at its axon terminals and is internalized into a signaling

endosome (SE) (Fig 4A). This SE is retrogradely trafficked back to the somatodendritic compartment to promote survival, synapse formation, and several other trophic functions[27,28]. Much effort by our group and others has gone into determining the fate of the retrogradely transported TrkA SE. Once the SE arrives in the soma it can undergo dynamic endosomal trafficking (i.e. recycling to the plasma membrane, re-internalizing into a more immature endosomal compartment) and has been shown to be incorporated into multivesicular bodies[38,51,52,166,167]. Using compartmentalized microfluidic devices and a transgenic mouse line expressing FLAG-tagged TrkA receptor, we showed that TrkA labeled in the distal axon could be retrogradely trafficked to the cell body and released on EVs (Fig. 4A-C). Further work is needed to investigate what regulates TrkA EV secretion and the functional responses these TrkA-containing EVs elicit in recipient cells. While much progress is being made in this field there are still many open questions regarding the full capacity of EVs as signaling modalities.

VII. Conclusion

The functional roles of EVs in many systems are just now beginning to be appreciated. Initially, researchers thought that the main function of EVs, most notably apoptotic bodies, is to serve as a mechanism by which cells release unwanted “trash”. This is certainly the case, but it is becoming increasingly clear that this is not their only function. It is now well established that EVs represent a novel form of both local and long-range intercellular communication in many tissues. Importantly, EVs can help spread quantal packets of information such as nucleic acids or other cytosolic cargoes while ensuring they don't get lost in the extracellular milieu.

In the nervous system, all examined cell types secrete and respond to EVs. In addition to EV-mediated signaling between neurons and other cells (such as astrocytes), there is increasing evidence that EVs constitute a new mode of neuron-to-neuron communication. EVs at the synapse can serve as functional hubs to communicate to surrounding cells the state of the synapse. For example, modulating neurotransmitter levels[157], or secreting molecules to break down synaptic scaffolding to allow for the growth or shrinkage of a spine[168]. In the case of development signaling one can envision that EVs might serve to establish a specific site as a putative synapse. While the precise functional roles of EVs are still being discovered, it is important to consider how both the donor and recipient cells regulate EV communication both synergistically and independently.

Given that EVs have both diagnostic and therapeutic potential, especially as they are relatively non-invasive both in the detection of neurological diseases and as drug delivery platforms, understanding the molecular players involved in the regulation of neuronal EV biogenesis, cargo loading, secretion, uptake, and functionality in recipient neurons is essential. Challenges and open questions regarding EV roles in neuron- to –neuron communication remain and understanding the basic cell biology of EVs is critical to understanding how EVs communicate and transfer cargo within tissues. Among these open questions are:

1) How many distinct cargos are secreted in EVs? Is their inclusion regulated by cell-type, cell status (synaptic activity, growth factor signaling, nutrient availability, cellular stress)? Does each cell make multiple “flavors” of EVs and how is that regulated?

2) Is uptake of EVs selective, i.e., not all cells will internalize all EVs? How is targeting of specific EV to its appropriate recipient achieved (different EV components and different recipient receptors)?

3) How do bioactive molecules contained within EVs (such as nucleic acids or other cytosolic cargoes) escape the EV to initiate signaling or metabolic changes in the recipient?

The technical challenges to obtain answers to these important questions, such as the small size of many EVs and the lack of selective markers, are increasingly being tackled by novel approaches which hold great promise for mechanistically unraveling EV biology, their physiological and pathological roles, and their promise as diagnostic and therapeutic tools. The future of EV research is bright!

Figures

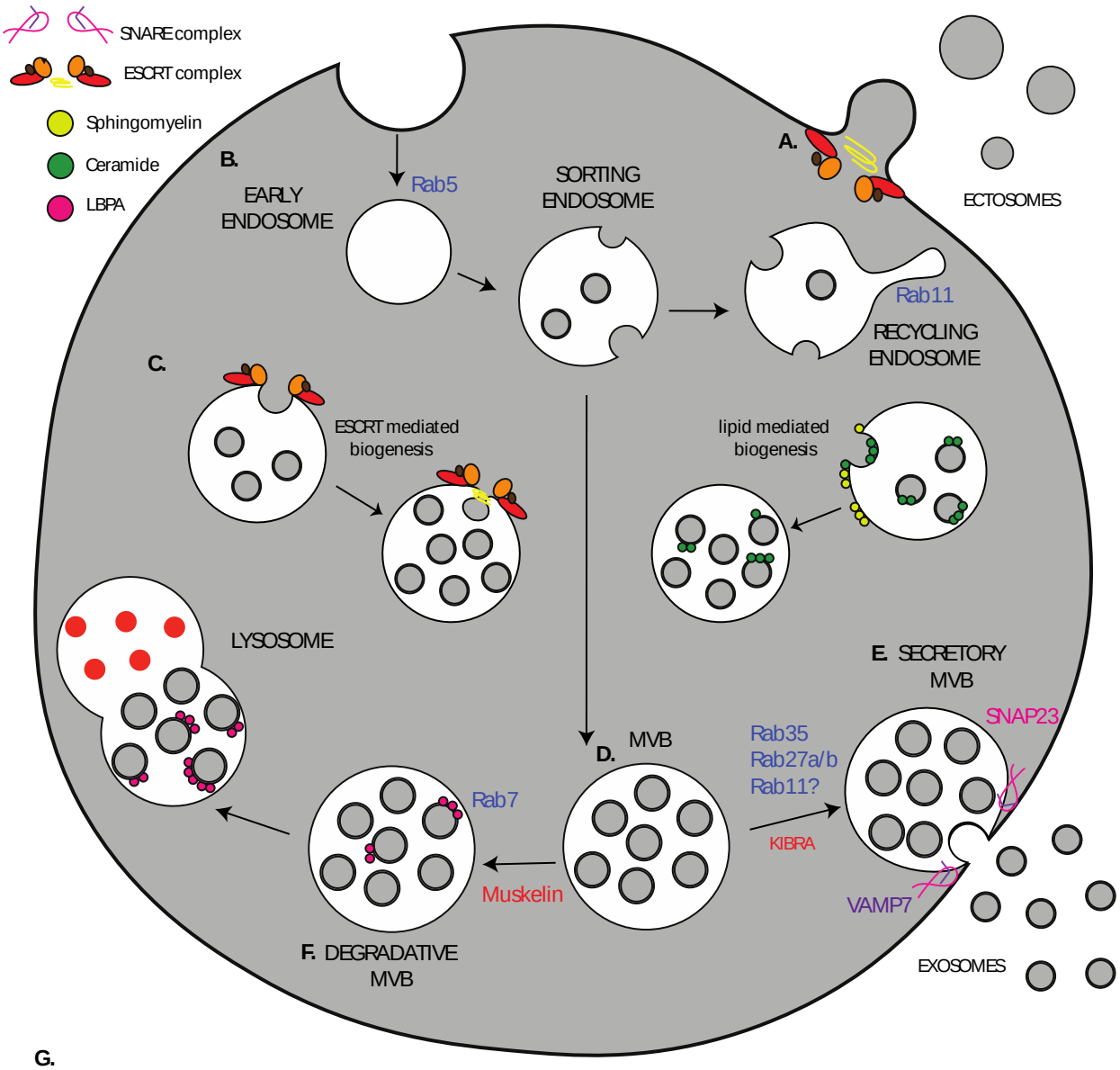

G.

Sphingomyelin

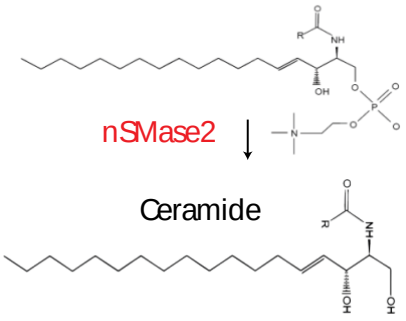

Lysobisphosphatidic Acid

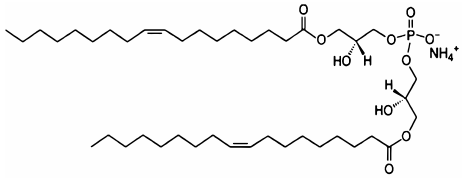

Figure 1. Mechanisms of EV Biogenesis. **A.** Ectosomes are formed by the budding off of the plasma membrane. This is likely facilitated by ESCRT but much of the machinery and regulation are still unknown. **B.** Endocytosed cargos enter the early endosome (Rab5+) and then converge in a dynamic compartment known as the sorting endosome. At the sorting endosome, cargos can be sorted to recycling routes (either rapid recycling directly to the plasma membrane or slower recycling via the Rab11+ recycling endosome). Non-recycling cargos destined for degradation are sorted to maturing endosomal compartments (such as multivesicular bodies, MVB) which ultimately fuse with the lysosome. Sorting endosomes begin to bud in small intraluminal vesicles (ILVs) from their limiting membrane **C.** ILVs can be formed by a variety of lipid or protein mediated pathways. Shown is ESCRT-dependent biogenesis (left) and lipid mediated biogenesis (right). Lipid mediated invagination occurs at sphingomyelin-enriched microdomains on the limiting membrane of multivesicular bodies (MVBs). Conversion of sphingomyelin into ceramide facilitates the inward budding. **D.** The MVB then undergoes a fate decision, fusion with the lysosome for degradation or fusion with the plasma membrane for secretion. While the precise checkpoint at which an MVB fate is decided is unknown here we depict the checkpoint as occurring after a mature MVB filled with many ILVs has formed. **E.** Secretion is guided by Rabs 11, 27a, 27b and 35 as well as the scaffolding protein KIBRA. A SNARE complex mediates MVB-plasma membrane fusion and ILVs are then secreted into the extracellular space as exosomes. **F.** Degradative MVBs destined for fusion with the lysosome are Rab7+ and are trafficked to the lysosome with the help of the cargo adaptor, Muskelin. **G.** Molecular structures of sphingomyelin, ceramide and LBPA.

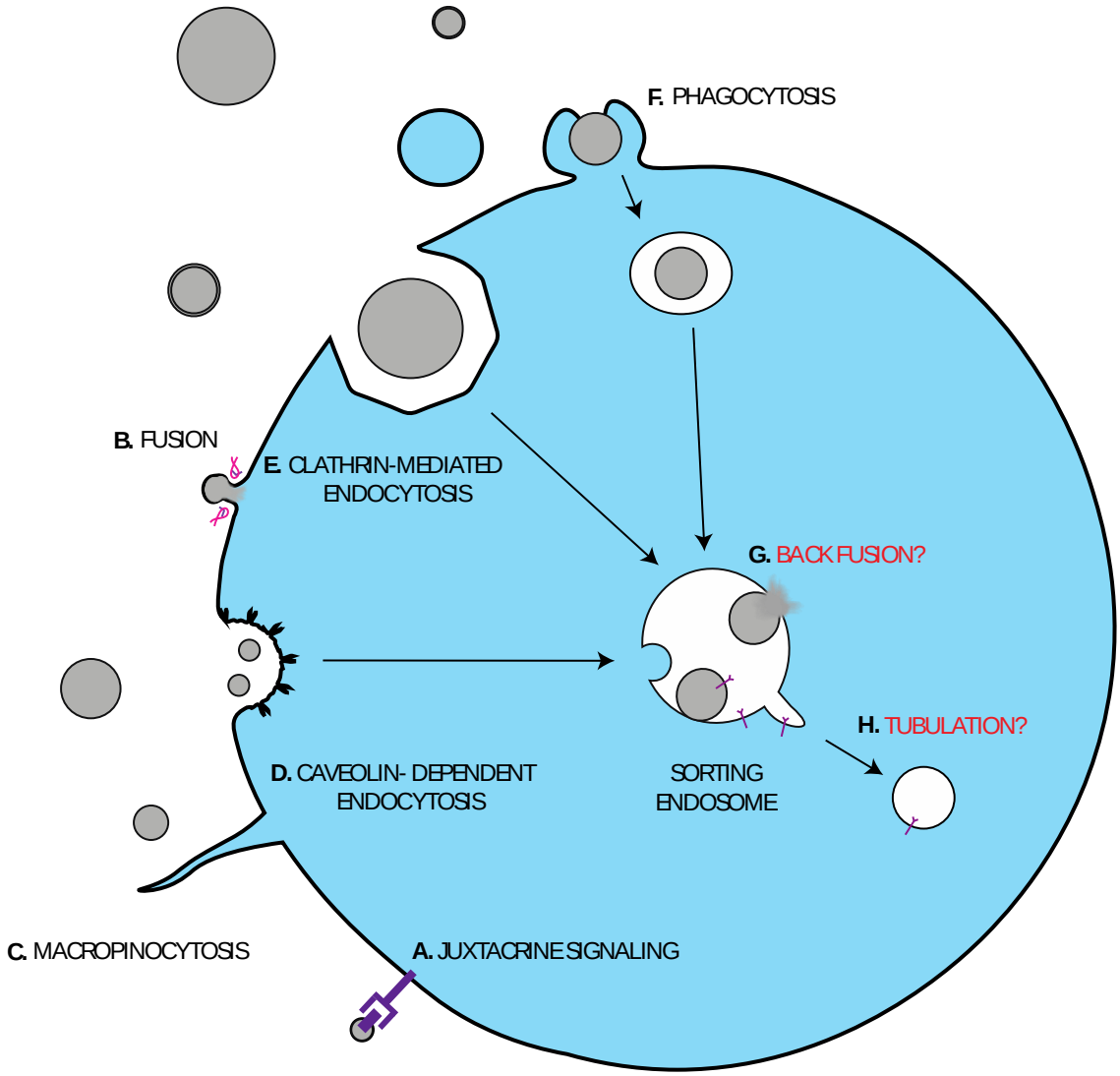

Figure 2. Mechanisms of EV Uptake. EVs can be internalized through a variety of pathways some of which are illustrated here. **A. Juxtacrine signaling.** EVs can potentially signal without being internalized by binding to a receptor and transducing a signal. **B. Fusion with plasma membrane.** EVs can potentially directly fuse with the plasma membrane to deliver their contents into the cytoplasm of the recipient. **C-F. Internalization of EV.** EVs can enter recipients by several pathways, including macropinocytosis (C), caveolin-mediated endocytosis (D), clathrin-mediated

endocytosis (E), and phagocytosis (F). Once EVs are internalized how the cargo is accessed by the cytosol is an open area of research. Some potential mechanisms include back fusion to retrieve cytosolic cargo (**G**), or back-fusion followed by tubulation to retrieve transmembrane receptor cargo (**H**).

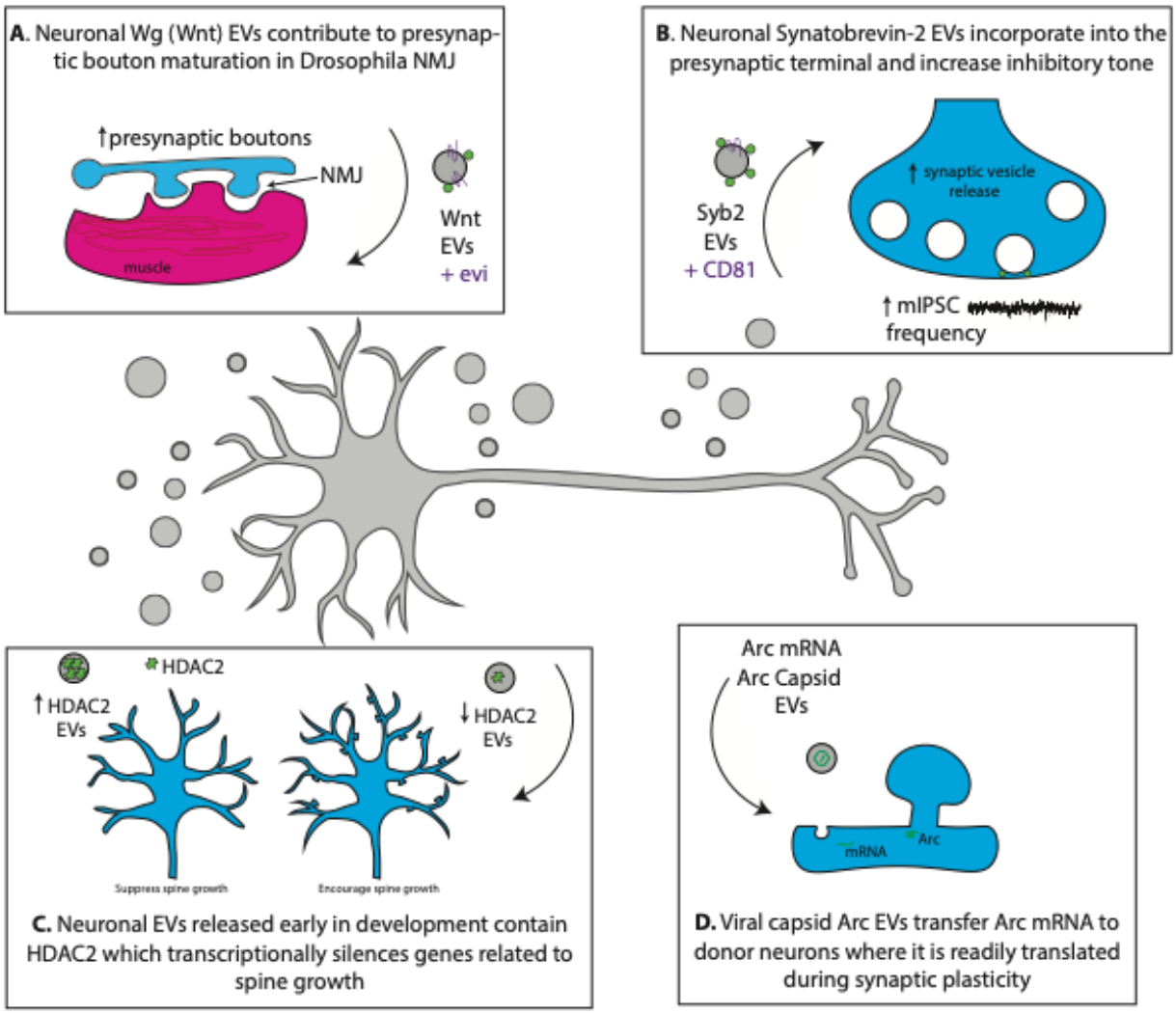

Figure 3. Neuron-derived EVs signal to other neurons and impact synaptic function. **A.** EVs containing the morphogen Wg (Wnt) are secreted by the presynaptic terminal and can influence the maturation of presynaptic boutons. **B.** Synaptobevin can

be transferred to the presynaptic terminal of hippocampal neurons where it is readily incorporated into the recycling pool of synaptic vesicles. Increases in synaptobrevin increase spontaneous inhibitory neurotransmission. **C.** Young neurons (3 DIV) secrete EVs containing HDAC2 which transcriptionally suppresses spine growth in recipient neurons. As neurons develop and mature, HDAC2 EV secretion decreases allowing for the maturation of spines along the dendrites. **D.** In response to synaptic plasticity, the immediate early gene, Arc, is rapidly assembled into a viral-like capsid that is secreted as an EV containing ARC mRNA. Recipient neurons then translate Arc mRNA into protein which acts as a key regulator of synaptic plasticity.

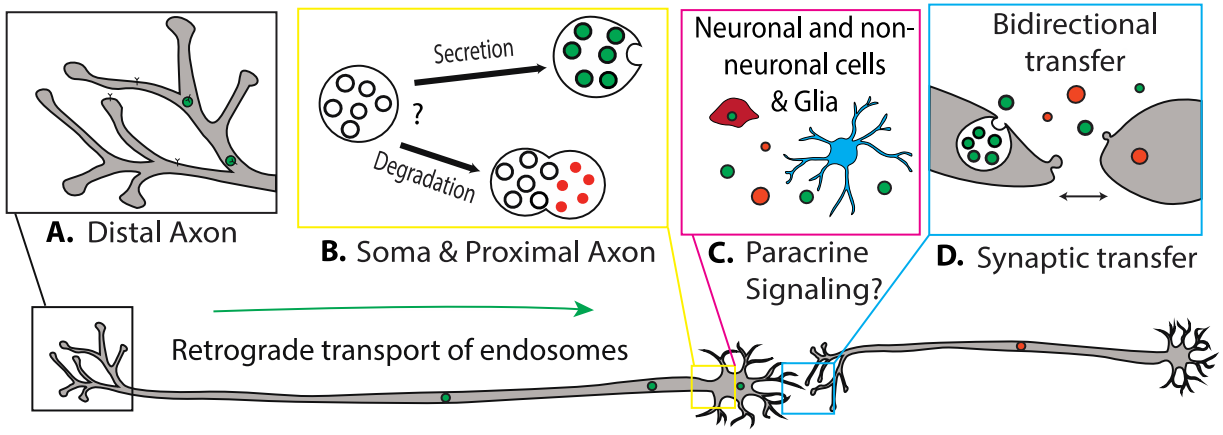

Figure 4. Long distance biosynthetic pathway for EV generation. A. Cargo originating in the distal axon can be internalized into endosomes to be retrogradely trafficked and secreted in EVs. **B.** In the cytoplasm of the recipient, internalized EVs, now endosomes, can be either trafficked throughout the cell, secreted, or degraded by the lysosome. **C.** EVs released at the somatodendritic compartment can signal to nearby cell types such as other neurons and glia. **D.** Bidirectional transfer of EVs across the synapse could coordinate transsynaptic communication and tune circuit function.

Chapter III. Sympathetic Neurons Secrete Retrogradely Transported TrkA on Extracellular Vesicles

This chapter is published as “Sympathetic neurons secrete retrogradely transported TrkA on extracellular vesicles.” Ashley J. Mason, Austin B. Keeler, Farah Kabir, Bettina Winckler and Christopher Deppmann. *Scientific Reports.* **13**, 3657 (2023). All experiments were carried out by Ashley J Mason with assistance from Austin Keeler and Farah Kabir.

Abstract

Proper wiring of the peripheral nervous system relies on neurotrophic signaling via nerve growth factor (NGF). NGF secreted by target organs (i.e., eye) binds to the TrkA receptor expressed on the distal axons of postganglionic neurons. Upon binding, TrkA is internalized into a signaling endosome and retrogradely trafficked back to the soma and into the dendrites to promote cell survival and postsynaptic maturation, respectively. Much progress has been made in recent years to define the fate of the retrogradely trafficked TrkA signaling endosome, yet it has not been fully characterized. Here we investigate extracellular vesicles as a novel route of neurotrophic signaling.

Using the mouse superior cervical ganglion (SCG) as a model, we isolate EVs derived from sympathetic cultures and characterize them using immunoblot assays, nanoparticle tracking analysis, and cryo-electron microscopy. Furthermore, using a compartmentalized culture system, we find that TrkA derived from endosomes originating in the distal axon can be detected on EVs secreted from the somatodendritic domain. In addition, inhibition of classic TrkA downstream pathways, specifically in somatodendritic compartments, greatly decreases TrkA packaging into EVs. Our results suggest a novel trafficking route for TrkA: it can travel long distances to the cell body, be packaged into EVs, and be secreted. Secretion of TrkA via EVs appears to be regulated by its own downstream effector cascades, raising intriguing future questions about novel functionalities associated with $TrkA^{+}$ EVs.

Introduction

The development of the sympathetic peripheral nervous system relies on neurotrophic signaling stemming from the interactions between nerve growth factor (NGF) and its cognate receptor, TrkA. NGF secreted from sympathetic target organs like the salivary gland or eye, binds TrkA present on distal tips of axons and is subsequently internalized into a signaling endosome (SE). This SE is then retrogradely trafficked back to the somatodendritic compartment to promote survival, synapse formation, and several other trophic functions[22,28,30]. Much effort by our group and several others has gone into determining the fate of the retrogradely transported $TrkA^+$ SE. We have shown previously that the activated retrogradely trafficked $TrkA^+$ SE can induce association with the cytoskeletal protein, Coronin-1a, which slows degradation of TrkA by evading fusion with the lysosome[51]. The $TrkA^+$ SE instead undergoes Coronin-1a dependent recycling to the plasma membrane and subsequent re-internalization[51] of TrkA, a pathway we have termed “retrograde transcytosis”. Interestingly, it has been shown that the $TrkA^+$ SE arrives in the soma as a multivesicular body (MVB)[38].

Morphologically, MVBs are defined by the presence of intraluminal vesicles (ILVs) that are formed through budding-in events from the endosomal limiting membrane. Functionally, MVBs are mature, late endosomal compartments largely destined for degradation. However, it has become increasingly clear that an alternative fate is for MVBs to fuse with the plasma membrane causing the release of their ILVs as extracellular vesicles (EVs). Although the study of EVs has greatly expanded over the past decade, very little is known about EVs secreted by peripheral neurons and what cargos they contain[6]. EVs, derived from either the plasma membrane or the endosomal system, have been implicated in a variety of functions ranging from cargo transport to

intercellular signaling[79,169–171]. Given our previous findings that retrograde TrkA$^+$ SEs can fuse with the somatodendritic plasma membrane,[51,172] taken together with the observations that TrkA$^+$ SEs can exist as MVBs, we reason that sympathetic neurons may be able to release EVs containing retrograde cargos like TrkA.

In this work, we investigate EVs as a potential trafficking pathway for TrkA by conducting a comprehensive analysis of their secretion from sympathetic neurons. First, we rigorously show that EVs can indeed be secreted from peripheral cells in accordance with the guidelines set forth by the International Society for Extracellular Vesicles (ISEV) in their position paper "Minimal Information for Studies of Extracellular Vesicles" (MISEV)[77]. Next, using microfluidic devices (MFDs) and the neurocircuit tracer, WGA, we show that cargo originating in the distal axon can undergo retrograde transport to the soma where it is packaged and released in EVs, thus establishing EV biogenesis as a possible fate of distal axon derived, long-distance signaling endosomes in peripheral neurons. Finally, we show that TrkA, internalized in distal axons, is secreted on EVs in the somatodendritic compartment. Importantly, this secretion is regulated by TrkA-dependent signaling pathways. This work suggests a potential new mode of trophic signaling that may have an impact in the development, maintenance, and pathogenesis of the nervous system.

Results

Sympathetic neurons release extracellular vesicles

We first wanted to determine if EVs are secreted by mouse sympathetic cell cultures. To investigate this, mixed sympathetic cultures containing neurons, satellite

glia, and fibroblasts were established for 7 days *in vitro* (DIV) and EVs were isolated from the conditioned media (CM) using differential centrifugation (Fig. 1A)[173]. We collected two EV fractions: the pellet from the 20,000 x g spin (P20) and the pellet from the 100,000 x g spin (P100) (Fig. 1A). We initially chose to analyze both the P20 and P100 fractions. It is noteworthy that while these fractions sediment vesicles and nanoparticles based on density, they still exhibit significant heterogeneity in terms of EV size and biogenic origin. Both the P20 and P100 fractions were resuspended in PBS for subsequent nanoparticle tracking analysis (NTA) (Fig. 1A, B). Quantification of NTA-tracked particles showed a greater concentration of particles in the P20 fraction compared to the P100 fraction (Fig. 1C). Size distribution histograms from NTA show a mean diameter of 134 nm and 136 nm for the P20 and P100 fractions, respectively (Fig. 1 E, F). To support the notion that these fractions are enriched for EVs, we blotted against canonical EV markers: CD63, CD81, and Alix (Fig. 1D, Supplementary Fig. S1). All three EV-associated markers were detected in the cell pellet, P20 and P100 fractions of three independent mouse litters (litter L1-L3; Fig. 1D). Importantly, cytochrome C, a mitochondrial marker, and calreticulin, an ER resident protein, were not detected in the P20 and P100 fractions, indicating undetectable contamination by intracellular organelles (Fig. 1D, Supplementary Fig. S1). Lastly, neither CD63, CD81, Alix, calreticulin, nor cytochrome C was detected in a “media only” condition (lane: ∅) where no cells were plated (Fig. 1D, Supplementary Fig. S1). We also used NTA to determine the concentration of particles in this “media-only” condition where no cells were plated. We observed $5.23 \times 10^7 \pm 5.21 \times 10^6$ particles/mL for the P20 fraction and $5.38 \times 10^7 \pm 5.07 \times 10^6$ particles/mL for the P100 fraction representing 1.94% and 9.36% of the

particles observed in Figure 1C, respectively (Supplementary Fig. S2). Lastly, we conducted a series of solution controls and found that the concentration of particles derived from these sources is minimal (ranging from 1.16×10^6 to 5.50×10^6 particles/mL) (Supplementary Fig. S2). Additionally, we determined the optimal cell density and growth duration necessary to robustly produce and detect EVs in our cultures. We found that we could reliably detect EV markers by immunoblot (Supplementary Fig. S2) and greater than $3x10^9$ particles/mL by NTA at starting cell densities above 80,000 cells that were grown for 7 DIV (Supplementary Fig. S2). Therefore, we used greater than 80,000 cells for all experiments.

NTA and immunoblot are good indicators for the presence of EVs in both the P20 and P100 fractions derived from sympathetic cultures, but we wanted to also visualize these isolated EVs by microscopy. Thus, we assessed the size and morphology of sympathetic culture-derived EVs using cryo-transmission electron microscopy (Cryo-EM). We collected high-magnification micrographs of the P20 and P100 fractions and observed many particles delimited by a membrane bilayer, consistent with them being EVs (Fig. 2A). The full-size distribution histogram of both the P20 (black bars) and P100 (gray bars) fractions are shown separately and together (Fig. 2B). For the P20 and P100 fractions the mean EV diameter was 146 nm and 153 nm, and the median EV diameter was 115 nm and 95 nm, respectively. We did not observe any vesicles in micrographs from either the P20 or P100 fractions of “media only” controls where no cells were plated. However, in low magnification micrographs of both the P20 and P100 fractions, we found that the P20 fractions contained large electron-dense aggregates that were difficult to measure as discrete vesicles and were therefore not included in the

size distribution histograms (shown in Fig. 2B) (Supplementary Fig. S3). Since the P20 fraction contained these large aggregates, we restricted our analysis to P100 fractions going forward. Lastly, to better contextualize our EVs within the literature, we performed a meta-analysis of the sizes of ILVs and EVs from PC12 cells and sympathetic neurons from published micrographs[5,14]. The sizes of these published EVs and ILVs range from 30-110 nm (Supplementary Fig. S4). Furthermore, we conducted a detailed characterization of all particles in our fractions, including those with a single membrane, as well as EVs encapsulated within other EVs (Supplementary Fig. S4).

Sympathetic EVs contain cargo derived from the distal axon

Given that a subset of EVs are derived from an endosomal origin and peripheral neurons can contain axons that extend many microns out from the cell body. We wondered whether cargos that originate in these distal axons can be trafficked back to the cell body and secreted as EVs. To do this, we cultured SCG neurons in microfluidic devices (MFDs) which allowed us to separate the cell bodies (CB) of neurons from their distal axons (DA) by a series of microgrooves (Fig. 3A). Next, under fluidic isolation, we added an AlexaFluor 488 conjugated wheat germ agglutinin (WGA-AF488), a well-known neuronal tracer, to the DA chamber to label SCG neurons at their distal axons (Fig. 3A). We collected and pooled CM from the CB chamber of six MFDs and isolated EVs by differential centrifugation 15 hours after adding WGA-AF488 (Fig. 3A). The ZetaView NTA instrument is equipped with a filter allowing measurement of fluorescently labeled particles. We employed this to measure the total number of particles secreted (scatter) from the sympathetic cultures and the number of WGA-

AF488^{+} particles secreted from SCG neurons (fluorescent) (Fig. 3 B, C). By scatter, 4.05 x 10^{9} ± 9.71 x 10^{8} particles/mL were detected with 2.01 x 10^{8} ± 1.99 x 10^{7} WGA-AF488^{+} particles/mL (Fig. 3C). Importantly, both scatter and fluorescent particle counts from a media-only condition where no cells were plated in MFDs were minimal, indicating that WGA-AF488 does not diffuse against the microfluidic isolation from the DA to the CB chamber in the absence of cells (Supplementary Fig. S5). Based on these findings we conclude that cargo originating in the distal axon can retrogradely traffic in the axon and be released as EVs from the somatodendritic domain.

Sympathetic EVs contain active retrogradely trafficked TrkA receptors

Once we determined that axonally derived cargos could be secreted in EVs, we wanted to determine if TrkA, a well-established retrogradely trafficked endosomal cargo, could be recovered in EVs from sympathetic neurons. Using immunoblotting of P20 and P100 EVs derived from SCG cells grown in mass culture (three separate litters L1-L3), we detect TrkA (Fig. 4A) on purified EVs in the P100 fraction. Next, we wanted to determine if the TrkA that was secreted on EVs was phosphorylated and therefore activated. We repeated the experiment with three additional litters and observed that pTrkA was detectable in the P100 EV fraction, indicating that some activated TrkA is secreted on EVs (Fig. 4B).

In order to determine whether axonally derived TrkA could be packaged into EVs upon retrograde arrival to the soma, we employed the MFD setup as described in Figure 3A. We made use of a mouse line containing a FLAG tag that was knocked in frame with the extracellular domain of the TrkA locus (*TrkA*$^{FLAG/FLAG}$ transgenic mice)

(Fig. 4C)[174]. This allows selective labeling of pre-endocytic TrkA receptors on the distal axon plasma membrane by adding an anti-FLAG antibody conjugated to AlexaFluor 488 (anti-FLAG-AF488) just to the DA chamber of the MFD as previously reported (Fig. 4C)[52]. Fifteen hours after anti-FLAG-AF488 antibody addition to the DA, we collected and pooled the CM from the CB chamber of six MFDs to isolate EVs (Fig. 4C). Using scatter and fluorescent NTA, we detected $5.09 \times 10^9 \pm 8.56 \times 10^8$ total particles/mL and $3.03 \times 10^8 \pm 2.91 \times 10^7$ fluorescent particles/mL after the addition of anti-FLAG-AF488 antibody (Fig. 4D-F). To ensure that these fluorescent particles were indeed anti-FLAG antibodies bound to TrkA and not due to non-specific uptake of anti-FLAG antibody, we added an irrelevant anti-epitope antibody, anti-V5-AF488, to *TrkA*$^{FLAG/FLAG}$ cells (Fig. 4E,F). As expected, the anti-V5-AF488 antibody did not significantly change the total number of particles secreted ($4.32 \times 10^9 \pm 3.71 \times 10^8$ particles/mL, Fig. 4E) nor did it result in significant fluorescent particle detection (3.24×10^7, $\pm 9.16 \times 10^6$ particles/mL, Fig. 4F) indicating that the anti-V5-AF488 antibody was not non-specifically endocytosed at significant levels. Next, we added an anti-FLAG-AF488 antibody to wild-type sympathetic cultures which do not express the *TrkA*$^{FLAG/FLAG}$ gene. We did not detect significant fluorescent particles thus confirming that the anti-FLAG-AF488 needed to bind the FLAG epitope on the FLAG-tagged TrkA receptor to be internalized and secreted as EVs (Supplementary Fig. S5).

Inhibition of phosphoinositide 3-kinase and phospholipase-C-γ reduces the number of TrkA EVs

The ligand-bound activated TrkA receptor transduces its signal via several canonical downstream pathways such as phosphatidylinositol-3-kinase (PI3K) and phospholipase-C-ɣ (PLC-ɣ) (Fig. 5A). Interestingly, these downstream pathways often determine the maturation and trafficking of the $TrkA^+$ SE[17,18]. We tested whether these pathways are important for $TrkA^+$ EV release. Using *TrkA*$^{FLAG/FLAG}$ SCG neurons cultured in MFDs, we simultaneously added anti-FLAG-AF488 to the DA chamber and different inhibitors to the CB chamber for 15 hours and then prepared EVs by differential centrifugation from CM collected and pooled from the CB chamber of six MFDs (Fig. 5B). Inhibition of PI3K using the chemical inhibitor, LY294002, did not change the total number of particles secreted (Fig. 5C), but did cause a significant decrease in the number of fluorescent TrkA particles detected in the P100 fraction (Fig. 5D) compared to a DMSO control. Interestingly, inhibition of PLC-ɣ using U73122 caused a significant increase in the total number of particles detected (Fig. 5E). Despite this increase in total particles detected in U73122-treated cells, there was a significant decrease in the number of fluorescent TrkA particles detected compared to control (Fig. 5F). In order to determine if the changes in EV secretion might be due to the inhibitor treatments causing increased cell death and/or morphological and functional alterations, we characterized several indicators of poor health and morphology in DMSO-treated and inhibitor-treated cultures. Etoposide was used to induce cell death as a positive control for our chosen readouts (Supplementary Fig. S6). Importantly, size analysis of the cell bodies of SCG neurons after the different inhibitor treatments did not show any significant differences compared to a DMSO control nor was there any cell loss or evidence of pyknotic nuclei that might account for the differences in EV secretion

(Supplementary Figs. S6, S7). In addition, the total cell number did not change between the inhibitor-treated cultures and the DMSO-treated cultures, and neither did the cell counts of SCG neurons, satellite glia cells, and other cells (Supplementary Figs. S6, S7). Lastly, the same number of MAP2+ neurons had internalized and transported anti-FLAG-AF488 antibody from the DA to the CB chamber, indicating that neuron health was not affected by the inhibitor treatment (Supplementary Fig. S7).

Discussion

Retrograde trafficking of TrkA is essential for sympathetic neuron survival[175,176]. The TrkA^{+} SE has recently been shown to arrive in the cell body from the distal axon as a multivesicular body; the precursor organelle for exosome formation[38]. Furthermore, these TrkA^{+} MVBs were shown to contain activated TrkA receptors that remain in complex with PLC-ɣ[38]. Previously, we have shown that the retrogradely trafficked TrkA^{+} SE can undergo recycling to the plasma membrane[51]. In sympathetic neurons, another neurotrophin receptor, p75NTR, has been shown to be routed away from the lysosome and secreted in EVs[164]. Based on these data, we speculated that activated TrkA receptors could be packaged and secreted in EVs. Indeed, using compartmentalized cultures and *TrkA$^{FLAG/FLAG}$* transgenic mice, we show that TrkA originating in the distal axon is retrogradely trafficked to the cell body in SEs and then subsequently secreted in EVs. We thoroughly characterize these sympathetic EVs using nanoparticle tracking analysis, immunoblot assays, and cryo-EM in accordance with MISEV guidelines. Lastly, we demonstrate that activation of different downstream pathways of TrkA affects its secretion in EVs.

Rigorous application of MISEV guidelines demonstrates that EVs are secreted from sympathetic cultures.

We find through immunoblot, NTA, and cryo-EM analysis that both the P20 and P100 fractions contain a diverse and heterogeneous set of EVs with a range of sizes and densities. We use several controls in all experiments to ensure that we could robustly detect EVs above baseline. In addition to solution controls, we experimented with both cell density and duration in culture. Increasing the density of seeded cells increases EV concentration; however not entirely linearly. We speculate that this is because we do not use any inhibitor of cell division in these sympathetic cultures. As such, these mouse SCG cultures contain a mixture of different cell types such as satellite glia, other glia cells, as well as some fibroblasts and endothelial cells, all of which can secrete EVs. After 7 DIV, the number of mitotic (non-neuronal) cells has increased, likely accounting for the increase in the concentration of EVs at higher cell densities. At 2 DIV the cultures have yet to stabilize and the conditioned media from these samples contains cell fragments and debris from the trituration and cell plating process. These experiments highlight the importance of consistency in all parameters related to EV collection (DIV, density, duration of media conditioning) to accurately compare EV secretion across different conditions or genotypes. These parameters have been thoroughly described within the MISEV guidelines[77].

Sympathetic cultures secrete a diverse set of EVs with many sizes.

Size analysis of sympathetic EVs by NTA and cryo-EM shows that the majority of EVs fall below 300 nm in diameter. We use two methods of sizing to measure these sympathetic EVs as both methods have their limitations. The ZetaView NTA measures the hydrodynamic radius of nanoparticles with a resolution limit of around 70-90 nm. Therefore NTA sizing analysis excludes smaller vesicles[177,178,]. In contrast, cryo-EM detects smaller EVs, but due to aggregation and concentration issues, larger EVs are excluded from the analysis. Our cryo-EM sizing shows two distinct peaks for both the P20 and P100 fraction, a sharper taller peak centered around 45 nm and a broader, wider peak around 180 nm (Fig. 2B). We measured the size of published sympathetic EVs and found that EVs derived from NGF-differentiated PC12 cells and primary sympathetic cultures were below 100 nm in diameter[164]. Although we were able to measure EVs from other sympathetic neurons, they are not directly comparable to our results because we used Cryo-EM while the published literature used transmission electron microscopy (TEM)[38,164,179]. Lastly, we note that we see small non-lipid bilayer encapsulated EVs by cryo-EM. The EV field is increasingly reporting these small EVs that lack a bilayer as exomeres or extracellular particles that co-isolate with EVs[180–182]. We also see EVs enveloped inside other EVs. There is speculation as to whether these EVs are naturally encapsulated inside each other or whether this is an artifact of ultracentrifugation resulting in membranes fusing into other membranes[179,183]. However, this does not appear to be EVs imaged on a different z-plane from each other since their membranes curve or deform around other EVs (Supplementary Fig. S4).

Cargos transported retrogradely from the axon can be secreted in EVs from the somatodendritic domain

The origin and packaging of EV cargos in neurons is still relatively unknown[170]. Endosomes are one of the intracellular compartments for trafficking EV cargos within the cell prior to secretion. Due to their high motility, endosomes can traffic cargo both locally and across long distances within neurons[184]. We used a fluorescently labeled lectin, wheat germ agglutinin (WGA), to visualize its trafficking through the cell from the distal axon to the cell body[185]. We show that WGA that originated in the distal axon can be packaged into EVs released at the cell body. WGA is primarily used as a neuronal circuit tracer to trace interconnected neurons;[186] however, the mechanism by which WGA traverses synapses is still debated[187]. We speculate that these neuronal-derived EVs might serve as one mechanism by which WGA can “hop” the synapse from one neuron to another. Our sympathetic neuronal cultures contain a mixture of all superior cervical ganglion cell types including satellite glia cells which can also secrete EVs. We show that a small proportion of all EVs secreted from our sympathetic cultures contain WGA and therefore are of neuronal origin. Since we only added WGA to the DA of MFDs it is only being internalized by axons of neurons that grew through the microgrooves to reach the DA chamber. We note that we cannot determine what proportion of neuronally secreted EVs contain WGA since the CB chamber from which conditioned media is collected contains many neurons whose axons did not traverse the microgrooves and were thus not able to pick up WGA. Future experimentation will be needed to more precisely determine the proportion of somatodendritically secreted EVs that contain retrograde cargo transported from the axon.

A novel EV cargo, TrkA, is derived from axonal retrograde endosomes and remains phosphorylated in the secreted EV.

We identified TrkA as a neuronally secreted EV cargo in sympathetic cultures by Western blots. Remarkably, TrkA only partitions into the P100 fraction. While a potential function for $TrkA^+$ EVs is not currently known, a proportion of these TrkA-containing EVs remains catalytically active as evidenced through phosphorylated TrkA immunoblots and might thus be capable of signaling in recipient cells. We also showed that TrkA which was internalized in the distal axon was able to be included in EVs secreted from the somatodendritic domain. Since only sympathetic neurons express TrkA and extend axons to the distal axon chamber, the $TrkA^+$ EVs are definitely secreted by the sympathetic neurons themselves. The other cell types found in our cultures do not express the TrkA receptor nor do they span the microgrooves of MFDs and do not contribute to $TrkA^+$ EV counts in our experiments. We thus discovered a new trafficking route for retrogradely derived TrkA, i.e., secretion in EVs.

TrkA-positive EV secretion is regulated by signaling cascades in the somatodendritic domain.

The binding of NGF to TrkA triggers autophosphorylation of tyrosine residues located on its intracellular domain thereby initiating a kinase cascade on the downstream effector signaling pathways: Ras/MAPK, PI3K and PLC-γ[11,176,188–190]. Activation of different downstream pathways of TrkA has been shown to affect the trafficking and functional output of the $TrkA^+$ SE. For example, blocking PI3K in the

distal axon prevents the initiation of retrograde transport of the TrkA$^+$ SE[191]. Additionally, recruitment of PLC-ɣ to the TrkA receptor promotes internalization of the ligand-receptor complex in the distal axon[25]. Based on these data, we wanted to test whether TrkA signaling affects the production of TrkA$^+$ EVs. Our findings suggest that inhibition of PI3K signaling in the cell body of sympathetic neurons influences the production of TrkA$^+$ EVs without affecting total EV secretion. Additionally, inhibition of PLC-ɣ signaling in the cell body of sympathetic neurons reduces TrkA$^+$ EVs, but also causes a striking increase in the total number of EVs released. The mechanisms underlying these inhibitors' effects on EV secretion remain unknown and it is important to consider that PI3K and PLC-ɣ are downstream of several different receptors in addition to TrkA. Lastly, broadly inhibiting these pathways might alter the trafficking and release of EVs independent of the cargo as shown by the increase in the number of particles released when PLC-ɣ is inhibited (Fig. 5E).

In summary, we have rigorously characterized EVs derived from primary sympathetic cultures through protein analysis, cryo-transmission electron microscopy, and nanoparticle tracking analysis. We have shown that EVs released from sympathetic cultures are heterogenous in size and morphology. Our findings thus expand the sparse literature on sympathetic EVs. Finally, we demonstrate the successful isolation of labeled EVs from specific neuronal domains. Specifically, we demonstrate that TrkA internalized at the distal axon can be secreted in EVs from the somatodendritic domain. Future studies investigating the mechanisms underlying TrkA partitioning into secretion-competent organelles will help elucidate the effects different inhibitors have on TrkA$^+$ EV

numbers. Our results thus demonstrate a novel trafficking route for TrkA: it can travel long distances to the cell body, be packaged into EVs, and be secreted. Secretion of TrkA via EVs appears to be regulated by its own downstream effector cascades, raising intriguing future questions about novel functionalities associated with $TrkA^+$ EVs. Functional and recipient studies in the future will discover the purpose of secreting EVs containing phosphorylated activated $TrkA^+$ and the functional output of $TrkA^+$ EVs in their intended recipient cells.

Materials and Methods

REAGENT or RESOURCE	**SOURCE**	**IDENTIFIER**
Antibodies		
Rabbit Anti- Cytochrome C	Abcam	**Cat # ab133504; RRID:AB_2802115**
Rabbit Anti- CD63	Abcam	**Cat # ab217345; RRID:AB_2754982**
Alexa Fluor 680 AffiniPure Donkey anti-Rabbit IgG	Jackson ImmunoResearch	Cat # 711-625-152 RRID: AB_2340627
Rabbit Anti- Calreticulin	Cell Signaling Technology	Cat # 12238S RRID: AB_2688013
Sheep Anti- Tyrosine Hydroxylase	Millipore	Cat # AB1542 RRID: AB_90755
Alexa Fluor 790 AffiniPure Donkey anti-Rabbit IgG	Jackson ImmunoResearch	Cat # 711-655-152 RRID: AB_2340628
Rabbit Anti- CD81	Cell Signaling Technology	Cat # 10037S RRID:AB_2714207
Rabbit Anti – Alix	Cell Signaling Technology	Cat # 92880 RRID:AB_2800192
Rabbit Anti-BLBP	Abcam	Cat # ab279649; RRID:AB
Chicken Anti-MAP2	EnCor Biotechnology	Cat # CPCA-MAP2 RRID: AB_2138173
Anti- FLAG DYKDDDDK tag (D6W5B) Rabbit mAb Alexa R 488	Cell Signaling Technology	Cat # 15008S Lot 2 and 3 RRID: N/A
Biological samples		
NGF	In house, purified from mouse salivary glands	

Chemicals, peptides, and recombinant proteins		
Poly-D-Lysine	Sigma	Cat # P7886
Prime XV IS-21	Sigma	Cat # 91142
Hyaluronidase	Sigma	Cat # H3884
Collagenase	Worthington	Cat # LS004196
Laminin	Invitrogen	Cat # 23017-01
BSA	Sigma	Cat # A9647
Polyacrylamide gels 4-12%	Genscript	Cat # M00654
Trypsin	Sigma	Cat # T4799
WGA-AF488	Fisher Scientific	Cat # W11261
PBS	Gibco	Cat # 14190-144
Milk	Lab Scientific	Cat # M0841
Beta mercaptoethanol	BioRad	Cat # 161-0716
DMEM no phenol	Gibco	Cat # 31053-028
GlutaMAX	Gibco	Cat # 35050-061
FBS	R & D Systems	Cat # S11195H
LY294002	Sigma	Cat # L9908
U-73122	Sigma	Cat # U6756
DAPI	ThermoFisher	Cat # D3571
Experimental models: Organisms/strains		
C57 Bl/6J mice	Jackson Laboratory	
$TrkA^{FLAG/FLAG}$	Gift from D. Ginty	Harvard
Hardware, Software and algorithms		
Odyssey CLx	LI-COR	
Optima TLX Ultracentrifuge	Beckman-Coulter	
Trans-Blot Turbo Transfer	Bio Rad	
Image J		https://imagej.nih.gov/ij/
Tecnai F20 Twin Electron Microscope	FEI	
Prism 9	Graphpad	graphpad.com
ZetaView PMX-120	Particle-Metrix	particle-metrix.com
Illustrator	Adobe	adobe.com
Other		
Microcentrifuge tubes	USAscientific	Cat # 1415-2500
Tissue culture plates	Fisher Scientific	Cat # 150628
Polycarbonate centrifuge tubes	Beckman	Cat # 343778
Sylgard 184 Silicone elastomer kit	Krayden	Cat # DC2065622

Animals

All animal use complied with the Association for Assessment and Accreditation of Laboratory Animals Care policies and was approved by the University of Virginia Animal

Care and Use Committee protocol #3422 (Winckler lab) and protocol #3795 (Deppmann lab). All mice were maintained on a C57Bl/6J background. Males and females were mixed in all experiments. Mouse lines used: C57BL/6J and TrkA$^{FLAG/FLAG}$ [174]. All methods were performed in accordance with ARRIVE (Animal Research: Reporting of In Vivo Experiments) guidelines (https://arriveguidelines.org) and regulations.

ARRIVE guidelines: All cells used in this study were derived from postnatal day 3 mice (*Mus Musculus*). Cells from both male and female mice were pooled. All mice were maintained on a C57Bl/6J background. Specific strains used are mentioned in the appropriate results and figure legends. Each experiment was repeated at least three times on three independent litters of mice (6-10 pups per litter) and appropriate controls were included. The total number of animals used in this study was 148 mouse neonates. Dissected tissue from mouse neonates was pooled before trituration and plating of cells, therefore all cells were randomized between control and treatment groups. No animals were excluded from analysis. Outcome measures, experimental procedures, and statistical methods are described below. Results with appropriate descriptive statistics are described in the figure legend for each experiment.

Primary sympathetic neuronal cultures

Postnatal day 3 (P3) mouse pups were euthanized by decapitation and the superior cervical ganglia were microdissected as previously described, and kept in ice-cold DMEM until enzymatic digestion[52]. Ganglia were transferred to an enzymatic solution containing 0.01 g/mL BSA, 0.4 mg/mL hyaluronidase, and 4 mg/mL collagenase for 20

mins at 37°C. This solution was aspirated off and replaced with a 2.5% trypsin solution for 15 mins at 37°C. Cells were then washed in DMEM containing 10% FBS 3x and then subjected to trituration using a P1000 pipette and then a P200 pipette. Cells were then spun down at 300 x g and resuspended in complete media. A small 10 µL aliquot of cells was counted on a hemocytometer. Cells were plated at a density of no less than 100,000 cells in a 12-well plate that had been precoated with poly-D-lysine and 1mg/mL laminin and washed 3x with sterile PBS. Cells were kept in an incubator at 37°C at 10% CO_2 and the media was changed every 48 hours. Because serum is known to contain EVs, cells were grown in serum-free complete media supplemented by Prime XV IS-21. Complete media contains the following: DMEM without phenol red, GlutaMAX, Prime XV IS-21, and 50 ng/mL NGF.

Compartmentalized WGA feeding assay

Sympathetic neurons were dissected as described above and dissociated neurons were plated in microfluidic devices as previously described[192,193]. Cells were plated at a density of 14,000 cells per MFD. To encourage axonal crossing of the microgrooves, neurons were exposed to 30 ng/mL NGF in the CB chamber and 80 ng/mL NGF in the DA chamber. At 6 DIV, 150 µL of complete media was added to the CB chamber and 100 µL of WGA-AF488 (1:200) in complete media was added to the DA chamber. Conditioned media was collected from the CB chamber 15 hours after the addition of WGA-AF488 and EVs were isolated.

Compartmentalized Anti-FLAG antibody feeding assay

Sympathetic neurons from *TrkA*$^{FLAG/FLAG}$ animals were dissected and plated at 14,000 cells per microfluidic device as previously described[192,193]. At 6 DIV, 150 µL of complete media was added to the CB chamber and 100 µL of anti-FLAG-AF488 antibody (1:200) in complete media was added to the DA chamber. Conditioned media was collected from the CB chamber 15 hours after the addition of the anti-FLAG-AF488 antibody and EVs were isolated. For inhibitor treatments, 100 µL of complete media containing inhibitors (LY294002 50 µM, U-73122 1 µM, or 0.1% v/v DMSO) was added to the CB chamber and 150 µL of anti-FLAG-AF488 antibody (1:200) in complete media was added the DA chamber. Conditioned media was collected from the CB chamber 15 hours after the addition of the anti-FLAG-AF488 and inhibitors and EVs were isolated.

EV Isolation and Characterization

Methods of EV isolation and characterization were performed in accordance with the guidelines set forth by the International Society for Extracellular Vesicles' position paper entitled "Minimal Information for the Study of Extracellular Vesicles"[77].

1) EV isolation and differential centrifugation

Conditioned media was collected from cells after 48 hours and placed into 1.5 mL microcentrifuge tubes on ice. In experiments using mass cultures, conditioned media from a single well in a 12-well plate was used. In experiments using MFDs, conditioned media collected from the CB chamber of six MFDs were combined. The conditioned media was then centrifuged at 300 x g for 10 mins at 4°C to pellet the cells. The supernatant was transferred to a clean 1.5 mL microcentrifuge tube and centrifuged at

2,000 x g for 10 mins at 4°C to pellet dead cells. The supernatant was transferred to a clean 1.5 mL microcentrifuge tube and spun at 20,000 x g for 30 mins. The pellet from this step is the P20 fraction. The supernatant was transferred to polycarbonate tubes subjected to ultracentrifugation at 100,000 x g_{max} (rotor: TLA 120.2; k -factor: 42; 53,000 rpm) for 70 mins at 4°C. The pellet from this step is the P100 fraction.

2) Nanoparticle Tracking Analysis

NTA was conducted using the ZetaView PMX 120 equipped with a 488 nm laser and a long wave pass filter (cutoff 500 nm) and CMOS camera. Samples were diluted to 1 mL in PBS prior to analysis. Each sample was measured at 11 different positions over 3 cycles ensuring a minimum number of 1000 traces were recorded. Two technical replicates were performed for each sample. Samples were recorded at 25°C, pH 7.0 with a shutter speed and camera sensitivity of 75 at 30 frames per second. Automatically generated reports of particle counts were checked, and any outliers were removed to calculate the final concentration.

3) Western Blot

All samples were lysed directly in 1.2X Laemmli sample buffer containing 5% BME and boiled for 5 mins. Laemmli sample buffer recipe: 4% SDS (10% (w/v), 20% glycerol, 120 mM 1M Tris-Cl (pH 6.8), and 0.02% (w/v) bromophenol blue in water. Sympathetic cultures were washed with PBS and lysed directly on the plate with 200 µL of 1.2X Laemmli sample buffer. P20 and P100 fractions were lysed directly in micro/ultracentrifuge tubes with 30 µL of 1.2X Laemmli. The sample buffer was pipetted

up and down 50 times along the walls of the tubes to collect the entire pellet. Samples were run on 4-12 % polyacrylamide gels with 7 µL of cell pellet fractions and 15 µL of P20 and P100 fractions loaded per well. Protein gels were transferred to nitrocellulose membranes using the Trans-blot turbo, blocked in 5% milk for 1 hour, and incubated in primary antibody (Alix 1:1000, CD63 1:1000, CD81 1:1000, Cytochrome C 1:5000, Calreticulin 1:4000) diluted in 5% milk 0.1% TBST overnight at 4°C on a rocker. Membranes were then washed 3 x with 0.1% TBST and secondary antibodies (1:20,000) diluted in 0.1% TBST were incubated for 1 hour at room temperature. Blots were imaged using the Odyssey CLx imager and exposure was determined automatically by the software.

4) Electron Cryo-Microscopy

Cryo-TEM was performed by the molecular electron microscopy core at UVA. P20 and P100 fractions were resuspended in 30 mL PBS. An aliquot of the sample (~3.5 µL) was applied to a glow-discharged, perforated carbon-coated grid (2/1-3C C-Flat; Protochips, Raleigh, NC), manually blotted with filter paper, and rapidly plunged into liquid ethane. The grids were stored in liquid nitrogen, then transferred to a Gatan 626 cryo-specimen holder (Gatan, Warrrendale, PA) and maintained at ~180°C. Low-dose images were collected on a Tecnai F20 Twin transmission electron microscope (FEI {now ThermoFisher Scientific}, Hillsboro, OR) operating at 120 kV. The digital micrographs were recorded on a TVIPS XF416 camera (Teitz, Germany).

Immunocytochemistry

Cells were fixed in 4% PFA for 20 minutes at room temperature in the MFDs. Cells were washed 3 times with 1X PBS and then blocked and permeabilized in 5% normal donkey serum and 0.2% TritonX-100 for 20 minutes. Primary antibodies were diluted in 1% BSA and applied overnight at 4 °C. Secondary antibodies were diluted in 1% BSA and added for 30 mins at room temperature. MFDs were washed 3x with 1x PBS and imaged on an inverted Zeiss 980 microscope with an Airyscan detector using a 40X oil objective (NA 1.3)

Statistics and Measurements.

Vesicles from micrographs were measured at their widest diameter using the segment tool in Image J. Cell counts were determined using the cell counter plugin in Image J. Cell type was determined using the following: all cells ($DAPI^+$), SCG neurons ($MAP2^+$; $FLAG^+$ double positive) and satellite glia ($BLBP^+$). Cells were classified as “other” if they were $DAPI^+$, but did not show staining against MAP2, FLAG, or BLBP. Soma and nuclei area was determined by drawing an ROI around the cell body of SCG neurons ($MAP2^+$;$FLAG^+$ double positive) or nucleus ($DAPI^+$) and measuring the area in Image J. Statistical analyses were performed using Prism 9 software. All values are shown as mean ± SEM. Differences between samples were determined using unpaired, two-tailed t-tests. Statistical significance is a p-value < 0.05. The p-values are denoted on top of each bracket pair.

Acknowledgements

Transmission electron micrographs were recorded at the University of Virginia Molecular Electron Microscopy Core facility (RRID:SCR_019031), which is supported in part by the School of Medicine and built with NIH grant G20-RR31199. We acknowledge the Keck Center for Cellular Imaging for the use of the Zeiss 880/980 multi-photon Airyscan microscopy system (PI- AP; NIH-OD025156). This work was supported by R21NS111991 awarded to CD and BW, 2T32GM007055-44 and F31NS126020 awarded to A.M and F32NS103770-02 awarded to A.K.

Additional Information

Competing interests

The authors declare no competing interests.

Data Availability Statement

Datasets generated and analyzed in this current study are available from the corresponding authors upon reasonable request.

Author Contributions

Study design and concept: A.M. A.K, B.W, and C.D. Data collection: A.M, A.K. F.K. Data Analysis: A.M., A.K., F.K. Data Interpretation: A.M., A.K, B.W., C.D. Manuscript and writing: A.M., B.W., C,D. Manuscript editing: A.M., A.K., F.K., B.W., C.D.

Figures

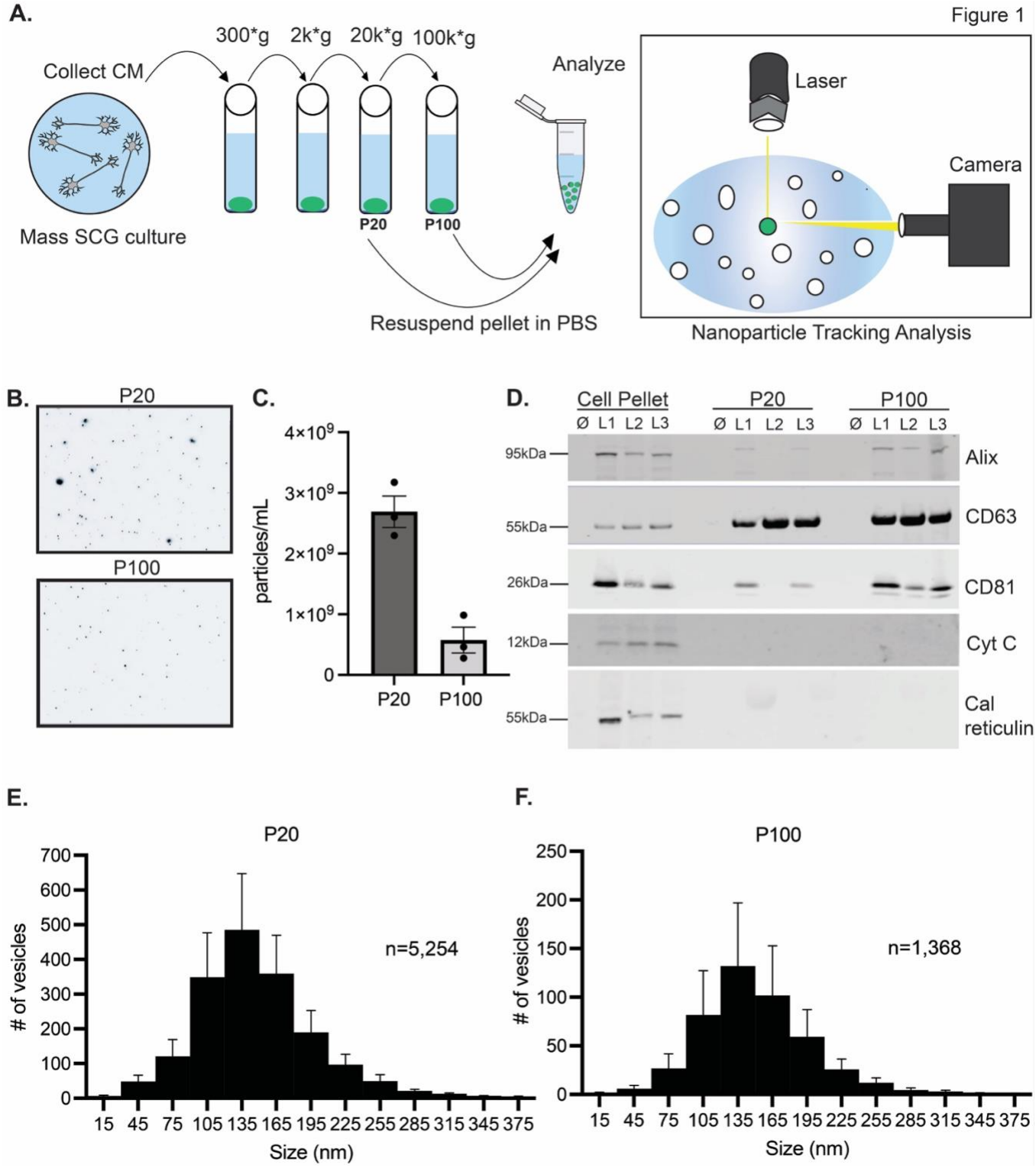
A.
Figure 1
Collect CM
300*g
2k*g
20k*g
100k*g
Analyze
Mass SCG culture
P20
P100
Resuspend pellet in PBS
Laser
Camera
Nanoparticle Tracking Analysis
B.
P20
P100
C.
4×10^9
3×10^9
2×10^9
1×10^9
0
particles/mL
P20
P100
D.
Cell Pellet
P20
P100
Ø L1 L2 L3
95kDa
55kDa
26kDa
12kDa
55kDa
Alix
CD63
CD81
Cyt C
Cal reticulin
E.
P20
# of vesicles
n=5,254
Size (nm)
F.
P100
# of vesicles
n=1,368
Size (nm)

Figure 1. EV isolation and analysis by immunoblot and NTA

A. Schematic of EV isolation from SCG cultures via centrifugation and downstream NTA by ZetaView. **B.** Still frames captured from NTA videos at t=30 secs. **C.** Quantification of the video analysis shown in B. Shown is mean ± SEM for three biological replicates. **D.** Immunoblot analysis of the canonical EV markers: Alix, CD63, CD81, and the intracellular markers: cytochrome C (mitochondria) and calreticulin (ER). Cell pellet, P20, and P100 fractions from three independent litters (L1, L2, L3) and a “no cell” media control (∅) are shown. These blots are cropped. Distinct blots are demarcated from each other by white spaces. **E, F.** Size distribution histogram of 5,254 particles from the P20 fraction and 1,368 particles from the P100 fraction for three biological replicates.

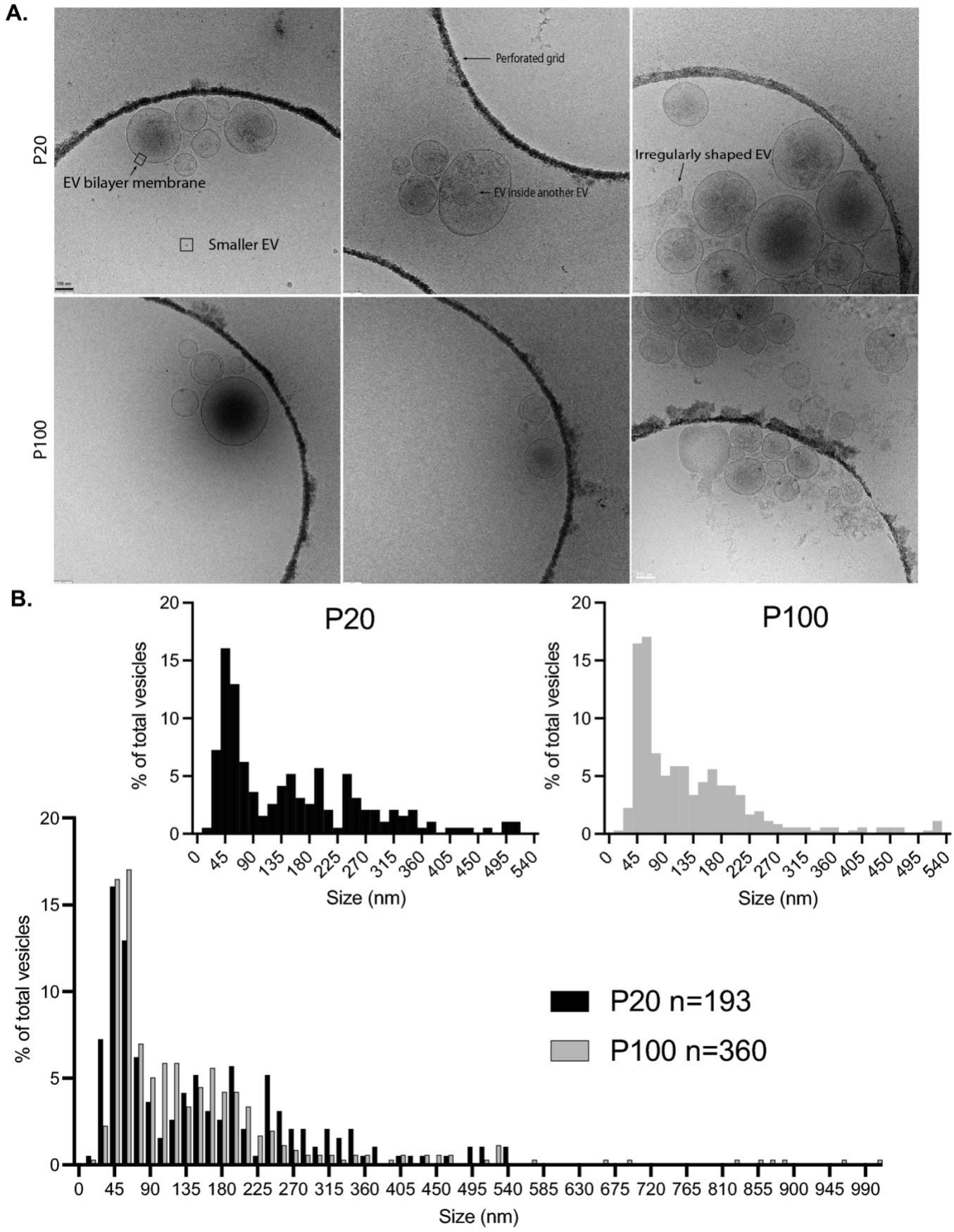
A.
P20
P100
EV bilayer membrane
Smaller EV
Perforated grid
EV inside another EV
Irregularly shaped EV
B.
P20
P100
% of total vesicles
Size (nm)
P20 n=193
P100 n=360
0 45 90 135 180 225 270 315 360 405 450 495 540 585 630 675 720 765 810 855 900 945 990

Figure 2. Morphology and sizing of EVs by cryo-EM.

A. Cryo-EM micrographs from the P20 (top row) and P100 (bottom row) fractions. Different types of EVs are annotated for easier appreciation of diverse EV morphologies. **B.** Size distribution histogram for all measured EVs from cryo-EM micrographs (P20: n=193 EVs, mean diameter 146.62 nm; P100: n=360 EVs, mean diameter 152.59 nm). The left histogram (black bars) is the sizing of the P20 fraction, and the right histogram (gray bars) is the sizing of the P100 fraction separated out from the histogram below. Data is from three biological replicates and the scale bar is 100 nm for all images.

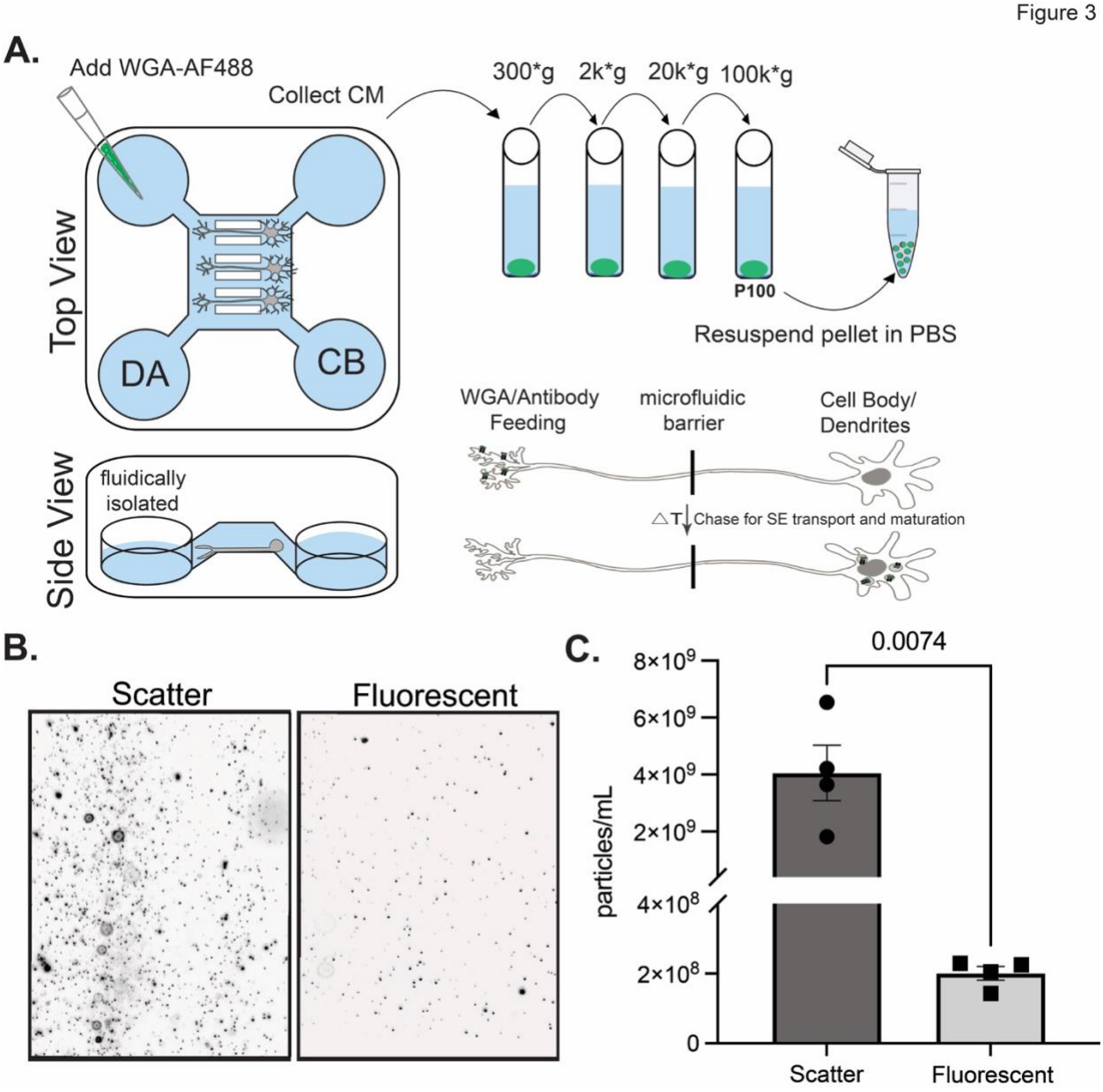

Figure 3. Somatodendritically secreted sympathetic EVs carry cargo originating in the distal axon

A. Schematic of the WGA-AF488 feeding assay in MFDs. WGA-AF488 was added to the distal axon (DA) chamber which was fluidically isolated from the cell body (CB) chamber. **B.** Still frames captured from NTA videos at t=30 secs in scatter and fluorescent mode. **C.** Quantification of the total number of particles (scatter) and the

number of fluorescent (WGA-AF488^{+}) particles collected from the P100 fraction after WGA-AF488 addition to the DA chamber of MFDs containing wild-type SCG neurons. Shown is the mean ± SEM for four biological replicates. P values are indicated above the pairwise brackets.

Figure 4

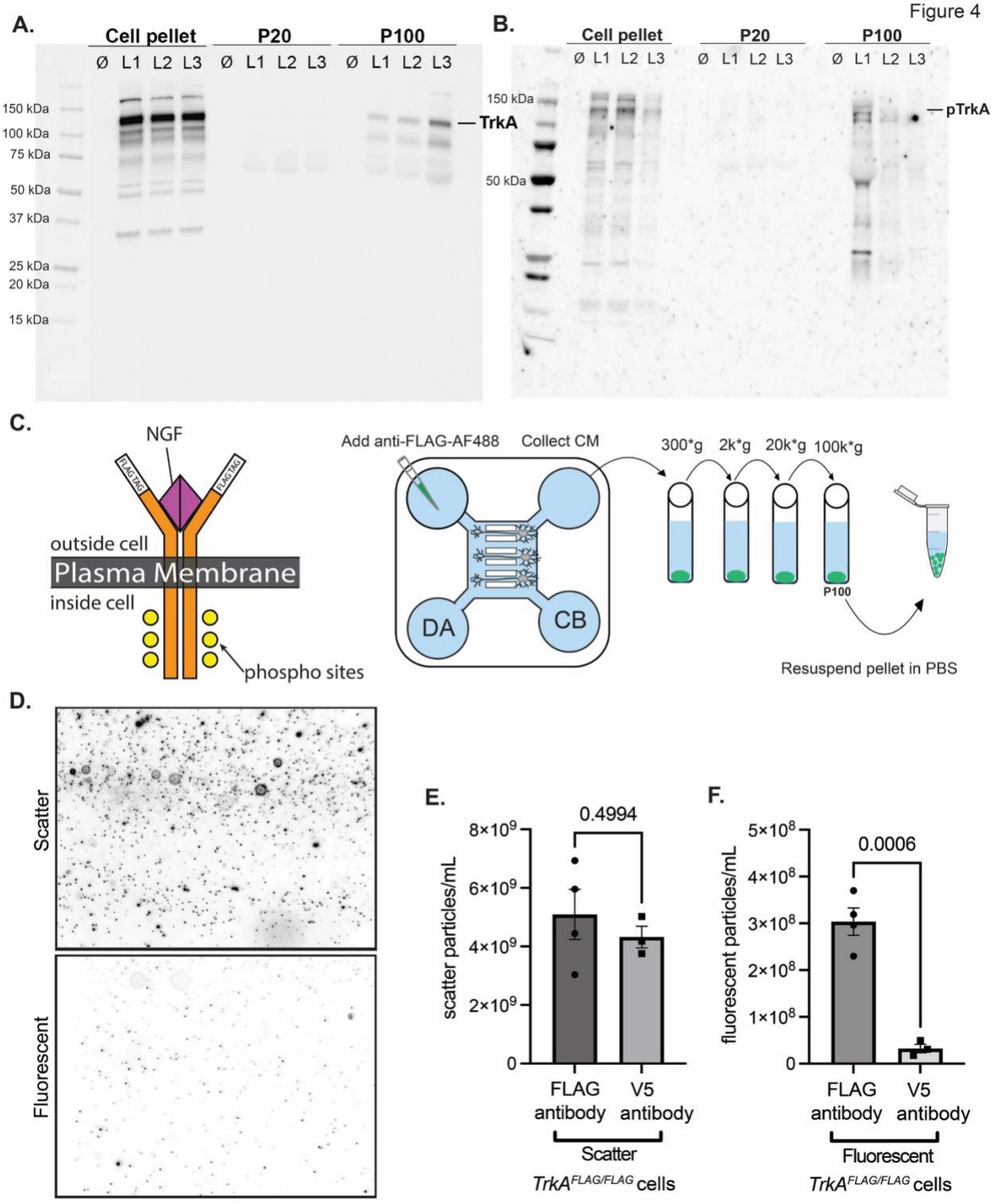
A.
Cell pellet
P20
P100
Ø L1 L2 L3 Ø L1 L2 L3 Ø L1 L2 L3
150 kDa
100 kDa
75 kDa
50 kDa
37 kDa
25 kDa
20 kDa
15 kDa
TrkA
B.
Cell pellet
P20
P100
Ø L1 L2 L3 Ø L1 L2 L3 Ø L1 L2 L3
150 kDa
50 kDa
pTrkA
C.
NGF
FLAG TAG
FLAG TAG
outside cell
Plasma Membrane
inside cell
phospho sites
Add anti-FLAG-AF488
Collect CM
DA
CB
300*g
2k*g
20k*g
100k*g
P100
Resuspend pellet in PBS
D.
Scatter
Fluorescent
E.
0.4994
8×10^9
6×10^9
4×10^9
2×10^9
0
scatter particles/mL
FLAG antibody
V5 antibody
Scatter
TrkA^FLAG/FLAG cells
F.
0.0006
5×10^8
4×10^8
3×10^8
2×10^8
1×10^8
0
fluorescent particles/mL
FLAG antibody
V5 antibody
Fluorescent
TrkA^FLAG/FLAG cells

Figure 4. Somatodendritically secreted sympathetic EVs contain the TrkA receptor that originated in the distal axon and was transported retrogradely to the soma.

A, B. Full immunoblot analysis of TrkA and phosphorylated TrkA (Y-490) in cell pellets, P20 and P100 EV fractions from three independent litters (L1, L2, L3) and a “no cell” media control (∅). Note: the three litters from **A.** are different from the three litters from **B. C.** Schematic showing the topology of FLAG-TrkA expressed from the mouse knockin locus in *TrkA*$^{FLAG/FLAG}$ mice (NGF: magenta triangle, phosphorylation sites: yellow circles). Sympathetic neurons from *TrkA*$^{FLAG/FLAG}$ mice were grown in MFDs. Anti-FLAG-AF488 antibody was fed to the distal axons (DA) and 15 hours later CM was collected from the cell body (CB) compartment and EVs were isolated by differential centrifugation. **D.** Still frames captured from NTA videos at t=30 secs in scatter (top) and fluorescent (Anti-FLAG-AF488^{+}) (bottom) mode. **E, F.** Quantification of the number of scatter or fluorescent (AF488+) particles detected after either Anti-FLAG-AF488 or V5-AF488 addition to the DA chamber of MFDs containing *TrkA*$^{FLAG/FLAG}$ SCG neurons. Shown is the mean ± SEM for four biological replicates. P values are indicated above the pairwise brackets.

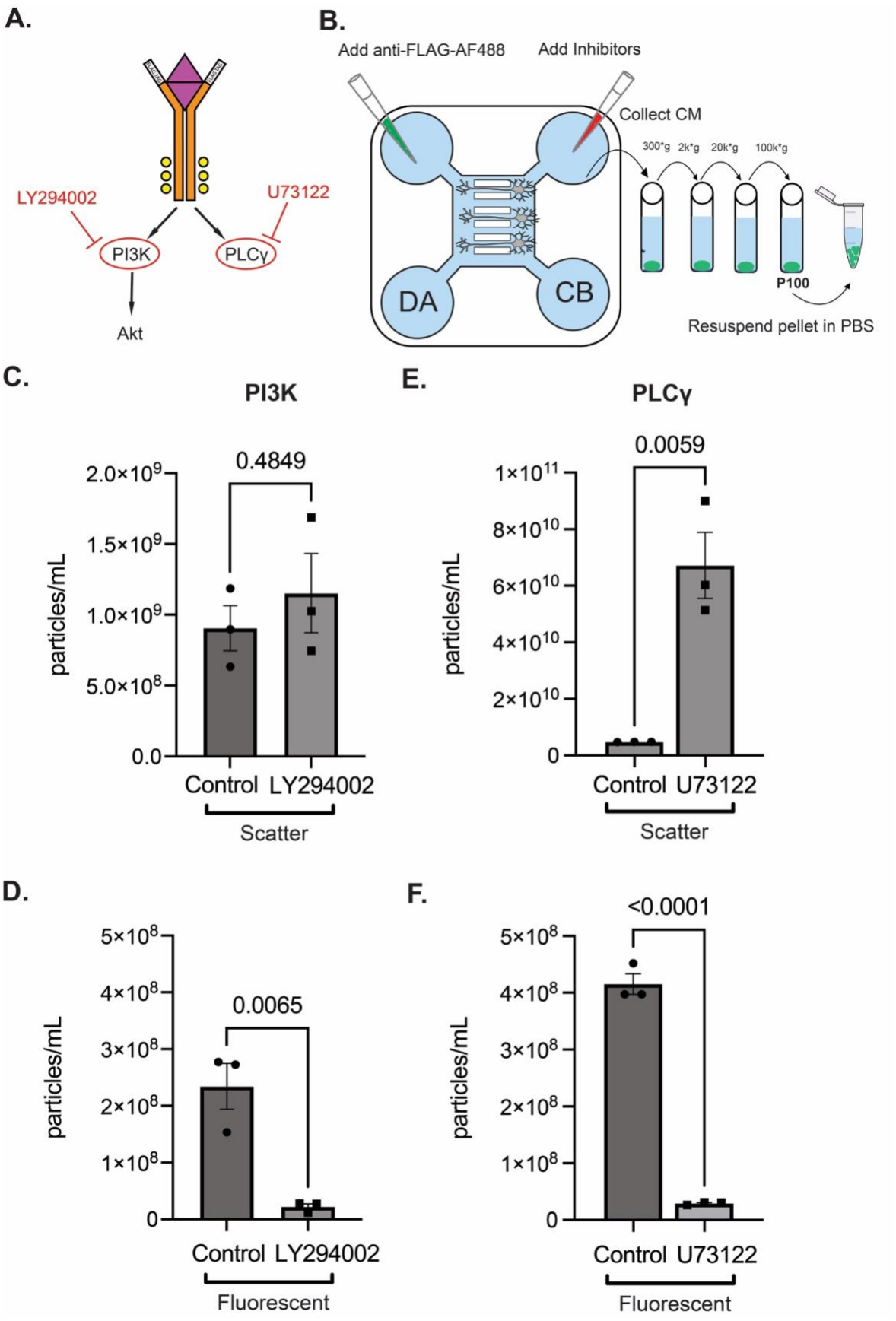
A.
LY294002
U73122
PI3K
PLCγ
Akt
B.
Add anti-FLAG-AF488
Add Inhibitors
Collect CM
300*g 2k*g 20k*g 100k*g
DA
CB
P100
Resuspend pellet in PBS
C.
PI3K
0.4849
2.0×10^9
1.5×10^9
1.0×10^9
5.0×10^8
0.0
particles/mL
Control LY294002
Scatter
E.
PLCγ
0.0059
1×10^11
8×10^10
6×10^10
4×10^10
2×10^10
0
particles/mL
Control U73122
Scatter
D.
0.0065
5×10^8
4×10^8
3×10^8
2×10^8
1×10^8
0
particles/mL
Control LY294002
Fluorescent
F.
<0.0001
5×10^8
4×10^8
3×10^8
2×10^8
1×10^8
0
particles/mL
Control U73122
Fluorescent

Figure 5. Inhibition of TrkA-dependent signaling pathways suppresses TrkA^{+} EV release

A. Schematic of the downstream pathways activated by TrkA phosphorylation and inhibitors that block them. **B.** Schematic of inhibitor and Anti-FLAG-AF488 antibody application to compartmentalized neurons to generate TrkA^{+} EVs. **C, D.** Quantification of the total number of scatter or fluorescent (Anti-FLAG-AF488^{+}) particles detected after anti-FLAG-AF488 antibody addition to the DA chamber of MFDs containing *TrkA$^{FLAG/FLAG}$* SCG neurons treated with the PI3K inhibitor, LY294002. **E, F.** Quantification of the total number of scatter or fluorescent (Anti-FLAG-AF488^{+}) particles detected after anti-FLAG-AF488 antibody addition to the DA chamber of MFDs containing *TrkA$^{FLAG/FLAG}$* SCG neurons treated with the PLC-ɣ inhibitor, U73122. Shown is the mean ± SEM for three biological replicates. P values are indicated above the pairwise brackets.

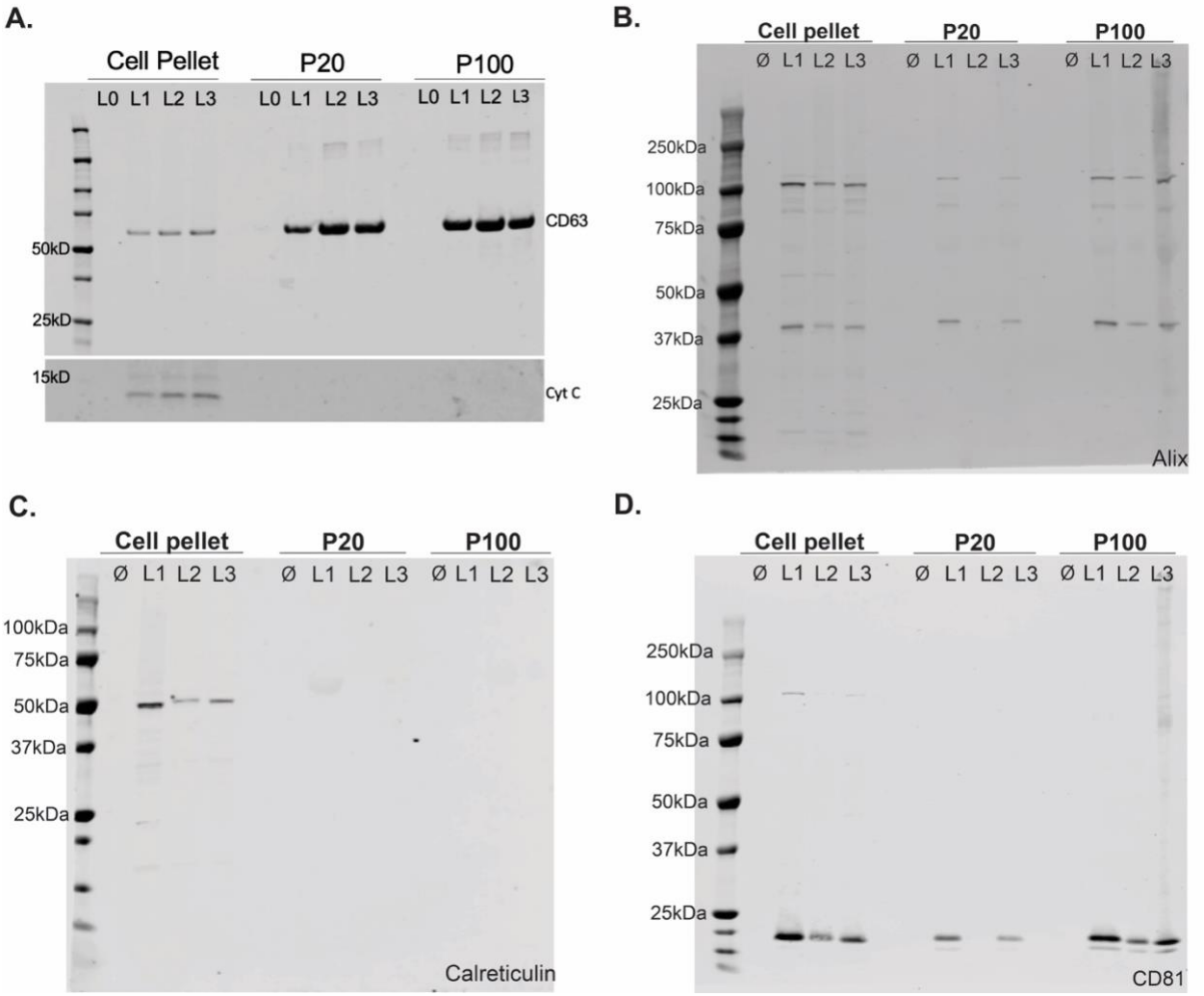

Supplementary Figure S1. Full-length immunoblots of EV and cell lysate markers that are shown in Figure 1D.

A. Full immunoblot that was physically cut in half before the addition of primary antibody against the EV marker tetraspanin, CD63 and the mitochondrial marker, Cytochrome C (Cyt C). **B.** Full immunoblot of the EV marker and accessory ESCRT protein, Alix. Full-length Alix is predicted to run around 95 kDa. The smaller band is either non-specific or represents a breakdown product of full-length Alix. **C.** Full immunoblot of the

endoplasmic reticulum marker, Calreticulin **D.** Full immunoblot of the EV marker tetraspanin, CD81 from the same blot in panel (**B)** that was stripped and re-probed.

Supplementary Figure S2

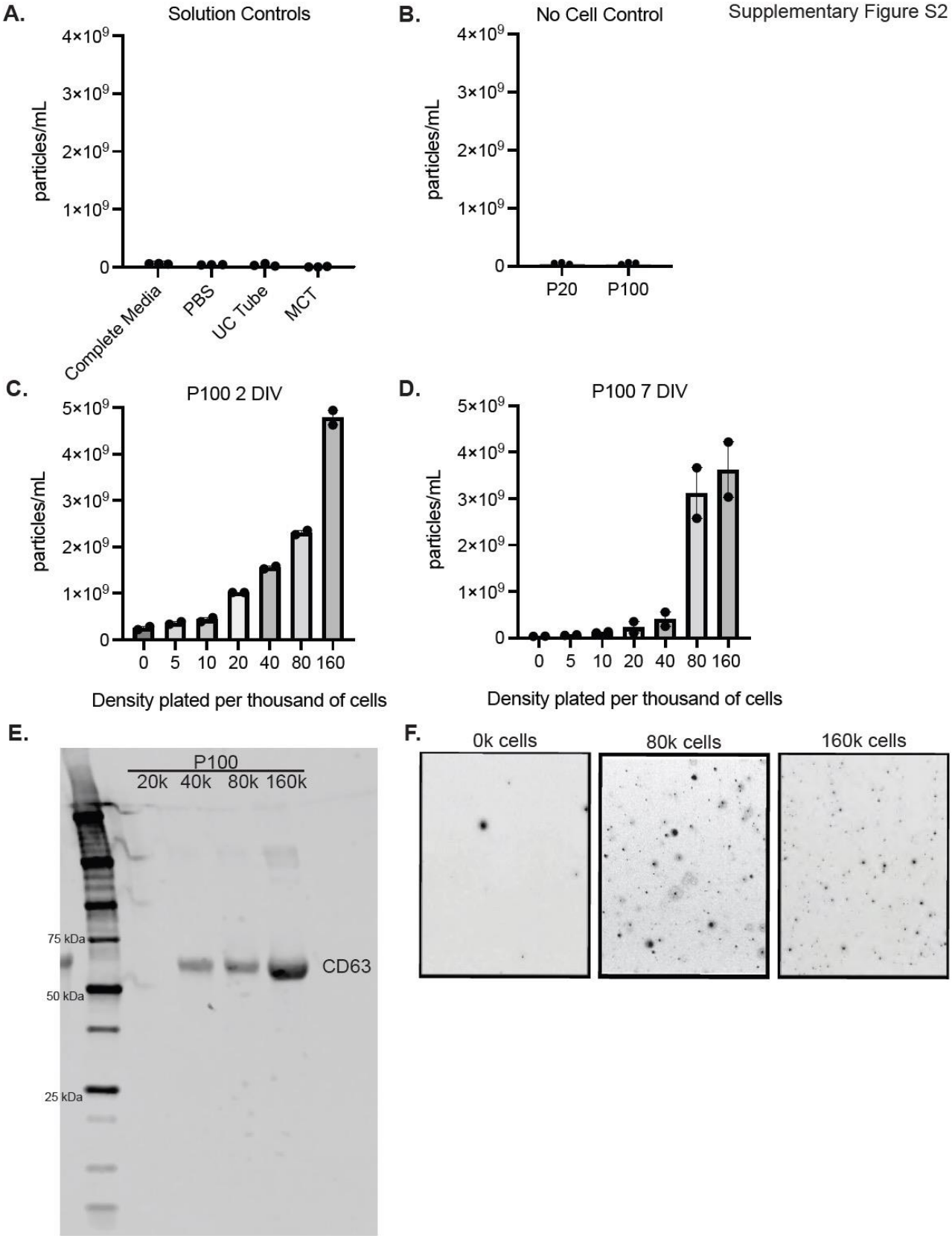

Supplementary Figure S2. Density and days in vitro affect EV production

A. One milliliter of each undiluted solution condition was analyzed by NTA for non-EV scattering particles. Complete media, PBS, UC tube (PBS that sat in a polycarbonate centrifuge tube for 3 hours), MCT (PBS that sat in a microcentrifuge tube for three hours). **B. "**No cell" only control consisting of complete media that was plated in a 12-well plate and changed every 48 hours before collection and differential centrifugation. **C-D.** Density and DIV curve from P100 fraction. Cells were plated at the density shown on the x-axis and grown for either 2 DIV (**C)** or 7 DIV **(D)** before CM was collected for EV isolation and NTA analysis. **E.** Immunoblot analysis of CD63 at different densities of plated SCG cells. **F.** Still frames captured from NTA videos at t=30 secs of EVs from different plated cell densities. **A - D**. Shown is mean ± SEM for three replicates.

Supplementary Figure S3

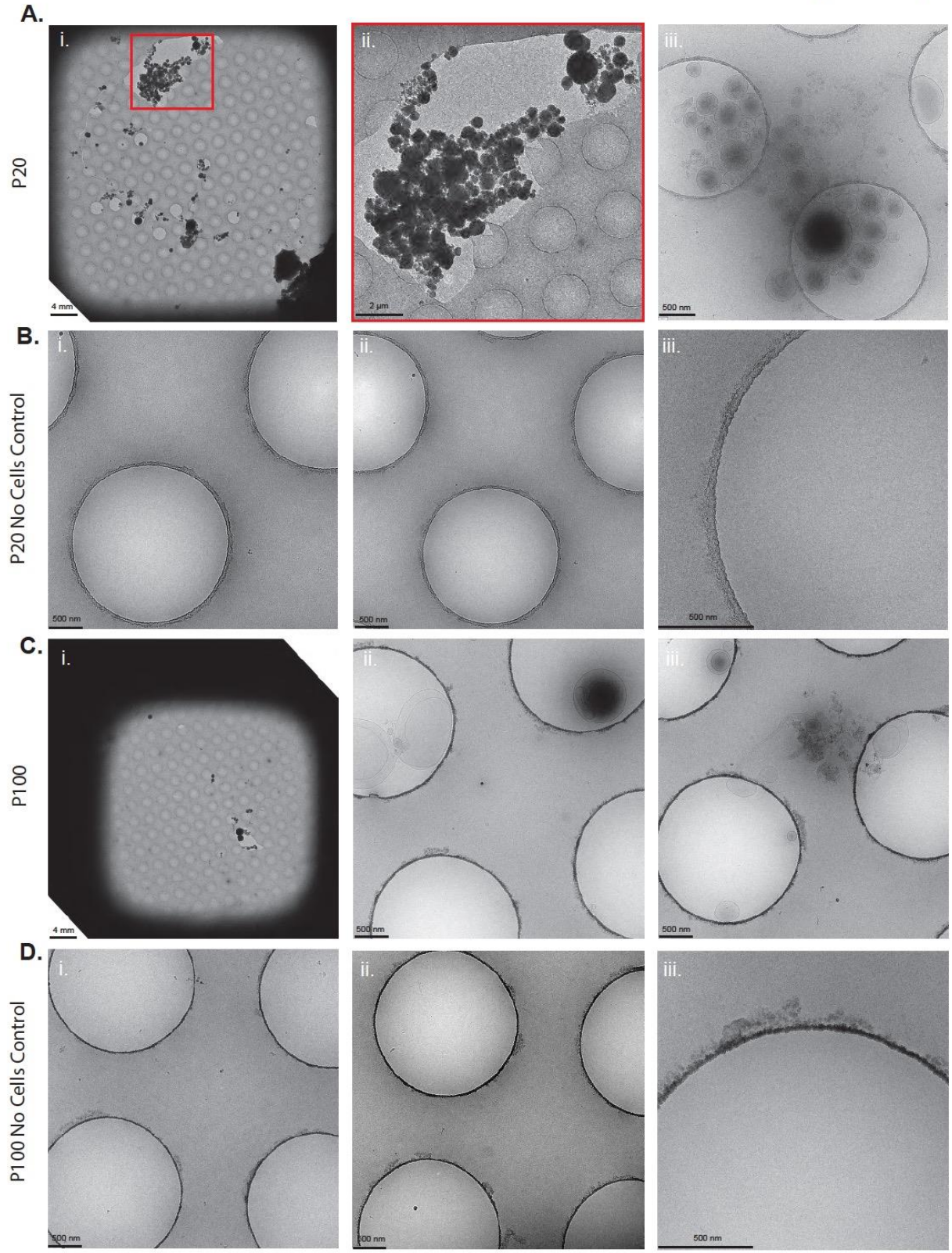

Supplementary Figure S3. Low magnification cryo-EM micrographs of EVs

A. Low magnification micrographs of the P20 fraction. i. Shown are large aggregates which cannot be measured as discrete EVs. Scale bar is 4 mm. ii. Zoomed in view of the red boxed inset in i. Scale bar is 2 μm. iii. Discrete double membrane-enclosed EVs are discernable with different-sized EVs with different electron densities. Scale bar is 500 nm. **B.** Low magnification micrographs of the P20 “no cell” controls (i., ii., and iii). Scale bar is 500 nm for all. **C.** Low magnification micrographs of P100 fraction. i. Full grid view of the P100 fraction with noticeably fewer large aggregates as compared to the P20 fraction. Scale bar is 4 mm. ii. EVs with interesting shapes and electron densities are viewable in the perforations. Scale bar is 500 nm. iii. Cluster of heterogeneous EVs. Scale bar is 500 nm. **D.** Low magnification micrographs of P100 “no cell” controls (i., ii., iii.). Scale bar is 500 nm for all.

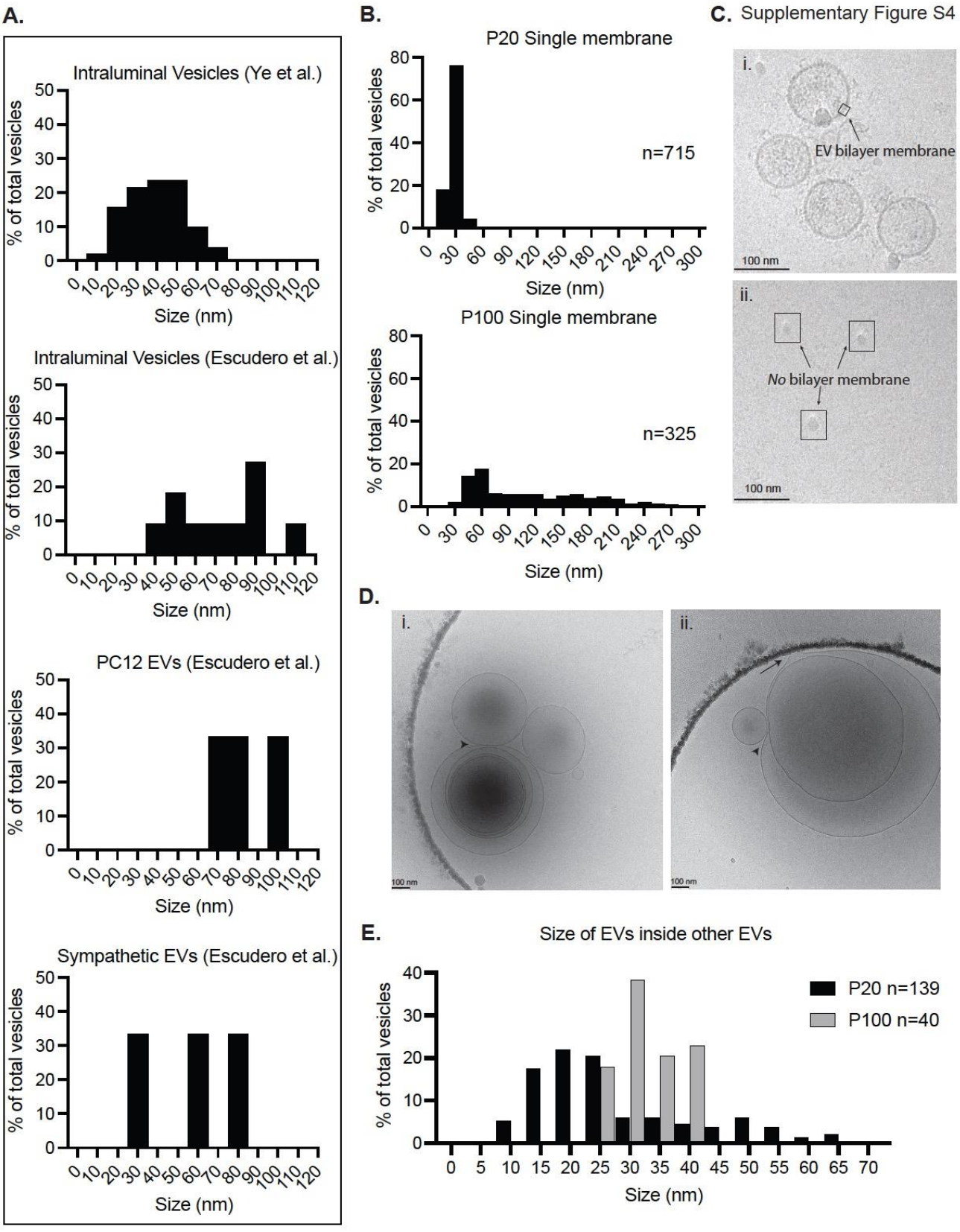
A.
Intraluminal Vesicles (Ye et al.)
% of total vesicles
Size (nm)
Intraluminal Vesicles (Escudero et al.)
PC12 EVs (Escudero et al.)
Sympathetic EVs (Escudero et al.)
B.
P20 Single membrane
n=715
P100 Single membrane
n=325
C. Supplementary Figure S4
i.
EV bilayer membrane
100 nm
ii.
No bilayer membrane
D.
E.
Size of EVs inside other EVs
P20 n=139
P100 n=40

Supplementary Figure S4. Heterogeneity in size and morphology of sympathetic EVs

A. Size distribution histogram showing intraluminal vesicles (ILVs) from sympathetic neuron transmission electron micrographs from Ye et al., 2018 (mean diameter 52.8 nm) and Escudero et al., 2014 (mean diameter 79.9 nm) as well as EVs derived from NGF-differentiated PC12 cells (mean diameter 80.0 nm) and sympathetic EVs (mean diameter 58.3 nm) from Escudero et al., 2014. **B.** Size distribution histogram of single membrane enclosed EVs from the P20 fraction (top) (n= 715 EVs, mean ± SEM is 21.04 nm ± 15.59 nm) and P100 fraction (bottom) (n= 325 EVs, mean ± SEM is 159.03 nm ± 191.56 nm) for three biological replicates. **C.** Zoomed in micrograph of small EVs. i. Small EVs with a distinct double membrane lipid bilayer. Scale bar is 100 nm. ii. Sub 30 nm diameter exomeres with only a single membrane. Scale bar is 100 nm. **D.** Heterogeneity in size and structure of EVs. i. micrograph demonstrating EVs inside EVs (data quantified in E), electron dense EVs, and EVs deforming around each other (arrowhead). ii. Micrograph showing EVs inside EVs, EV membranes deforming around each other (arrowhead), and long tubule-like projections from EV membranes (arrow). Scale bar is 100 nm for all images. **E.** Size distribution histogram of EVs enclosed inside of other EVs for both the P20 (mean ± SEM is 35.5 nm ± 26.79 nm) and P100 fraction (mean ± SEM is 24.59 nm ± 5.44 nm).

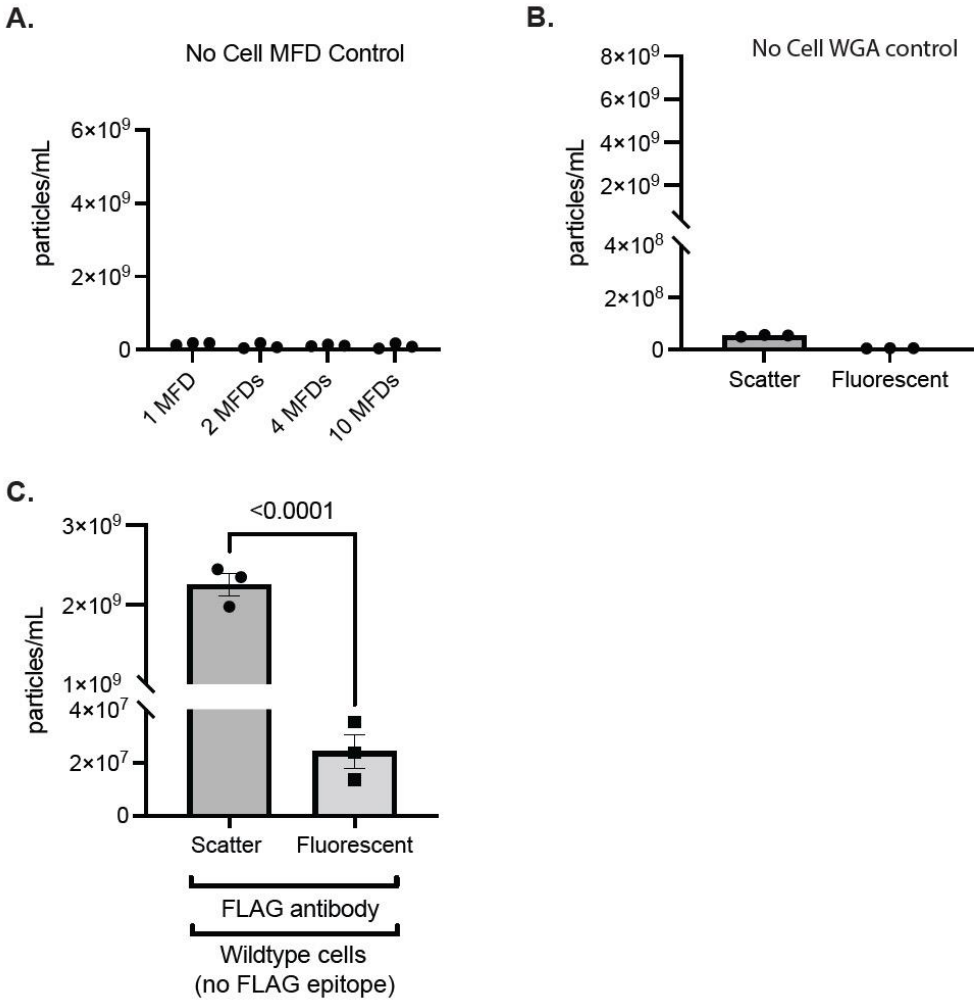

Supplementary Figure S5. Control for compartmentalized FLAG feeding assays

A. "No cell" MFD control consists of complete media that was plated and pooled from either 1, 2, 4, or 10 MFDs and changed every 48 hours before collection and differential centrifugation. Particle counts were 1.28 x 10^7, 2.23 x 10^7, 4.86 x 10^7, and 8.32 x 10^7 particles/mL for 1, 2, 4, and 10 MFDs, respectively. **B.** Quantification of the total number of particles (scatter) and the number of fluorescent (WGA-AF488$^+$) particles collected from the P100 fraction after WGA-AF488 addition to the DA chamber of MFDs

containing no cells. **C.** Quantification of the total number of particles (scatter) and the number of fluorescent (Anti-FLAG-AF488^{+}) particles collected from the P100 fraction after Anti-FLAG-AF488 addition to the DA chamber of MFDs containing wildtype (no FLAG epitope) SCG neurons. **A-C.** Shown is the mean ± SEM for three biological replicates. P-values are indicated above the pairwise brackets.

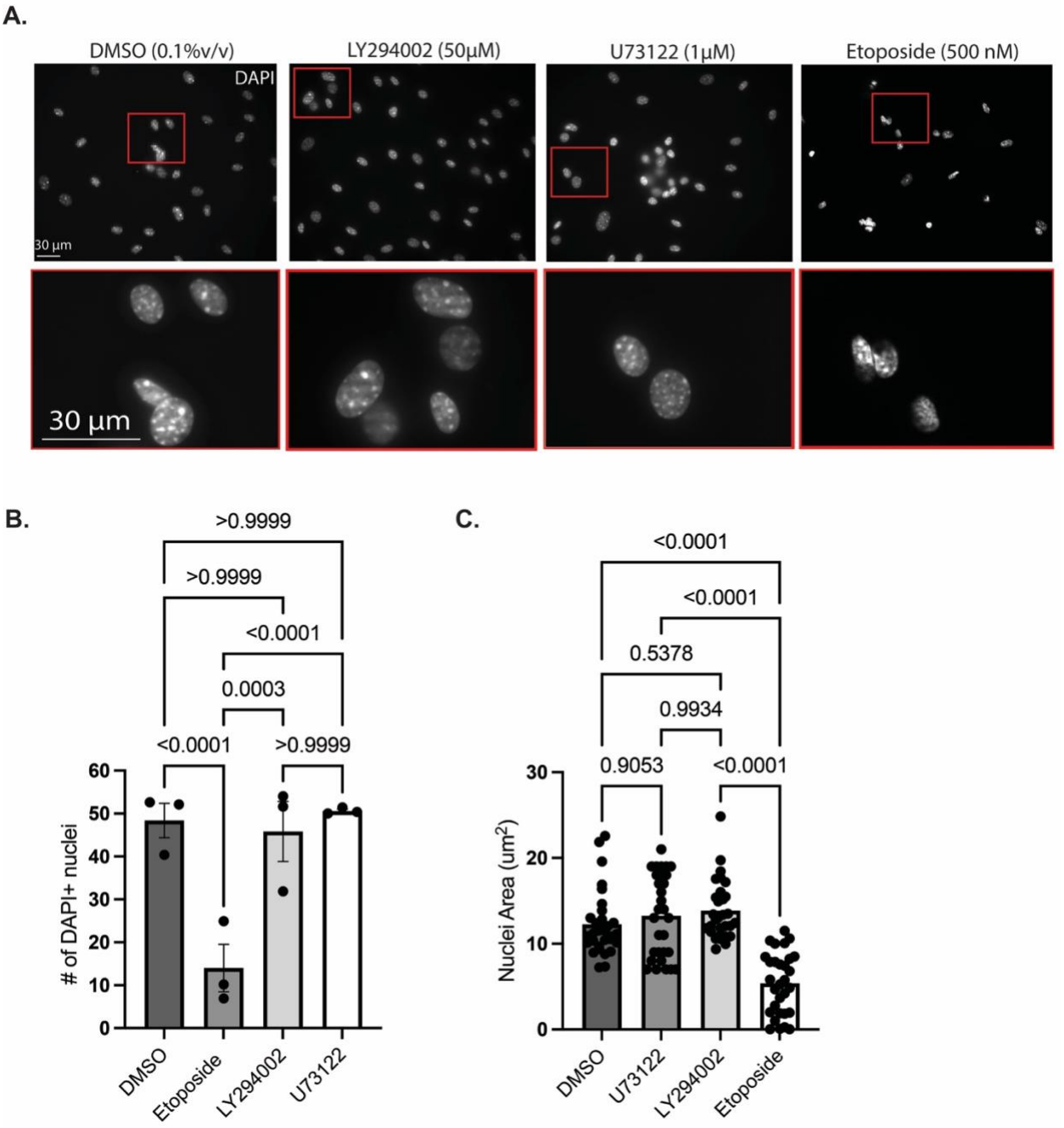

Supplementary Figure S6. TrkA inhibitors do not affect sympathetic culture viability

A. Images of nuclei from compartmentalized sympathetic cultures treated for 15 hours

with DMSO (inhibitor solvent), etoposide (positive control to promote cell death), or inhibitors in the cell body chamber. Zoomed in view of the red boxed inset is below. Scale bar is 30 μm. **B.** Quantification of the number of total cells ($DAPI^+$) present in each condition. Shown is the mean ± SEM for three biological replicates from 10 fields of view per replicate. **C.** Quantification of the nucleus area from 30 cells in each condition. **B-C.** P-values are indicated above the pairwise brackets.

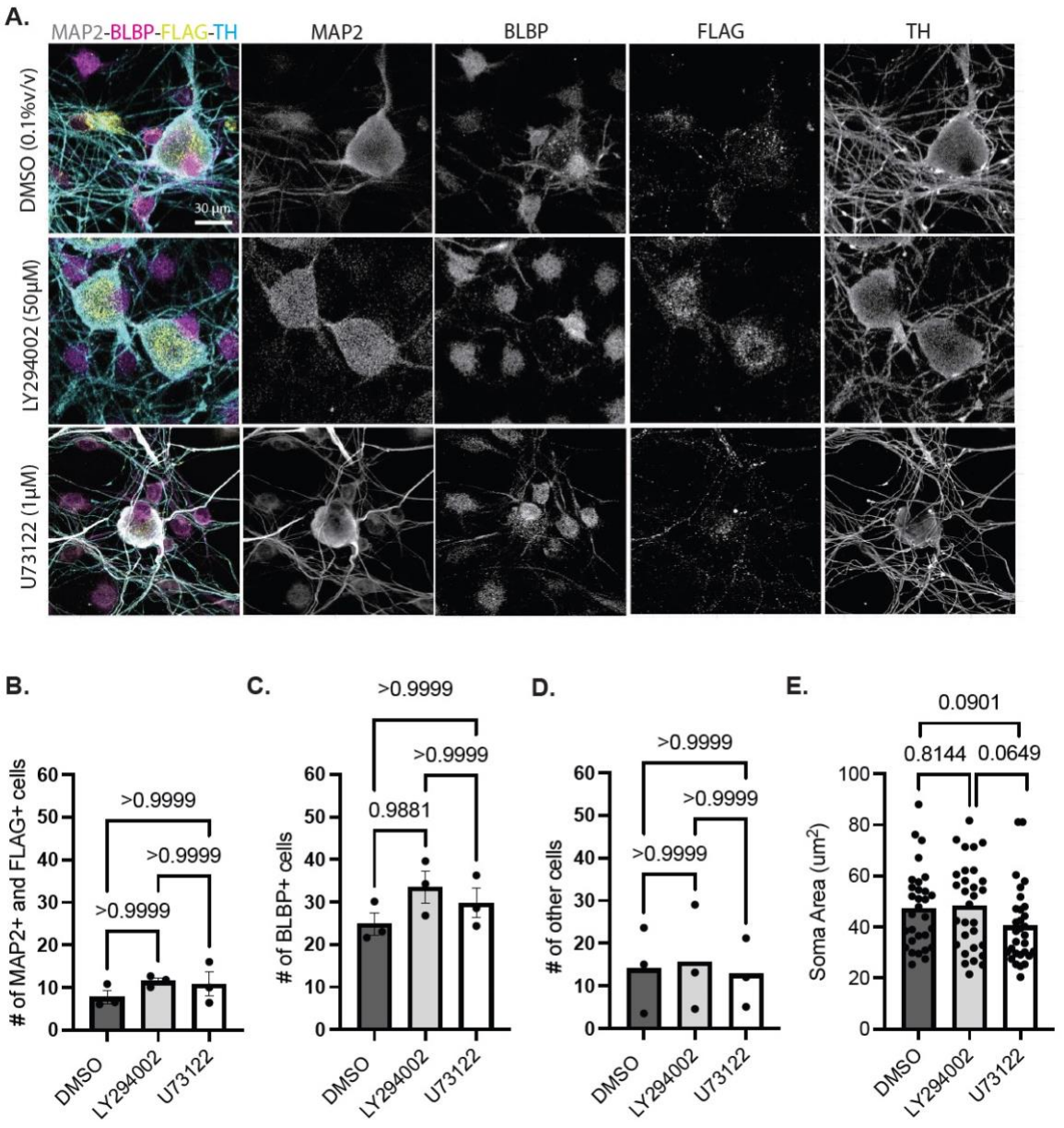

Supplementary Figure S7. TrkA inhibitors do not affect SCG neuron morphology

A. Images of the cell bodies of compartmentalized SCG neurons treated with DMSO (control) or inhibitors in the cell body chamber and anti-FLAG-AF488 antibody in the distal axon chamber for 15 hours. Staining against MAP2 (somatodendritic domain), BLBP (satellite glia), anti-FLAG-AF488, and TH (SCG neuron). Scale bar is 30 µm.

B-D. Quantification of the number of SCG neurons ($MAP2^+$; $FLAG^+$ double positive)**,**

satellite glia **(**$BLBP^+$), and other cells ($DAPI^+$ and $BLBP^-$; $FLAG^-$; $MAP2^-$) from each condition. Shown is mean ± SEM for three biological replicates from 10 fields of view per replicate. **E.** Quantification of the somata area of 30 SCG neurons that were $MAP2^+$; $FLAG^+$ double positive. P-values are indicated above the pairwise brackets.

Chapter IV. Sympathetic Extracellular Vesicles Promote the Survival of Spinal Cord Neurons

Ashley J Mason and Austin B. Keeler. All experiments were carried out by Ashley J. Mason with flow cytometry assistance from Austin Keeler.

Abstract

Survival of sympathetic neurons during development relies on the internalization and trafficking of the neurotrophin, nerve growth factor (NGF). Postganglionic neurons express the neurotrophin receptor TrkA, which upon binding NGF becomes active and signals for the survival of the neuron. Neurons that do not receive adequate amounts of NGF will undergo regulated cell death. Interestingly, the preganglionic neurons, which are the upstream presynaptic partners of the postganglionic neurons rely on NGF signaling as well. However, they do not have direct access to NGF, nor do they express TrkA. Thus, the mediator of survival signaling in these preganglionic neurons is unknown. Here we show that Extracellular Vesicles (EVs) derived from the postganglionic neurons provide trophic support to the preganglionic neurons. We found that addition of sympathetic EVs to spinal cord cultures *in vitro* supports their survival using both flow cytometry and live imaging microscopy. This work provides a foundation for the presence of neurotrophic EVs that modulate the survival of their recipient cells. Future work will further elucidate the signaling pathways and mechanisms behind this survival phenotype.

Introduction

In the peripheral nervous system, the sympathetic circuit consists of preganglionic spinal neurons residing in the intermediolateral (IML) cell column of the spinal cord[5,6,64,194–196] which send axons to the sympathetic ganglia to innervate postganglionic sympathetic neurons. In turn, these postganglionic neurons send axons to innervate peripheral organs. During development, more neurons are produced than

ultimately constitute the mature sympathetic circuit[197]. The decision to survive or die is regulated by nerve growth factor (NGF), which is secreted by target organs (i.e. salivary gland or eye)[198] and binds to the TrkA receptor on postganglionic axons. Only those postganglionic sympathetic neurons that receive sufficient amounts of target derived NGF will survive. Interestingly, cell survival of the preganglionic neurons is also NGF-dependent, even though they do not have direct access to soluble NGF nor do they express the TrkA receptor[199]. Survival of preganglionic neurons is quantitatively matched to the survival of postganglionic neurons, a concept termed 'target matching'[200]. In addition to survival signaling, NGF signaling regulates synaptogenesis between axons from preganglionic neurons and dendrites of the sympathetic neurons in the ganglion.

It is currently unknown how NGF signaling is communicated from sympathetic postganglionic neurons to the preganglionic neurons for survival and synaptogenesis. Long distance NGF-TrkA signaling in postsynaptic neurons is well studied and known to be propagated from the distal axon back to the cell body via internalization of the NGF-TrkA receptor complex into an endosome, commonly referred to as a signaling endosome (SE)[40,201]. The SE is then retrogradely trafficked along axonal microtubules to the cell body to elicit cell survival signaling cascades and transcriptional responses[40]. Here we demonstrate a novel mechanism of postganglionic-to-preganglionic cell-to-cell communication through extracellular vesicles (EVs). We show that exogenous application of EVs derived from SCG cultures provide neurotrophic signals to the preganglionic neurons that increase their survival *in vitro*. This work is the first step in

establishing the possibility of neurotrophic EVs that support the survival of preganglionic neurons.

Materials and Methods

REAGENT or RESOURCE	SOURCE	IDENTIFIER
Antibodies		
Sheep Anti-Nerve Growth Factor-**β** Antibody	Millipore	**AB1528SP**
Biological samples		
NGF	In house, purified from mouse salivary glands	
Chemicals, peptides, and recombinant proteins		
Poly-D-Lysine	Sigma	Cat # P7886
DMEM no phenol	Gibco	Cat # 31053-028
GlutaMAX	Gibco	Cat # 35050-061
Papain	Worthington Biochemical Corp	Cat # LS003119
Basal Medium Eagle	Gibco	Cat # 21010-046
N2 Supplements	Gibco	Cat # 17502-048
B27 supplement	ThermoFisher Scientific	Cat # 17504044
Neurobasal Media	Gibco	Cat # 21103-049
35mm glass bottom dish with 14mm micro-well # 1.5 coverglass	Cellvis	Cat # D35-14-1.5N
Hoechst 33342 Fluorescent Nucleic Acid Stain	Sarorius	Cat # 639
Incucyte Annexin V Red Dye	Sartorius	Cat # 4641
Incucyte Annexin V NIR Dye	Sartorius	Cat # 4768
HBSS	Gibco	Cat # 14175-095
Experimental models: Organisms/strains		
$ChAT^{BAC}$-eGFP	Jackson Laboratory	Strain # 007902
Hardware, Software and algorithms		
Optima TLX Ultracentrifuge	Beckman-Coulter	
Attune NxT Flow Cytometer	Thermo-Fisher	
Prism 9	Graphpad	graphpad.com
Illustrator	Adobe	adobe.com
Other		
Microcentrifuge tubes	USAscientific	Cat # 1415-2500

Tissue culture plates	Fisher Scientific	Cat # 150628
Polycarbonate centrifuge tubes	Beckman	Cat # 343778

Primary spinal cord cultures

Spinal cords from E18 mouse embryos were micro dissected and meninges were removed and kept in ice cold HBSS until enzymatic digestion. Spinal cords were then resuspended in 20 u/mL papain in 1mM L-cysteine and 0.5mM EDTA for 20 mins at 37°C. This solution was aspirated off and spinal cords were washed three times in plating media (BME, 5% FBS, N2 supplements, 1x GlutaMAX). Cells were triturated 20X with a P100 pipette tip and then strained through a 40μm cell strainer. After counting, cells were plated on poly-D-lysine and laminin coated coverslips and kept in an incubator at 37°C at 5% CO_2. Media was changed to Neurobasal media containing B27 supplements 16 hours after plating.

Flow Cytometry

Spinal cords were dissected from ChAT-GFP mice as described above and plated on 24 well plates at a density of 500,000 cells per well. After 4 hours, plating media was replaced with one of the following conditions: P100, P100 + anti-NGF neutralizing antibody (5uM), NGF (50ng/mL), supernatant from the 100,000 x g spin (SN100), and a control condition with media only. After 24 hours in each condition, dead floating cells were collected to be stained. The attached cells were dissociated with Accutase for 3 mins followed by a recovery in Neurobasal media containing 10% FBS for 15 mins at 37°C. The dead floating cells and the live cells were combined into one microcentrifuge tube and stained with 1:200 μL Annexin V Red and 1:800 μL of TO-PRO-3 at RT for 15

mins. The samples were then spun at 500 x g for 3 mins and resuspended in cell storage media. 10 μL of sample from all conditions were used to test and determine the voltage.

Survival Microscopy Assay

Spinal cords were dissected from ChAT-GFP animals as described above and plated on glass bottom dishes at a density of 200,000 cells per dish. After 4 hours, plating media was replaced with one of the following conditions: P100, P100 + anti-NGF neutralizing antibody (5uM), NGF (50ng/mL), supernatant from the 100,000 x g spin (SN100), and a control condition with media only. After 24 hours in each condition, Hoechst (0.5% v/v) and AnnexinV dye (Inucyte, 1:200) was added to the dishes for 15 minutes prior to imaging. Cells were then imaged on a Zeiss AxioZoom Observer.Z1 with Apotome 2.1 structured illumination and acquired with a 40x air objective. Ten fields of view (FOV) were imaged per condition.

EV Isolation

SCG cells from wildtype mice were dissected and plated at a density of 100,000 cells per well and cultured for 7 DIV. Conditioned media was collected from the SCG cells after 48 hours and placed into 1.5 mL microcentrifuge tubes on ice. The conditioned media was then centrifuged at 300 x g for 10 mins at 4°C to pellet cells and large debris. The supernatant was transferred to a clean 1.5 mL microcentrifuge tube and centrifuged at 2,000 x g for 10 mins at 4°C to pellet dead cells. The supernatant was transferred to a clean 1.5 mL microcentrifuge tube and spun at 20,000 x g for 30 mins. The pellet from

this step is the P20 fraction. The supernatant was transferred to polycarbonate tubes subjected to ultracentrifugation at 100,000 x g_{max} (rotor: TLA 120.2; k -factor: 42; 53,000 rpm) for 70 mins at 4°C. The pellet from this step is the P100 fraction.

Statistics and Measurements.

For the Survival Microscopy Assay, cell counts were determined using the cell counter plugin in Image J. Cell type was determined using the following: all cells ($Hoechst^+$), ChAT neurons (GFP^+) and apoptotic cells (Annexin V^+). For the Flow Cytometry Survival Assay, cells were first gated by GFP signal to select for ChAT-GFP neurons, then cells were classified as either TOPRO-3 positive (dead) or negative (alive). Statistical analyses were performed using Prism 9 software. All values are shown as mean ± SEM. Differences between samples were determined using one-way ANOVA with Tukey's Multiple Comparisons. Statistical significance is a p-value < 0.05. P-values are denoted on top of each bracket pair.

Results

We wanted to determine if EVs secreted by mouse sympathetic neurons could support the survival of their upstream preganglionic partners *in vitro*. The preganglionic neurons that synapse onto SCG neurons are visceral motor neurons. Therefore, to better identify these neurons, we cultured cells from embryonic (E18) spinal cords derived from a ChAT-GFP expressing mouse line enabling us to visualize GFP+ motor neurons. These cultures were then treated with one of the following conditions for 24 hours: complete media, serum free media, P100, NGF, P100 + anti-NGF antibody or the

SN100 fraction (Fig. 1A). ChAT-GFP expressing motor neurons comprise ~30% of all cells in the spinal cord and an even smaller proportion of these ChAT-GFP cells are visceral motor neurons [202]. Therefore, we first wanted to determine that the proportion of ChAT-GFP expressing neurons across our different treatment conditions. We observe that approximately 10% of cells in our cultures express GFP across all treatment groups (Fig. 1B). Next, we cultured the neurons for either 3, 5, or 7 DIV in either complete media or serum-free media to assess their normal growth and death trajectories. At all serum-free media condition (serum starved) time points the neurons did not survive (Fig. 1C). Meanwhile the cells grown in complete media continued to survive at all time points and developed long neurites after 7 DIV (Fig. 1C).

Once we established the baseline conditions for our assay, we began to assess the survival of spinal cord cells after culturing them in the different treatment conditions. After 24 hours of condition treatment, we imaged the cells live after staining them with Hoechst (to visualize nuclei) and Annexin V (to visualize apoptotic membranes) (Fig. 2A). The total number of cells that were undergoing apoptosis (Annexin V+) after treatment with the P100 EV fraction was significantly less when compared to cells treated with the supernatant from the 100,000 x g spin (SN100) (Fig. 2B). The number of ChAT-GFP+ cells that were undergoing apoptosis was significantly less in the P100 treated condition compared to either the NGF or SN100 treated conditions (Fig. 2C). Lastly, the number of dying ChAT-GFP+ cells compared to all other cell types in the cultures was significantly less in the P100 treated condition versus the SN100 or the serum-starved condition (Fig. 2D). Importantly, the total number of cells counted (Hoechst+) was consistent throughout all treatment groups with the exception of the

serum-starved condition in which there were fewer total numbers of cells in the cultures at 24 hours (Table 2).

Due to the limitations of the microscopy assay, namely, the inability to image more than 10 fields of view per coverslip without photobleaching, it was difficult to quantify a large number of cells per condition. Therefore, we conducted an additional survival assay using flow cytometry. Using the nuclei stain, TOPRO-3, we quantified the number of dead cells ChAT-GFP+ cells in our different treatment conditions. Cells treated with the P100 EV fraction or complete media had significantly more living cells (TOPRO-3^{low}) then cells treated with either NGF, P100 + anti-NGF antibody, SN100 or serum-free media (Fig. 2E). In accordance, the number of dead (TOPRO-3^{high}) cells was significantly higher in cells treated with either NGF, P100 + anti-NGF antibody, SN100 or serum-free media when compared to cells treated with the P100 EVs or complete media (Fig. 2F).

Discussion

Ontogenetic cell death has been described throughout the nervous system for many neuronal subtypes. The preganglionic spinal motor neurons that project onto the sympathetic postganglionic neurons exhibit this programmed cell death in response to inadequate trophic factor support[62,199,200,203–206]. Withdrawal of NGF from this system results in a decrease in the number of neurons in the sympathetic ganglia as well as a loss of synapses and preganglionic axon fibers in the nerve tract[67,199,207]. Since NGF-TrkA signaling is highly important to the integrity of this system during development, we purported that NGF-TrkA carrying EVs could mediate the transfer of neurotrophic

signals between the pre- and postganglionic neurons. To assess this question *in vitro* we employed two different assays to probe neuronal survival after treatment with postganglionic neuron derived EVs. We found that treatment with these P100 EVs in both assays was sufficient to increase the survival of ChAT-GFP+ neurons from the spinal cord. Importantly, incubation of the P100 EVs with anti-NGF antibody prior to their addition to the spinal cord cells blocked the pro-survival effect of the EVs on these neurons. We currently cannot resolve if this reduction in survival is due to inhibition of NGF-TrkA signaling by the anti-NGF antibody or if the anti-NGF antibody is non-specifically blocking EV function due to steric hindrance. Blocking EV uptake using an anti-CD9 antibody has been shown before using flow cytometry. In these experiments, fluorescent lipid dye labeled EVs were not internalized after incubation with an anti-CD9 antibody[208]. Interestingly, EV treatment not only increases the survival of ChAT-GFP+ neurons but also of other cells in the cultures (Fig. 2B). This suggests that other cargos present in the EVs might be acting on the cells in culture to promote survival or that TrkA signaling is also able to impact these other cell types. Further research would be needed to parse apart these specific functions.

The notion that EVs can provide trophic signaling is gaining traction within the field[94,209]. EVs have been shown to be involved in pathogenic spread of neurotoxic species such as alpha-synuclein, tau, etc[151,210,211]. Other studies have shown EVs can modulate synapse maturation and spine density as well as increase proliferation of neurons in certain brain regions[160,212,213]. While this study does not examine this survival

phenotype *in vivo*, it provides the initial understanding of the role of the EVs in the sympathetic nervous system as a messenger of pro-survival signaling cues.

Figures

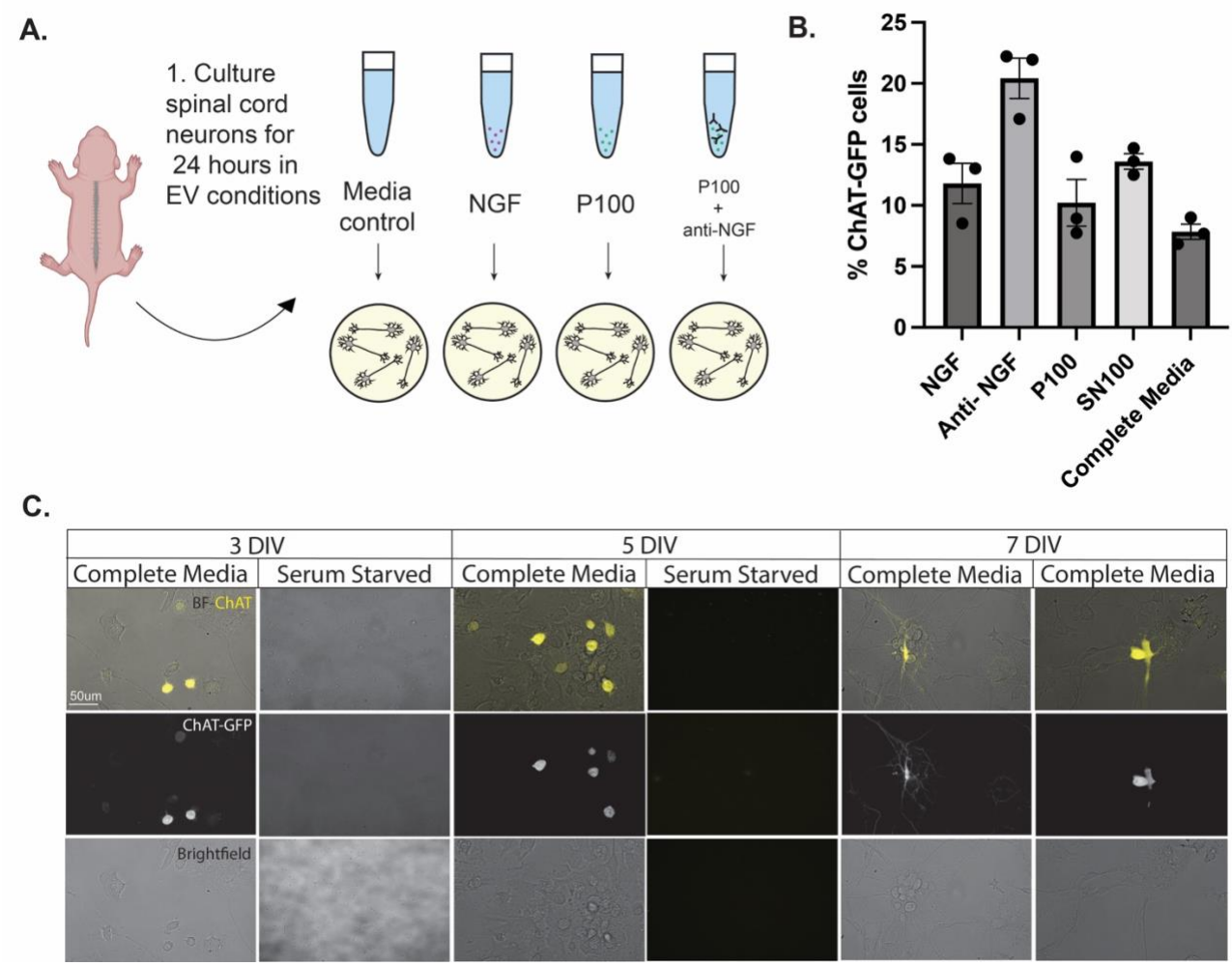

Figure 1. EV survival assay schematic and baseline parameters

A. Schematic of the EV survival assay. EVs or control conditions isolated from 7 DIV SCG cultures are added to spinal cord cultures for 24 hours before downstream analysis. **B.** Percentage of ChAT-GFP cells in each culture condition 24 hours after

plating. Shown is mean ± SEM for three biological replicates. **C.** Images of E18 ChAT-GFP spinal cord cultures grown in either complete media or media without serum (serum starved) for 3, 5 or 7 DIV.

	Total # cells (n=)	Total # GFP Cells (n=)
NGF	663	97
Anti-NGF	756	81
P100	722	83
SN100	771	94
Complete Media	816	96
Serum Starved	506	119

Table 2. Quantification of the total number of cells and the number of ChAT-GFP+ cells in each condition. Cell count is the summation of 10 fields of view from three biological replicates.

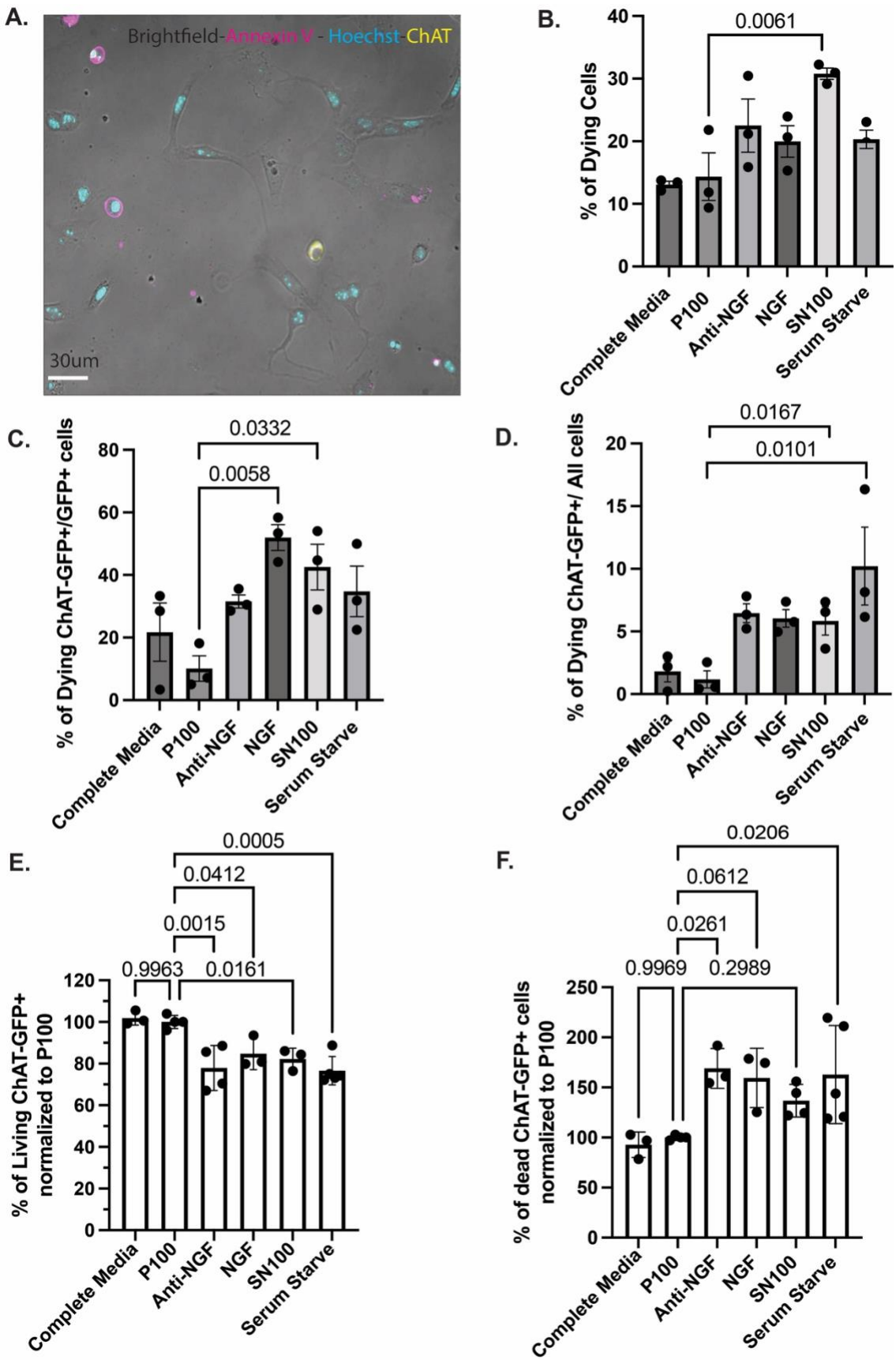
A.
Brightfield-Annexin V - Hoechst-ChAT
30um
B.
% of Dying Cells
0.0061
Complete Media
P100
Anti-NGF
NGF
SN100
Serum Starve
C.
% of Dying ChAT-GFP+/GFP+ cells
0.0332
0.0058
D.
% of Dying ChAT-GFP+/ All cells
0.0167
0.0101
E.
% of Living ChAT-GFP+ normalized to P100
0.0005
0.0412
0.0015
0.9963
0.0161
F.
% of dead ChAT-GFP+ cells normalized to P100
0.0206
0.0612
0.0261
0.9969
0.2989

Figure 2. EVs promote the survival of spinal cord neurons

A. Image of one field of view from spinal cord cultures 24 hours after P100 EV addition. Annexin V (magenta) labels apoptotic membranes, Hoechst (cyan) labels cell nuclei for total cell counts, and transgenic expression of ChAT-GFP (yellow) labels cholinergic motor neurons. **B-D.** Percentage of dying cells by live microscopy based on Annexin V staining per each condition. Shown is mean ± SEM for three biological replicates. P values are indicated above the pairwise brackets. **E-F.** Percentage of living or dead cells determined by flow cytometric analysis of TO-PRO-3 staining. Shown is mean ± SEM for three biological replicates. P values are indicated above the pairwise brackets.

Chapter V. Conclusion and Future Directions

This chapter will conclude my thesis work by summarizing the key findings of the study as stated by the research aims. I will place my work in the broader context of the field of extracellular vesicle biology and the field of neurotrophins. Herein, I will discuss any limitations and weakness of the study. Finally, I will conclude with present recommendations for future research on this work.

The key findings of this work are outlined below:

I. Rigorous characterization EVs derived from primary sympathetic cultures in accordance with internationally recognized field guidelines.
II. Exploration of EVs as a fate of retrogradely trafficked cargo in peripheral neurons.
III. Discovery of EVs as a novel fate of TrkA receptor trafficking.
IV. Determination of the regulation of sympathetic-derived EVs and TrkA positive EVs.
V. Implications of the functional significance of extracellular vesicles in recipient cells.

I. Rigorous application of MISEV guidelines to sympathetic-derived EVs

In this work, I set out to characterize EVs from the developing peripheral nervous system in accordance with field guidelines set forth by the International Society for Extracellular Vesicle's position paper entitled " Minimal Information for the Study of Extracellular Vesicles[77]." International standards were established to ensure the rigor and reproducibility of the studies examining EVs. Because EVs are small and difficult to detect both *in vitro* and *in vivo* it is essential that studies involving these particles ensure that there are multiple methods to detect and characterize them. In Mason et al 2023

(Chapter III), I characterize EVs using nanoparticle tracking analysis (NTA), immunoblotting, and Cryo-transmission electron microscopy (Cryo-EM). I analyze two different fractions of EVs, the P20 and P100 fraction. I find that the P20 fraction contains more EVs and other nanoparticles compared to the P100 fraction based on NTA analysis and cryo-EM. Furthermore, both fractions contain canonical EVs markers as evidence by immunoblot. There does seem to be some partitioning of EVs markers into the different fractions as evidence by more intense ALIX banding in the P100 fraction compared to the P20 fraction. Why would certain EV markers be partitioned to specific subsets of EVs? One possibility is that specific EV cargos are packaged into specific subtypes of EVs depending on the cell of origin, biogenic pathway origin (i.e., from an endosome or from the plasma membrane), or downstream function of the EV. More details and examples of these different subtypes of EVs are detailed in Chapter II. This is the first full characterization of EVs derived from cultured sympathetic neurons to the best of my knowledge. This finding builds on previous work by Escudero et al, describing EVs as a fate the neurotrophin p75NTR in sympathetic neurons[164].

Limitations

The main limitation of this finding is the inability to decipher subtypes of EVs based on their cell of origin or biogenic mechanism. EVs assessed in this study were derived from primary sympathetic cells which were harvested from mouse superior cervical ganglia (SCG). The SCG contains many different cells including, neurons, small intensely fluorescent interneurons, glia, endothelial cells, and other cell types. An anti-mitotic cell division inhibitor was not used in these studies because the drug normally used, AraC would result in culture loss when used with both the serum-free media and

the compartmentalized chambers necessary for these studies. There is another anti-mitotic inhibitor that might be compatible with serum-free media and microfluidic devices called, Aphidicolin, but it was not available to me during these experiments. Another limitation of this finding was the inability to quantify the protein content in these EVs by immunoblot. It was not feasible to perform a BCA or Bradford analysis in order to load equal concentrations of total protein into the protein gels due to the low yield of EVs from the starting conditioned media. Additionally, it was difficult to compare the quantity of protein across different fractions because there is currently no universal marker for EVs. Therefore, there was no loading control that could be implemented across the sample fractions to assess protein quantity. Fortunately, a qualitative analysis of canonical EV markers was sufficient to identify these fractions as EVs per MISEV standards.

Future directions

There are increasingly better and more accurate technologies becoming available for assessing EVs. Imaging Flow Cytometry is a tool that would allow for sizing and fluorescence-based phenotyping of EVs based on their surface markers[178]. Additionally, the ExoView R100 platform uses antibody-capture on a microarray chip to isolate EVs. This system allows for sizing, concentration, co-localization of tetraspanins and the ability to isolate EVs of interest using a flex-capture antibody against your protein of interest[177]. Lastly, this system allows for unprocessed conditioned media as the starting material thereby decreasing bias and loss of material that comes from other isolation methods. To fully characterize the cargo present on/in sympathetic-derived EVs a proteomic analysis could be utilized. Lastly, these experiments could be repeated

using an anti-mitotic cell division inhibitor in the cultures to select for only the EVs derived from a neuronal population.

II. Extracellular vesicles as a mechanism of intercellular communication of long-distance retrogradely trafficked cargo in peripheral neurons

Currently, research on EVs is focused on investigating their function, content, uptake and regulation[214,215]. EVs are a novel modality of intercellular signaling both locally and over long distances within the body[216–218]. More systemic circulation of EVs generally occurs through the vasculature allowing EVs to carry cargo from one organ or tissue system to another[217,218]. An alternative pathway for the transport of long-distance cargo is utilizing the endosomal system and then packaging the trafficked cargo for secretion in EVs[184,211]. Peripheral neurons are the ideal model system to test this pathway as they are highly polarized cells with axons extending millimeters and in some cases meters out from the cell body.

In my study, I used the lectin, wheat germ agglutinin, tagged with a fluorescent protein to visualize the long-distance trafficking of WGA. I grew neurons in compartmentalized chambers and added WGA only to the distal axon chambers. I found, using fluorescent NTA, that distally fed WGA was packaged into EVs. These WGA+ EVs contained WGA that had been retrogradely trafficked back from the axons. Furthermore, *in vivo*, I injected WGA into the salivary glands of mouse pups and tracked its transport from the axon terminals of postganglionic neurons to the spinal cord (Appendix II).

Limitations

While my work establishes that EV cargo can be derived from a distant source and subsequently packaged into EVs *in vitro*, my conclusion would be better supported if another method was used to confirm WGA on EVs besides NTA. Furthermore, it is difficult to ascertain what proportion of neurons are transporting retrogradely trafficked cargo as not all neurons in my compartmentalized devices sent axons through the microgrooves to the axonal chamber. Lastly, my *in vivo* experiments are limited by a secondary method to confirm that the WGA is indeed traversing the synapse on EVs. WGA reliably and robustly traverses the synapse and is therefore used widely as a circuit tracer in neuroscience. It is possible that one of the mechanisms by which WGA traverses the synapse is through the use of EVs. The surface glycans present on EVs contain a lot of sialic acid residues that readily bind WGA[185,219,220]. Thus, the EV surface might serve as a vehicle for the trafficking of WGA across synapses.

Future Directions

Open questions remain regarding long-distance transport of EVs including: 1. Which cargos are competent to undergo long distance transport and packaging in EVs? 2. What regulates cargo packaging into EVs and their subsequent secretion? In the context of my work on TrkA questions include: 1. Does TrkA get secreted on EVs and hop the synapse *in vivo*? 2. Which cells internalize TrkA? I have attempted to answer some of these questions. Evidence for TrkA traversing the synapse *in vivo* has been shown preliminarily by Dr. Austin Keeler in the Deppmann lab; however, I have been unable to successfully replicate this. In addition, we cannot detect TrkA in spinal cords using mass cytometry, *in vivo*. We have however, shown that TrkA can be detected in spinal cord cultures grown *in vitro* and treated with postganglionic neuron derived EVs.

New protocols have been published improving methods for extracting EVs from tissue[221]. It is reasonable that future progress can be made in answering these questions.

Lastly, I have made progress in establishing an experimental design to determine which cell types take up sympathetic EVs *in vitro* (see Appendix II). Fulfillment of these experiments in sympathetic cells would answer which cell types are internalizing EVs and how many EVs are being internalized. Others, in different model systems are beginning to study the uptake of EVs *in vitro*[156] as well as deciphering which cargos are selected for packaging into EVs[127,128,170].

III. Neurotrophins and their trafficking fates during development.

The trafficking of NGF begins with its internalization into a signaling and transport competent endosome at the distal tips of axons. This endocytosis is triggered upon ligand (i.e. NGF) binding to the TrkA receptor resulting in trans-autophosphorylation of tyrosine residues on the intracellular domain of TrkA[28,29]. This process recruits effectors that help internalize the NGF-TrkA receptor complex into a signaling endosome (SE). This SE can signal locally in the distal axons to initiate local mRNA translation and facilitate axonal growth [11,175,222]. The SE also undergoes long distance retrograde trafficking to the cell body[27]. Once in the cell body the SE can undergo a variety of fates. 1. It can be trafficked to the dendrites to promote post-synaptic maturation and PSD clustering[64]. 2. It can initiate survival signaling through transcriptional upregulation[223]. 3. It can undergo recycling to the cell body plasma membrane, a process called retrograde transcytosis[51,52]. 4. It can tune the cells responsiveness to NGF by routing naïve TrkA

receptors to be trafficked anterogradely to the distal axon tips[12,167]. 5. Lastly, the SE can fuse with the lysosome thus terminating its signaling capacity.

My work has focused on describing a new fate for TrkA and the TrkA signaling endosome, namely its incorporation into and secretion on EVs. EVs are extracellular compartments, but one of their preceding compartments are endosomes. The TrkA signaling endosome has been shown to exist as this biogenic compartment, the multivesicular body (MVB)[38]. Using neurons grown in a compartmentalized chamber and derived from a *TrkA*$^{FLAG/FLAG}$ transgenic mouse line, I was able track and label the TrkA receptor. Furthermore, I used fluorescent nanoparticle tracking analysis and Western blot, to show that the TrkA receptor is indeed secreted on EVs.

Limitations

There are several limitations to this study. The biggest challenge in working with EVs is the inability to separate out specific subtypes of EVs both reliably and robustly. Current methods include bead-based precipitation against an EV surface protein of interest or nanoFACS based sorting. These technologies rely on surface labeling of EVs and therefore are not useful for probing luminal content of EVs. Additionally, these technologies are still being adapted for nanoscale EV work and therefore are more easily implemented in cell model systems where the quantity of EVs secreted is much higher. The postganglionic cultures used in my system had total cell counts of around 100,000 neurons, much lower than other primary or transformed cell line cultures. The low number of neurons in the cultures resulted in a lower number of secreted EVs. When accounting for loss from EV isolation methods, it became difficult to separate out subtypes of EVs and still reliably detect EVs by Western blot or NTA. Therefore, the

TrkA on EVs detected by Western Blot from my work consists of all TrkA secreted by the cell and not just retrogradely transported TrkA. To overcome this, I used the fluorescent NTA assay to reliably detect retrogradely trafficked TrkA. Lastly, I wanted to confirm the presence of retrogradely trafficked TrkA using another method namely, immuno-gold labeling Cryo-EM. This work is still ongoing.

Future Directions

There are many open questions regarding the fate of the neurotrophin receptor, TrkA, once it reaches the cell body. It is still unknown when TrkA begins to associate with CD63 and other EV markers. One study showed co-localized of TrkA with CD63 in the proximal axon of sympathetic neurons, but further characterization wasn't undertaken [38]. Several experiments can be done to further investigate these associations. Firstly, using a triple transgenic mouse line expressing CD63-emGFP$^{loxP/stop/loxP}$, TrkA$^{FLAG/FLAG}$ and a DBH-Cre recombinase, we can selectively express CD63-GFP in sympathetic neurons while simultaneously tracking TrkA trafficking. These cells could be grown in compartmentalized cultures and anti-FLAG antibody can be added to the distal axon chamber. Using this experimental paradigm, the following questions could be answered: 1. How many FLAG-TrkA endosomes are CD63-GFP+? 2. How many TrkA+/CD63+ endosomes are in the dendrites? 3. Does CD63 colocalize with TrkA in the axons? Variations on this experiment could include adding different fluorescently labeled endosomal cargos such as transferrin or BSA to determine whether these cargos are sorted with or independently from TrkA. Additionally, lysosome disrupters such as bafilomycin A or leupeptin could be added to

examine if there is an increased sorting and secretion of EVs when lysosomal flux is perturbed.

IV. Regulation of sympathetic-derived and TrkA+ EVs

Regulating the trafficking of TrkA SE depends on the effectors and adaptors recruited to the phosphorylated tyrosine residues of the receptor's intracellular domain after NGF binding. These effectors initiate activation of a series of signaling pathways, Ras/MAPK, PI3K, and PLC-γ, within the cell [189,190,224]. These different signaling pathways differentially influence the trafficking of the TrkA SE. Internalization of the TrkA receptor after surface activation depends on PLC-γ signaling [25,189]. Meanwhile, PI3K signaling is necessary for the initiation of retrograde transport [191]. Other Trk receptors are similarly influenced by these downstream signaling effectors and coordinating Rabs.

My findings suggest that inhibition of PI3K signaling in the cell body of sympathetic neurons influences the production of TrkA+ EVs without affecting total EV secretion. Similarly, PLC-ɣ inhibition in the cell body also reduces $TrkA^{+}$ EVs, while simultaneously causing a marked increase in the total number of EVs released. Lastly, inhibition of MAPK does not cause any significant decrease in either the total number or TrkA+ number of EVs. It is clear that inhibiting these pathways downstream of TrkA activation affects TrkA+ EV numbers, but it is unclear at which stage, sorting or secretion, these drugs are affecting the TrkA receptor. Ultimately, the significance of these results has yet to be investigated, but experiments probing both biogenesis as well as functional outputs in recipient cells would be beneficial.

Limitations

While I showed that certain signaling pathways downstream of TrkA activation can affect the total number of TrkA+ EVs that are secreted I did not answer which step precisely is being regulated by the pathway in question. Furthermore, addition of these inhibitors to different compartments of the cell (i.e., dendrites, axons) might affect the trafficking and packaging of the TrkA receptors into EVs. Temporally manipulating the duration of drug application might also perturb TrkA EV biogenesis at different stages. These are widely acting inhibitors that affect many other receptors, not just TrkA, that utilize these signaling pathways throughout the cell.

Future Directions

To further assess mechanistically how these inhibitors are affecting TrkA EV secretion and/or packaging one could use live imaging to track TrkA and CD63 simultaneously. Using cells from the triple transgenic *CD63-emGFP$^{loxP/stop/loxP}$; TrkA$^{FLAG/FLAG}$; DBH^{Cre}* mouse line grown in compartmentalized devices one could add the different inhibitors to either the cell body or distal axon compartment after addition of anti-FLAG antibody and observe the trafficking and partitioning of CD63 and TrkA. This experimental paradigm can be further employed to test other drug conditions that inhibit or encourage EV release to probe and understand the biogenesis and secretion of TrkA EVs. Potential pathways of investigation include depolarizing the neurons using KCL to determine if neuronal activity could increase EV secretion. Alternatively, the neutral sphingomyelinase inhibitor GW4869 could be used to inhibit exosome formation, in an attempt to elucidate the biogenic compartment of TrkA EVs. One caveat is this drug does not perfectly inhibit all exosome biogenesis pathways just those mediated by

neutral sphingomyelinase. Experimental modulation of TrkA+ EV secretion could include the use of K252a to broadly impact tyrosine kinases. Lastly, an NGF deprivation course could be completed to determine whether NGF withdrawal affects TrkA+ EV secretion. This finding would be instrumental in understanding the contextual purpose of releasing TrkA+ EVs during neuronal development and circuit establishment. Ultimately the goal is to determine the molecular players that regulate TrkA EV release in a developmental context.

V. Functional significance of extracellular vesicles in recipient cells

During embryonic and early postnatal development more neurons are produced than will ultimately survive to adulthood [62,66,225–227]. Proper wiring of the nervous system relies on coordinated cell migration, axon pathfinding and defasciculation of axons as they reach their final targets. The intricate process of wiring the nervous system is coordinated both spatially and temporally, in part by guidance factors and growth cues [228]. In the model system used in my research, postganglionic neurons achieve proper innervation and subsequent survival by responding to NGF that is secreted by the target organs[229]. It is now well understood that NGF binds to the TrkA receptor at the axon tips and is incorporated into a signaling endosome. This SE is retrogradely trafficked back to the neuron's cell body where it elicits signaling that results in the transcriptional upregulation of genes important for neuronal survival and innervation. These postganglionic neurons are the first to die off if they don't receive adequate amounts of neurotrophic support. Their upstream preganglionic partners will also die off as the circuit prunes itself; however, the mechanism underlying which preganglionic neurons

die and which do not have not been fully elucidated. Interestingly, the preganglionic visceral motor neurons do not express the TrkA receptor, nor do they have access to NGF. Furthermore, the decision to live or die is not solely dictated by synaptic activity between the pre- and post-synaptic neuron. In an interesting preprint, researchers developed a mosaic model of sympathetic ganglia that contained synaptically active and synaptically silent (KO of an acetylcholine receptor subunit) sympathetic neurons *in vivo*. They found that converging inputs from preganglionic neurons do not require postsynaptic activity to refine as long the silenced postsynaptic postganglionic neurons share a target with a synaptically active postganglionic neuron [230]. This study suggests that something secreted by the target might being influencing the development and refinement of preganglionic inputs.

In my work, I hypothesized that distally derived retrogradely trafficked TrkA secreted from the somatodendritic domain of postganglionic neurons could be internalized by their upstream preganglionic partners to promote survival. I harvested and dissociated spinal cord neurons from ChAT-GFP expressing mice in order to visualize motor neurons and added postganglionic EVs to these cells. I then assessed survival using both microscopy and flow cytometry. I showed that spinal cord cells cultured in the presence of EVs from the P100 fraction reduces the number of dying neurons after 24 hours. Importantly, this effect is ablated when I incubate the P100 EVs with an anti-NGF antibody before addition to the cultures. This control suggests that NGF-TrkA signaling is important for survival or that the EVs need to be internalized in order to affect the recipient's survival.

Limitations

The main limitation of this study is that the preganglionic motor neuron population is relatively small with about a 1:4 ratio of preganglionic to postganglionic cells in the rodent superior cervical ganglia [203]. This makes it difficult dissect and culture enough preganglionic neurons to study their survival. Additionally, these preganglionic neurons are visceral motor neurons therefore their primary neurotransmitter is acetylcholine. However, they do not synapse onto muscles, but instead onto postganglionic neurons. While recent transcriptomic analyses of these preganglionic neurons have been conducted it is still difficult to identify them using a specific cell identity marker [202,231,232]. Because of both low cell numbers and lack of a single specific marker for these preganglionic neurons it is difficult to sort and culture just the preganglionic neurons. Therefore, I used a ChAT-GFP mouse to attempt to classify motor neurons as one subtype of cells that responded with a survival phenotype after EV application.

Another limitation of this study is deciphering which population of EVs are eliciting the survival phenotype and what cargos these EVs contain. Based on my study, incubating the P100 EV fraction with an anti-NGF antibody was enough to ablate survival signaling. It is unknown, if this is because the EVs are unable to be internalized due to steric hindrance when an anti-NGF antibody is applied or if the anti-NGF antibody is acting as a neutralizing antibody thus binding up NGF and preventing activation of the TrkA receptor and therefore downstream survival signaling in the recipient cell. Furthermore, it might be another cargo present on or in these EVs that is actually responsible for the survival phenotype. Addition of an anti-NGF antibody is preventing delivery of this subtype of EV to the recipient cell.

The final limitation of this finding is the assays used to determine survival. Flow cytometry allows for robust counting of cells; however, the cells need to be dissociated into a single cell suspension to create a laminar flow through the cytometry cell. This dissociation step can damage the plasma membrane of otherwise healthy cells and create a false positive of Annexin V binding to these cells. I attempted to mitigate this disruption by incubating the cells in serum for 15 minutes prior to cytometric analysis. Additionally, I conducted a survival assay using live epifluorescence imaging. This technique only allowed me to investigate 10 fields of view per condition and therefore a lot fewer cells were counted. Together, these two survival assays utilizing different techniques allows for a much clearer understanding of the functional biology of these EVs.

Future Directions

Additional controls to further elucidate the role of TrkA+ EVs on promoting the survival of spinal cord neurons could be to incubate the EVs with a non-specific antibody to determine if the anti-NGF antibody is actually blocking TrkA function or its just preventing internalization due to steric hindrance. Other studies have incubated fluorescently labeled EVs with an anti-CD9 antibody and this was sufficient enough to prevent uptake of these EVs as examined by flow cytometry[208]. Additionally, uptake could be blocked or reduced by decreasing the temperature at which the spinal cord cells are incubated with the EVs. If the EVs still support spinal cord cell survival without internalization than a potential explanation might be that these sympathetic EVs bind and transmit their signal via external plasma membrane bound receptors. However, this

experiment has some caveats as 4°C might also reduce intracellular metabolism and signaling downstream of EV surface binding and signal transmission.

An alternative explanation for the survival signaling provided by EVs might be the result of synergistic signaling between another neurotrophin receptor, p75NTR, and TrkA. It is possible that both TrkA and p75NTR could co-isolate together on EVs or both TrkA and P75NTR might heterodimerize and be secreted on the same EV[233,234]. Alternatively, TrkA and p75NTR could be secreted in distinct subpopulations of EVs with divergent functions. Lastly, to establish a more complete proteomic understanding of all the cargos that are present in these sympathetic-derived EVs mass spectrometry could be utilized. Specific experiments that would be interesting to conduct include a proteomic analysis on EVs derived from neuron only cultures versus EVs derived from mixed culture conditions. Additionally, by performing quantitative proteomics using TMT LC-MS3 (tandem mass tag liquid chromatography mass spectrometry 3), one could compare EVs derived from NGF treated cultures versus NGF deprived cultures. This proteomic analysis would allow one to quantify differences in protein enrichment between these different groups. If for instance, NGF deprivation reduces TrkA in EVs then those EVs could be added to cultures to assay their effectiveness on promoting survival. Additionally, proteomic analysis of EVs would provide a more complete appreciation of all the cargos present in sympathetic EVs. My speculation is that there are other important cargos that might work independently or synergistically to promote the survival of spinal cord neurons.

Lastly, it is important to decipher the mechanism underlying spinal cord survival signaling after sympathetic EV incubation. The main technique that could be used to

assess the signaling changes in spinal cord neurons in response to EVs is signaling mass cytometry (CyTOF). Signaling CyTOF allows for the extracellular and intracellular labeling of protein targets of interest. A panel of antibodies can be designed to probe both cell identity as well as proteins involved in signaling pathways. I developed a preliminary panel to assess signaling changes in spinal cord neurons after incubation with EVs and conducted preliminary experiments as proof of concept. Completion of these studies would further elucidate the downstream signaling pathways activated by EVs and shed more understanding on the type of cargos that are triggering these responses.

The study of extracellular vesicles is currently a burgeoning field and while it is accepted that all cells have the capacity to secrete EVs their purpose and function outside of their cell of origin has been poorly characterized. This is due, in part, to the heterogeneity of these EV as well as the lack of tools to properly isolate, assess, and track these vesicles. My work has established the existence of neurotrophic EVs that influence the survival of spinal cord motor neurons. Additionally, I have characterized a novel pathway for trafficking of the neurotrophin receptor, TrkA. While this study had limitations, the full implications and impact of this work are yet to be discovered. Future research in this area will further inform our understanding of neurotrophic signaling and intercellular communication.

References

1. Davies, A. The Neurotrophic Hypothesis: Where does it stand? *Philos. Trans. R. Soc. Lond. B, Biol. Sci.* (1996).
2. Levi-Montalcini, R. & Hamburger, V. Selective growth stimulating effects of mouse sarcoma on the sensory and sympathetic nervous system of the chick embryo. *J. Exp. Zool.* **116,** 321–361 (1951).
3. Levi-Montalcini, R. & Hamburger, V. A diffusible agent of mouse sarcoma, producing hyperplasia of sympathetic ganglia and hyperneurotization of viscera in the chick embryo. *J. Exp. Zool.* **123,** 233–287 (1953).
4. Cohen, S. & Levi-Montalcini, R. A NERVE GROWTH-STIMULATING FACTOR ISOLATED FROM SNAKE VENOM. *Proc. Natl. Acad. Sci. USA* **42,** 571–574 (1956).
5. Levi-Montalcini, R. & Booker, B. Destruction of the sympathetic ganglia in mammals by an antiserum to a nerve-growth protein. *Proc. Natl. Acad. Sci. USA* **46,** 384–391 (1960).
6. Levi-Montalcini, R. & Booker, B. Excessive growth of the sympathetic ganglia evoked by a protein isolated from mouse salivary glands. *Proc. Natl. Acad. Sci. USA* **46,** 373–384 (1960).
7. Nishino, J. *et al.* Gfrα3, a component of the artemin receptor, is required for migration and survival of the superior cervical ganglion. *Neuron* **23,** 725–736 (1999).
8. Maisonpierre, P. C. *et al.* Neurotrophin-3: a neurotrophic factor related to NGF and

BDNF. *Science* **247,** 1446–1451 (1990).

9. Long, J. B., Jay, S. M., Segal, S. S. & Madri, J. A. VEGF-A and Semaphorin3A: modulators of vascular sympathetic innervation. *Dev. Biol.* **334,** 119–132 (2009).
10. Honma, Y. *et al.* Artemin is a vascular-derived neurotropic factor for developing sympathetic neurons. *Neuron* **35,** 267–282 (2002).
11. Kuruvilla, R. *et al.* A neurotrophin signaling cascade coordinates sympathetic neuron development through differential control of TrkA trafficking and retrograde signaling. *Cell* **118,** 243–255 (2004).
12. Ascaño, M., Richmond, A., Borden, P. & Kuruvilla, R. Axonal targeting of Trk receptors via transcytosis regulates sensitivity to neurotrophin responses. *J. Neurosci.* **29,** 11674–11685 (2009).
13. Makita, T., Sucov, H. M., Gariepy, C. E., Yanagisawa, M. & Ginty, D. D. Endothelins are vascular-derived axonal guidance cues for developing sympathetic neurons. *Nature* **452,** 759–763 (2008).
14. Raper, J. & Mason, C. Cellular strategies of axonal pathfinding. *Cold Spring Harb. Perspect. Biol.* **2,** a001933 (2010).
15. Sutter, A., Riopelle, R. J., Harris-Warrick, R. M. & Shooter, E. M. Nerve growth factor receptors. Characterization of two distinct classes of binding sites on chick embryo sensory ganglia cells. *J. Biol. Chem.* **254,** 5972–5982 (1979).
16. Saragovi, H. U. *et al.* A TrkA-selective, fast internalizing nerve growth factor-antibody complex induces trophic but not neuritogenic signals. *J. Biol. Chem.* **273,** 34933–34940 (1998).
17. Huang, E. J. & Reichardt, L. F. Trk receptors: roles in neuronal signal transduction.

Annu. Rev. Biochem. **72,** 609–642 (2003).

18. Huang, E. J. & Reichardt, L. F. Neurotrophins: roles in neuronal development and function. *Annu. Rev. Neurosci.* **24,** 677–736 (2001).
19. Martin-Zanca, D., Barbacid, M. & Parada, L. F. Expression of the trk proto-oncogene is restricted to the sensory cranial and spinal ganglia of neural crest origin in mouse development. *Genes Dev.* **4,** 683–694 (1990).
20. Smeyne, R. J. *et al.* Severe sensory and sympathetic neuropathies in mice carrying a disrupted Trk/NGF receptor gene. *Nature* **368,** 246–249 (1994).
21. Campenot, R. B. Local control of neurite development by nerve growth factor. *Proc. Natl. Acad. Sci. USA* **74,** 4516–4519 (1977).
22. Howe, C. L., Valletta, J. S., Rusnak, A. S. & Mobley, W. C. NGF Signaling from Clathrin-Coated Vesicles. *Neuron* **32,** 801–814 (2001).
23. Atwal, J. K., Massie, B., Miller, F. D. & Kaplan, D. R. The TrkB-Shc Site Signals Neuronal Survival and Local Axon Growth via MEK and PI3-Kinase. *Neuron* **27,** 265–277 (2000).
24. Zhou, F.-Q., Zhou, J., Dedhar, S., Wu, Y.-H. & Snider, W. D. NGF-induced axon growth is mediated by localized inactivation of GSK-3beta and functions of the microtubule plus end binding protein APC. *Neuron* **42,** 897–912 (2004).
25. Bodmer, D., Ascaño, M. & Kuruvilla, R. Isoform-specific dephosphorylation of dynamin1 by calcineurin couples neurotrophin receptor endocytosis to axonal growth. *Neuron* **70,** 1085–1099 (2011).
26. Howe, C. L. & Mobley, W. C. Signaling endosome hypothesis: A cellular mechanism for long distance communication. *J. Neurobiol.* **58,** 207–216 (2004).

27. Howe, C. L. & Mobley, W. C. Long-distance retrograde neurotrophic signaling. *Curr. Opin. Neurobiol.* **15,** 40–48 (2005).

28. Grimes, M. L. *et al.* Endocytosis of activated TrkA: evidence that nerve growth factor induces formation of signaling endosomes. *J. Neurosci.* **16,** 7950–7964 (1996).

29. Huang, C. S. *et al.* Nerve growth factor signaling in caveolae-like domains at the plasma membrane. *J. Biol. Chem.* **274,** 36707–36714 (1999).

30. Hosang, M. & Shooter, E. M. The internalization of nerve growth factor by high-affinity receptors on pheochromocytoma PC12 cells. *EMBO J.* **6,** 1197–1202 (1987).

31. Stenmark, H. Rab GTPases as coordinators of vesicle traffic. *Nat. Rev. Mol. Cell Biol.* **10,** 513–525 (2009).

32. Grosshans, B. L., Ortiz, D. & Novick, P. Rabs and their effectors: achieving specificity in membrane traffic. *Proc. Natl. Acad. Sci. USA* **103,** 11821–11827 (2006).

33. Wilson, J. M. *et al.* EEA1, a tethering protein of the early sorting endosome, shows a polarized distribution in hippocampal neurons, epithelial cells, and fibroblasts. *Mol. Biol. Cell* **11,** 2657–2671 (2000).

34. Delcroix, J.-D. *et al.* NGF signaling in sensory neurons. *Neuron* **39,** 69–84 (2003).

35. Valdez, G. *et al.* Trk-signaling endosomes are generated by Rac-dependent macroendocytosis. *Proc. Natl. Acad. Sci. USA* **104,** 12270–12275 (2007).

36. Deinhardt, K. *et al.* Rab5 and Rab7 control endocytic sorting along the axonal retrograde transport pathway. *Neuron* **52,** 293–305 (2006).

37. Saxena, S., Bucci, C., Weis, J. & Kruttgen, A. The small GTPase Rab7 controls the endosomal trafficking and neuritogenic signaling of the nerve growth factor receptor TrkA. *J. Neurosci.* **25,** 10930–10940 (2005).
38. Ye, M., Lehigh, K. M. & Ginty, D. D. Multivesicular bodies mediate long-range retrograde NGF-TrkA signaling. *Elife* **7,** (2018).
39. Hanafusa, H. *et al.* LRRK1 phosphorylation of Rab7 at S72 links trafficking of EGFR-containing endosomes to its effector RILP. *J. Cell Sci.* **132,** (2019).
40. Heerssen, H. M., Pazyra, M. F. & Segal, R. A. Dynein motors transport activated Trks to promote survival of target-dependent neurons. *Nat. Neurosci.* **7,** 596–604 (2004).
41. Bhattacharyya, A. *et al.* High-resolution imaging demonstrates dynein-based vesicular transport of activated Trk receptors. *J. Neurobiol.* **51,** 302–312 (2002).
42. Zhang, K. *et al.* Defective axonal transport of Rab7 GTPase results in dysregulated trophic signaling. *J. Neurosci.* **33,** 7451–7462 (2013).
43. Turegano-Lopez, M., Santuy, A., DeFelipe, J. & Merchan-Perez, A. Size, shape, and distribution of multivesicular bodies in the juvenile rat somatosensory cortex: A 3D electron microscopy study. *Cereb. Cortex* **30,** 1887–1901 (2020).
44. Philippidou, P. *et al.* Trk retrograde signaling requires persistent, Pincher-directed endosomes. *Proc. Natl. Acad. Sci. USA* **108,** 852–857 (2011).
45. Claude, P., Hawrot, E., Dunis, D. A. & Campenot, R. B. Binding, internalization, and retrograde transport of 125I-nerve growth factor in cultured rat sympathetic neurons. *J. Neurosci.* **2,** 431–442 (1982).
46. Tsukita, S. & Ishikawa, H. The movement of membranous organelles in axons.

Electron microscopic identification of anterogradely and retrogradely transported organelles. *J. Cell Biol.* **84,** 513–530 (1980).

47. Sandow, S. L. *et al.* Signalling organelle for retrograde axonal transport of internalized neurotrophins from the nerve terminal. *Immunol. Cell Biol.* **78,** 430–435 (2000).
48. Weible, M. W. & Hendry, I. A. What is the importance of multivesicular bodies in retrograde axonal transport in vivo? *J. Neurobiol.* **58,** 230–243 (2004).
49. Von Bartheld, C. S. & Altick, A. L. Multivesicular bodies in neurons: distribution, protein content, and trafficking functions. *Prog. Neurobiol.* **93,** 313–340 (2011).
50. Altick, A. L., Baryshnikova, L. M., Vu, T. Q. & von Bartheld, C. S. Quantitative analysis of multivesicular bodies (MVBs) in the hypoglossal nerve: evidence that neurotrophic factors do not use MVBs for retrograde axonal transport. *J. Comp. Neurol.* **514,** 641–657 (2009).
51. Suo, D. *et al.* Coronin-1 is a neurotrophin endosomal effector that is required for developmental competition for survival. *Nat. Neurosci.* **17,** 36–45 (2014).
52. Barford, K. *et al.* Transcytosis of TrkA leads to diversification of dendritic signaling endosomes. *Sci. Rep.* **8,** 4715 (2018).
53. Rodrigues, M. L. *et al.* Vesicular polysaccharide export in Cryptococcus neoformans is a eukaryotic solution to the problem of fungal trans-cell wall transport. *Eukaryotic Cell* **6,** 48–59 (2007).
54. Tatischeff, I. *et al.* Dictyostelium discoideum cells shed vesicles with associated DNA and vital stain Hoechst 33342. *Cell Mol. Life Sci.* **54,** 476–487 (1998).
55. Regente, M. *et al.* Vesicular fractions of sunflower apoplastic fluids are associated

with potential exosome marker proteins. *FEBS Lett.* **583,** 3363–3366 (2009).

56. Chargaff, E. & West, R. The biological significance of the thromboplastic protein of blood. *J. Biol. Chem.* **166,** 189–197 (1946).

57. Pan, B. T., Teng, K., Wu, C., Adam, M. & Johnstone, R. M. Electron microscopic evidence for externalization of the transferrin receptor in vesicular form in sheep reticulocytes. *J. Cell Biol.* **101,** 942–948 (1985).

58. Harding, C., Heuser, J. & Stahl, P. Receptor-mediated endocytosis of transferrin and recycling of the transferrin receptor in rat reticulocytes. *J. Cell Biol.* **97,** 329–339 (1983).

59. Johnstone, R. M., Adam, M., Hammond, J. R., Orr, L. & Turbide, C. Vesicle formation during reticulocyte maturation. Association of plasma membrane activities with released vesicles (exosomes). *J. Biol. Chem.* **262,** 9412–9420 (1987).

60. Voyvodic, J. T. Development and regulation of dendrites in the rat superior cervical ganglion. *J. Neurosci.* **7,** 904–912 (1987).

61. Forehand, C. J. Density of somatic innervation on mammalian autonomic ganglion cells is inversely related to dendritic complexity and preganglionic convergence. *J. Neurosci.* **5,** 3403–3408 (1985).

62. Lichtman, J. W. & Purves, D. The elimination of redundant preganglionic innervation to hamster sympathetic ganglion cells in early post-natal life. *J. Physiol. (Lond.)* **301,** 213–228 (1980).

63. Rubin, E. Development of the rat superior cervical ganglion: initial stages of synapse formation. *J. Neurosci.* **5,** 697–704 (1985).

64. Sharma, N. *et al.* Long-distance control of synapse assembly by target-derived NGF. *Neuron* **67,** 422–434 (2010).

65. Lehigh, K. M., West, K. M. & Ginty, D. D. Retrogradely Transported TrkA Endosomes Signal Locally within Dendrites to Maintain Sympathetic Neuron Synapses. *Cell Rep.* **19,** 86–100 (2017).

66. Wright, L. L., Cunningham, T. J. & Smolen, A. J. Developmental neuron death in the rat superior cervical sympathetic ganglion: cell counts and ultrastructure. *J Neurocytol* **12,** 727–738 (1983).

67. Schäfer, T., Schwab, M. E. & Thoenen, H. Increased formation of preganglionic synapses and axons due to a retrograde trans-synaptic action of nerve growth factor in the rat sympathetic nervous system. *J. Neurosci.* **3,** 1501–1510 (1983).

68. Snider, W. D. Nerve growth factor enhances dendritic arborization of sympathetic ganglion cells in developing mammals. *J. Neurosci.* **8,** 2628–2634 (1988).

69. Ugolini, G. Specificity of rabies virus as a transneuronal tracer of motor networks: transfer from hypoglossal motoneurons to connected second-order and higher order central nervous system cell groups. *J. Comp. Neurol.* **356,** 457–480 (1995).

70. Klingen, Y., Conzelmann, K.-K. & Finke, S. Double-labeled rabies virus: live tracking of enveloped virus transport. *J. Virol.* **82,** 237–245 (2008).

71. Reardon, T. R. *et al.* Rabies Virus CVS-N2c(ΔG) Strain Enhances Retrograde Synaptic Transfer and Neuronal Viability. *Neuron* **89,** 711–724 (2016).

72. Abrami, L. *et al.* Hijacking multivesicular bodies enables long-term and exosome-mediated long-distance action of anthrax toxin. *Cell Rep.* **5,** 986–996 (2013).

73. Maximova, O. A., Bernbaum, J. G. & Pletnev, A. G. West Nile Virus Spreads

Transsynaptically within the Pathways of Motor Control: Anatomical and Ultrastructural Mapping of Neuronal Virus Infection in the Primate Central Nervous System. *PLoS Negl. Trop. Dis.* **10,** e0004980 (2016).

74. Schwab, M. E., Suda, K. & Thoenen, H. Selective retrograde transsynaptic transfer of a protein, tetanus toxin, subsequent to its retrograde axonal transport. *J. Cell Biol.* **82,** 798–810 (1979).
75. Schwab, M. & Thoenen, H. Selective trans-synaptic migration of tetanus toxin after retrograde axonal transport in peripheral sympathetic nerves: a comparison with nerve growth factor. *Brain Res.* **122,** 459–474 (1977).
76. Rind, H. B., Butowt, R. & von Bartheld, C. S. Synaptic targeting of retrogradely transported trophic factors in motoneurons: comparison of glial cell line-derived neurotrophic factor, brain-derived neurotrophic factor, and cardiotrophin-1 with tetanus toxin. *J. Neurosci.* **25,** 539–549 (2005).
77. Théry, C. *et al.* Minimal information for studies of extracellular vesicles 2018 (MISEV2018): a position statement of the International Society for Extracellular Vesicles and update of the MISEV2014 guidelines. *J Extracell Vesicles* **7,** 1535750 (2018).
78. Pérez-González, R. *et al.* A Method for Isolation of Extracellular Vesicles and Characterization of Exosomes from Brain Extracellular Space. *Methods Mol. Biol.* **1545,** 139–151 (2017).
79. Hill, A. F. Extracellular vesicles and neurodegenerative diseases. *J. Neurosci.* **39,** 9269–9273 (2019).
80. Pistono, C., Bister, N., Stanová, I. & Malm, T. Glia-Derived Extracellular Vesicles:

Role in Central Nervous System Communication in Health and Disease. *Front. Cell Dev. Biol.* **8,** 623771 (2020).

81. Krämer-Albers, E.-M. Extracellular Vesicles at CNS barriers: Mode of action. *Curr. Opin. Neurobiol.* **75,** 102569 (2022).
82. Shen, B., Wu, N., Yang, J.-M. & Gould, S. J. Protein targeting to exosomes/microvesicles by plasma membrane anchors. *J. Biol. Chem.* **286,** 14383–14395 (2011).
83. Cocucci, E. & Meldolesi, J. Ectosomes and exosomes: shedding the confusion between extracellular vesicles. *Trends Cell Biol.* **25,** 364–372 (2015).
84. Nabhan, J. F., Hu, R., Oh, R. S., Cohen, S. N. & Lu, Q. Formation and release of arrestin domain-containing protein 1-mediated microvesicles (ARMMs) at plasma membrane by recruitment of TSG101 protein. *Proc. Natl. Acad. Sci. USA* **109,** 4146–4151 (2012).
85. Muralidharan-Chari, V. *et al.* ARF6-regulated shedding of tumor cell-derived plasma membrane microvesicles. *Curr. Biol.* **19,** 1875–1885 (2009).
86. Antonyak, M. A., Wilson, K. F. & Cerione, R. A. R(h)oads to microvesicles. *Small GTPases* **3,** 219–224 (2012).
87. Huotari, J. & Helenius, A. Endosome maturation. *EMBO J.* **30,** 3481–3500 (2011).
88. Anand, S., Samuel, M., Kumar, S. & Mathivanan, S. Ticket to a bubble ride: Cargo sorting into exosomes and extracellular vesicles. *Biochim. Biophys. Acta Proteins Proteom.* **1867,** 140203 (2019).
89. Henne, W. M., Buchkovich, N. J. & Emr, S. D. The ESCRT pathway. *Dev. Cell* **21,** 77–91 (2011).

90. Juan, T. & Fürthauer, M. Biogenesis and function of ESCRT-dependent extracellular vesicles. *Semin. Cell Dev. Biol.* **74,** 66–77 (2018).

91. Wollert, T. & Hurley, J. H. Molecular mechanism of multivesicular body biogenesis by ESCRT complexes. *Nature* **464,** 864–869 (2010).

92. Tang, S. *et al.* ESCRT-III activation by parallel action of ESCRT-I/II and ESCRT-0/Bro1 during MVB biogenesis. *Elife* **5,** (2016).

93. Colombo, M. *et al.* Analysis of ESCRT functions in exosome biogenesis, composition and secretion highlights the heterogeneity of extracellular vesicles. *J. Cell Sci.* **126,** 5553–5565 (2013).

94. Coulter, M. E. *et al.* The ESCRT-III Protein CHMP1A Mediates Secretion of Sonic Hedgehog on a Distinctive Subtype of Extracellular Vesicles. *Cell Rep.* **24,** 973–986.e8 (2018).

95. Crivelli, S. M. *et al.* Function of ceramide transfer protein for biogenesis and sphingolipid composition of extracellular vesicles. *J Extracell Vesicles* **11,** e12233 (2022).

96. Ferreira, J. V. *et al.* LAMP2A regulates the loading of proteins into exosomes. *Sci. Adv.* **8,** eabm1140 (2022).

97. Wollert, T. *et al.* The ESCRT machinery at a glance. *J. Cell Sci.* **122,** 2163–2166 (2009).

98. Subra, C., Laulagnier, K., Perret, B. & Record, M. Exosome lipidomics unravels lipid sorting at the level of multivesicular bodies. *Biochimie* **89,** 205–212 (2007).

99. Arya, S. B., Chen, S., Jordan-Javed, F. & Parent, C. A. Ceramide-rich microdomains facilitate nuclear envelope budding for non-conventional exosome

formation. *Nat. Cell Biol.* **24,** 1019–1028 (2022).

100. Castro, B. M., Prieto, M. & Silva, L. C. Ceramide: a simple sphingolipid with unique biophysical properties. *Prog. Lipid Res.* **54,** 53–67 (2014).
101. Sezgin, E., Levental, I., Mayor, S. & Eggeling, C. The mystery of membrane organization: composition, regulation and roles of lipid rafts. *Nat. Rev. Mol. Cell Biol.* **18,** 361–374 (2017).
102. Choezom, D. & Gross, J. C. Neutral sphingomyelinase 2 controls exosome secretion by counteracting V-ATPase-mediated endosome acidification. *J. Cell Sci.* **135,** (2022).
103. Fukushima, M. *et al.* StAR-related lipid transfer domain 11 (STARD11)-mediated ceramide transport mediates extracellular vesicle biogenesis. *J. Biol. Chem.* **293,** 15277–15289 (2018).
104. Barman, B. *et al.* VAP-A and its binding partner CERT drive biogenesis of RNA-containing extracellular vesicles at ER membrane contact sites. *Dev. Cell* **57,** 974–994.e8 (2022).
105. Stuffers, S., Sem Wegner, C., Stenmark, H. & Brech, A. Multivesicular endosome biogenesis in the absence of ESCRTs. *Traffic* **10,** 925–937 (2009).
106. Goursot, A., Mineva, T., Bissig, C., Gruenberg, J. & Salahub, D. R. Structure, dynamics, and energetics of lysobisphosphatidic acid (LBPA) isomers. *J. Phys. Chem. B* **114,** 15712–15720 (2010).
107. Hullin-Matsuda, F. *et al.* De novo biosynthesis of the late endosome lipid, bis(monoacylglycero)phosphate. *J. Lipid Res.* **48,** 1997–2008 (2007).
108. Rubinsztein, D. C., Shpilka, T. & Elazar, Z. Mechanisms of autophagosome

biogenesis. *Curr. Biol.* **22,** R29-34 (2012).

109. Kobayashi, T. *et al.* A lipid associated with the antiphospholipid syndrome regulates endosome structure and function. *Nature* **392,** 193–197 (1998).
110. Wubbolts, R. *et al.* Proteomic and biochemical analyses of human B cell-derived exosomes. Potential implications for their function and multivesicular body formation. *J. Biol. Chem.* **278,** 10963–10972 (2003).
111. Laulagnier, K. *et al.* Mast cell- and dendritic cell-derived exosomes display a specific lipid composition and an unusual membrane organization. *Biochem. J.* **380,** 161–171 (2004).
112. Miranda, A. M. *et al.* Neuronal lysosomal dysfunction releases exosomes harboring APP C-terminal fragments and unique lipid signatures. *Nat. Commun.* **9,** 291 (2018).
113. Kobayashi, T. *et al.* Separation and characterization of late endosomal membrane domains. *J. Biol. Chem.* **277,** 32157–32164 (2002).
114. Sobo, K., Chevallier, J., Parton, R. G., Gruenberg, J. & van der Goot, F. G. Diversity of raft-like domains in late endosomes. *PLoS One* **2,** e391 (2007).
115. Le Blanc, I. *et al.* Endosome-to-cytosol transport of viral nucleocapsids. *Nat. Cell Biol.* **7,** 653–664 (2005).
116. Perrin, P. *et al.* Retrofusion of intralumenal MVB membranes parallels viral infection and coexists with exosome release. *Curr. Biol.* (2021). doi:10.1016/j.cub.2021.06.022
117. Gagescu, R. *et al.* The recycling endosome of Madin-Darby canine kidney cells is a mildly acidic compartment rich in raft components. *Mol. Biol. Cell* **11,** 2775–2791

(2000).

118. Palmulli, R. *et al.* CD63 regulates cholesterol storage within endosomes and its distribution via exosomes. *Res. Sq.* (2022). doi:10.21203/rs.3.rs-2194192/v1
119. Möbius, W. *et al.* Recycling compartments and the internal vesicles of multivesicular bodies harbor most of the cholesterol found in the endocytic pathway. *Traffic* **4,** 222–231 (2003).
120. Kobayashi, T. *et al.* Late endosomal membranes rich in lysobisphosphatidic acid regulate cholesterol transport. *Nat. Cell Biol.* **1,** 113–118 (1999).
121. Heisler, F. F. *et al.* Muskelin Coordinates PrPC Lysosome versus Exosome Targeting and Impacts Prion Disease Progression. *Neuron* **99,** 1155–1169.e9 (2018).
122. Song, L. *et al.* KIBRA controls exosome secretion via inhibiting the proteasomal degradation of Rab27a. *Nat. Commun.* **10,** 1639 (2019).
123. Ashley, J. *et al.* Retrovirus-like Gag Protein Arc1 Binds RNA and Traffics across Synaptic Boutons. *Cell* **172,** 262–274.e11 (2018).
124. Pastuzyn, E. D. *et al.* The Neuronal Gene Arc Encodes a Repurposed Retrotransposon Gag Protein that Mediates Intercellular RNA Transfer. *Cell* **172,** 275–288.e18 (2018).
125. Buzas, E. I. Opportunities and challenges in studying the extracellular vesicle corona. *Nat. Cell Biol.* (2022). doi:10.1038/s41556-022-00983-z
126. Korkut, C. *et al.* Regulation of postsynaptic retrograde signaling by presynaptic exosome release. *Neuron* **77,** 1039–1046 (2013).
127. Walsh, R. B. *et al.* Opposing functions for retromer and Rab11 in extracellular

vesicle traffic at presynaptic terminals. *J. Cell Biol.* **220,** (2021).

128. Blanchette, C. R. *et al.* Local regulation of extracellular vesicle traffic by the synaptic endocytic machinery. *J. Cell Biol.* **221,** (2022).
129. Vilcaes, A. A., Chanaday, N. L. & Kavalali, E. T. Interneuronal exchange and functional integration of synaptobrevin via extracellular vesicles. *Neuron* **109,** 971–983.e5 (2021).
130. Catalano, M. & O'Driscoll, L. Inhibiting extracellular vesicles formation and release: a review of EV inhibitors. *J Extracell Vesicles* **9,** 1703244 (2020).
131. Mathieu, M., Martin-Jaular, L., Lavieu, G. & Théry, C. Specificities of secretion and uptake of exosomes and other extracellular vesicles for cell-to-cell communication. *Nat. Cell Biol.* **21,** 9–17 (2019).
132. Desnos, C. *et al.* Rab27A and its effector MyRIP link secretory granules to F-actin and control their motion towards release sites. *J. Cell Biol.* **163,** 559–570 (2003).
133. Ostrowski, M. *et al.* Rab27a and Rab27b control different steps of the exosome secretion pathway. *Nat. Cell Biol.* **12,** 19–30; sup pp 1 (2010).
134. Krämer-Albers, E.-M. *et al.* Oligodendrocytes secrete exosomes containing major myelin and stress-protective proteins: Trophic support for axons? *Proteomics Clin Appl* **1,** 1446–1461 (2007).
135. Hsu, C. *et al.* Regulation of exosome secretion by Rab35 and its GTPase-activating proteins TBC1D10A-C. *J. Cell Biol.* **189,** 223–232 (2010).
136. Koles, K. *et al.* Mechanism of evenness interrupted (Evi)-exosome release at synaptic boutons. *J. Biol. Chem.* **287,** 16820–16834 (2012).
137. Zylbersztejn, K. & Galli, T. Vesicular traffic in cell navigation. *FEBS J.* **278,** 4497–

4505 (2011).

138. Südhof, T. C. & Rothman, J. E. Membrane fusion: grappling with SNARE and SM proteins. *Science* **323,** 474–477 (2009).
139. Vats, S. & Galli, T. Role of SNAREs in Unconventional Secretion-Focus on the VAMP7-Dependent Secretion. *Front. Cell Dev. Biol.* **10,** 884020 (2022).
140. Coco, S. *et al.* Subcellular localization of tetanus neurotoxin-insensitive vesicle-associated membrane protein (VAMP)/VAMP7 in neuronal cells: evidence for a novel membrane compartment. *J. Neurosci.* **19,** 9803–9812 (1999).
141. Hessvik, N. P. & Llorente, A. Current knowledge on exosome biogenesis and release. *Cell Mol. Life Sci.* **75,** 193–208 (2018).
142. Verweij, F. J. *et al.* Quantifying exosome secretion from single cells reveals a modulatory role for GPCR signaling. *J. Cell Biol.* **217,** 1129–1142 (2018).
143. Fauré, J. *et al.* Exosomes are released by cultured cortical neurones. *Mol. Cell. Neurosci.* **31,** 642–648 (2006).
144. Lachenal, G. *et al.* Release of exosomes from differentiated neurons and its regulation by synaptic glutamatergic activity. *Mol. Cell. Neurosci.* **46,** 409–418 (2011).
145. Gauthier, S. A. *et al.* Enhanced exosome secretion in Down syndrome brain - a protective mechanism to alleviate neuronal endosomal abnormalities. *Acta Neuropathol. Commun.* **5,** 65 (2017).
146. Fussi, N. *et al.* Exosomal secretion of α-synuclein as protective mechanism after upstream blockage of macroautophagy. *Cell Death Dis.* **9,** 757 (2018).
147. Coleman, B. M. & Hill, A. F. Extracellular vesicles--Their role in the packaging and

spread of misfolded proteins associated with neurodegenerative diseases. *Semin. Cell Dev. Biol.* **40,** 89–96 (2015).

148. Hartmann, A., Muth, C., Dabrowski, O., Krasemann, S. & Glatzel, M. Exosomes and the Prion Protein: More than One Truth. *Front. Neurosci.* **11,** 194 (2017).
149. Mathews, P. M. & Levy, E. Exosome production is key to neuronal endosomal pathway integrity in neurodegenerative diseases. *Front. Neurosci.* **13,** 1347 (2019).
150. Li, T., Tan, X., Li, S., Al-Nusaif, M. & Le, W. Role of Glia-Derived Extracellular Vesicles in Neurodegenerative Diseases. *Front. Aging Neurosci.* **13,** 765395 (2021).
151. Khadka, A., Spiers, J. G., Cheng, L. & Hill, A. F. Extracellular vesicles with diagnostic and therapeutic potential for prion diseases. *Cell Tissue Res.* (2022). doi:10.1007/s00441-022-03621-0
152. Herrmann, I. K., Wood, M. J. A. & Fuhrmann, G. Extracellular vesicles as a next-generation drug delivery platform. *Nat. Nanotechnol.* **16,** 748–759 (2021).
153. Xu, M. *et al.* Engineered exosomes: desirable target-tracking characteristics for cerebrovascular and neurodegenerative disease therapies. *Theranostics* **11,** 8926–8944 (2021).
154. Mulcahy, L. A., Pink, R. C. & Carter, D. R. F. Routes and mechanisms of extracellular vesicle uptake. *J Extracell Vesicles* **3,** 24641 (2014).
155. Verweij, F. J. *et al.* The power of imaging to understand extracellular vesicle biology in vivo. *Nat. Methods* **18,** 1013–1026 (2021).
156. O'Brien, K., Ughetto, S., Mahjoum, S., Nair, A. V. & Breakefield, X. O. Uptake,

functionality, and re-release of extracellular vesicle-encapsulated cargo. *Cell Rep.* **39,** 110651 (2022).

157. Men, Y. *et al.* Exosome reporter mice reveal the involvement of exosomes in mediating neuron to astroglia communication in the CNS. *Nat. Commun.* **10,** 4136 (2019).
158. Yoshihara, M., Adolfsen, B., Galle, K. T. & Littleton, J. T. Retrograde signaling by Syt 4 induces presynaptic release and synapse-specific growth. *Science* **310,** 858–863 (2005).
159. Sharma, P. *et al.* Exosomes regulate neurogenesis and circuit assembly. *Proc. Natl. Acad. Sci. USA* **116,** 16086–16094 (2019).
160. Zhang, L. *et al.* Small Extracellular Vesicles Control Dendritic Spine Development through Regulation of HDAC2 Signaling. *J. Neurosci.* **41,** 3799–3807 (2021).
161. Korkut, C. *et al.* Trans-synaptic transmission of vesicular Wnt signals through Evi/Wntless. *Cell* **139,** 393–404 (2009).
162. Gross, J. C., Chaudhary, V., Bartscherer, K. & Boutros, M. Active Wnt proteins are secreted on exosomes. *Nat. Cell Biol.* **14,** 1036–1045 (2012).
163. Gong, J., Körner, R., Gaitanos, L. & Klein, R. Exosomes mediate cell contact-independent ephrin-Eph signaling during axon guidance. *J. Cell Biol.* **214,** 35–44 (2016).
164. Escudero, C. A. *et al.* The p75 neurotrophin receptor evades the endolysosomal route in neuronal cells, favouring multivesicular bodies specialised for exosomal release. *J. Cell Sci.* **127,** 1966–1979 (2014).
165. Mason, A. J., Keeler, A. B., Kabir, F., Winckler, B. & Deppmann, C. Sympathetic

neurons secrete retrogradely transported TrkA on extracellular vesicles. *Sci. Rep.* **13,** 3657 (2023).

166. Barford, K., Deppmann, C. & Winckler, B. The neurotrophin receptor signaling endosome: Where trafficking meets signaling. *Dev. Neurobiol.* **77,** 405–418 (2017).
167. Connor, B., Moya-Alvarado, G., Yamashita, N. & Kuruvilla, R. Transcytosis-mediated anterograde transport of TrkA receptors is necessary for sympathetic neuron development and function. *Proc. Natl. Acad. Sci. USA* **120,** e2205426120 (2023).
168. Padamsey, Z. *et al.* Activity-Dependent Exocytosis of Lysosomes Regulates the Structural Plasticity of Dendritic Spines. *Neuron* **93,** 132–146 (2017).
169. van Niel, G. *et al.* Challenges and directions in studying cell-cell communication by extracellular vesicles. *Nat. Rev. Mol. Cell Biol.* **23,** 369–382 (2022).
170. Blanchette, C. R. & Rodal, A. A. Mechanisms for biogenesis and release of neuronal extracellular vesicles. *Curr. Opin. Neurobiol.* **63,** 104–110 (2020).
171. Colombo, M., Raposo, G. & Théry, C. Biogenesis, secretion, and intercellular interactions of exosomes and other extracellular vesicles. *Annu. Rev. Cell Dev. Biol.* **30,** 255–289 (2014).
172. Yamashita, N., Joshi, R., Zhang, S., Zhang, Z.-Y. & Kuruvilla, R. Phospho-Regulation of Soma-to-Axon Transcytosis of Neurotrophin Receptors. *Dev. Cell* **42,** 626–639.e5 (2017).
173. Théry, C., Amigorena, S., Raposo, G. & Clayton, A. Isolation and characterization of exosomes from cell culture supernatants and biological fluids. *Curr. Protoc. Cell*

Biol. **Chapter 3,** Unit 3.22 (2006).

174. Mandai, K. *et al.* LIG family receptor tyrosine kinase-associated proteins modulate growth factor signals during neural development. *Neuron* **63,** 614–627 (2009).
175. Harrington, A. W. *et al.* Recruitment of actin modifiers to TrkA endosomes governs retrograde NGF signaling and survival. *Cell* **146,** 421–434 (2011).
176. Ginty, D. D. & Segal, R. A. Retrograde neurotrophin signaling: Trk-ing along the axon. *Curr. Opin. Neurobiol.* **12,** 268–274 (2002).
177. Bachurski, D. *et al.* Extracellular vesicle measurements with nanoparticle tracking analysis - An accuracy and repeatability comparison between NanoSight NS300 and ZetaView. *J Extracell Vesicles* **8,** 1596016 (2019).
178. van der Pol, E. *et al.* Particle size distribution of exosomes and microvesicles determined by transmission electron microscopy, flow cytometry, nanoparticle tracking analysis, and resistive pulse sensing. *J. Thromb. Haemost.* **12,** 1182–1192 (2014).
179. Linares, R., Tan, S., Gounou, C., Arraud, N. & Brisson, A. R. High-speed centrifugation induces aggregation of extracellular vesicles. *J Extracell Vesicles* **4,** 29509 (2015).
180. Anand, S., Samuel, M. & Mathivanan, S. Exomeres: A new member of extracellular vesicles family. *Subcell. Biochem.* **97,** 89–97 (2021).
181. Zhang, Q. *et al.* Transfer of functional cargo in exomeres. *Cell Rep.* **27,** 940–954.e6 (2019).
182. Zhang, G. & Yang, P. A novel cell-cell communication mechanism in the nervous system: exosomes. *J. Neurosci. Res.* **96,** 45–52 (2018).

183. Linares, R., Tan, S., Gounou, C. & Brisson, A. R. Imaging and quantification of extracellular vesicles by transmission electron microscopy. *Methods Mol. Biol.* **1545,** 43–54 (2017).

184. Polanco, J. C., Li, C., Durisic, N., Sullivan, R. & Götz, J. Exosomes taken up by neurons hijack the endosomal pathway to spread to interconnected neurons. *Acta Neuropathol. Commun.* **6,** 10 (2018).

185. Broadwell, R. D. & Balin, B. J. Endocytic and exocytic pathways of the neuronal secretory process and trans-synaptic transfer of wheat germ agglutinin-horseradish peroxidase in vivo. *J. Comp. Neurol.* **242,** 632–650 (1985).

186. Borges, L. & Sidman, R. Axonal transport of lectins in the peripheral nervous system. *J. Neurosci.* **5,** 647–653 (1982).

187. Trojanowski, J. Q. Native and derivatized lectins for in vivo studies of neuronal connectivity and neuronal cell biology. *J. Neurosci. Methods* **9,** 185–204 (1983).

188. Kaplan, D. R. & Miller, F. D. Neurotrophin signal transduction in the nervous system. *Curr. Opin. Neurobiol.* **10,** 381–391 (2000).

189. Stephens, R. M. *et al.* Trk receptors use redundant signal transduction pathways involving SHC and PLC-γ1 to mediate NGF responses. *Neuron* **12,** 691–705 (1994).

190. Holgado-Madruga, M., Moscatello, D. K., Emlet, D. R., Dieterich, R. & Wong, A. J. Grb2-associated binder-1 mediates phosphatidylinositol 3-kinase activation and the promotion of cell survival by nerve growth factor. *Proc. Natl. Acad. Sci. USA* **94,** 12419–12424 (1997).

191. Kuruvilla, R., Ye, H. & Ginty, D. D. Spatially and functionally distinct roles of the

PI3-K effector pathway during NGF signaling in sympathetic neurons. *Neuron* **27,** 499–512 (2000).

192. Park, J. W., Vahidi, B., Taylor, A. M., Rhee, S. W. & Jeon, N. L. Microfluidic culture platform for neuroscience research. *Nat. Protoc.* **1,** 2128–2136 (2006).
193. Yong, Y., Hughes, C. & Deppmann, C. A microfluidic culture platform to assess axon degeneration. *Methods Mol. Biol.* **2143,** 83–96 (2020).
194. Deppmann, C. D. *et al.* A model for neuronal competition during development. *Science* **320,** 369–373 (2008).
195. Ascano, M., Bodmer, D. & Kuruvilla, R. Endocytic trafficking of neurotrophins in neural development. *Trends Cell Biol.* **22,** 266–273 (2012).
196. Glebova, N. O. & Ginty, D. D. Growth and survival signals controlling sympathetic nervous system development. *Annu. Rev. Neurosci.* **28,** 191–222 (2005).
197. Hamburger, V. & Levi-Montalcini, R. Proliferation, differentiation and degeneration in the spinal ganglia of the chick embryo under normal and experimental conditions. *J. Exp. Zool.* **111,** 457–501 (1949).
198. Glebova, N. O. & Ginty, D. D. Heterogeneous requirement of NGF for sympathetic target innervation in vivo. *J. Neurosci.* **24,** 743–751 (2004).
199. Schober, A. & Unsicker, K. Growth and neurotrophic factors regulating development and maintenance of sympathetic preganglionic neurons. *Int Rev Cytol* **205,** 37–76 (2001).
200. Oppenheim, R. W., Maderdrut, J. L. & Wells, D. J. Cell death of motoneurons in the chick embryo spinal cord. VI. Reduction of naturally occurring cell death in the thoracolumbar column of Terni by nerve growth factor. *J. Comp. Neurol.* **210,** 174–

189 (1982).

201. Zweifel, L. S., Kuruvilla, R. & Ginty, D. D. Functions and mechanisms of retrograde neurotrophin signalling. *Nat. Rev. Neurosci.* **6,** 615–625 (2005).
202. Blum, J. A. *et al.* Single-cell transcriptomic analysis of the adult mouse spinal cord reveals molecular diversity of autonomic and skeletal motor neurons. *Nat. Neurosci.* **24,** 572–583 (2021).
203. Brooks-Fournier, R. & Coggeshall, R. E. The ratio of preganglionic axons to postganglionic cells in the sympathetic nervous system of the rat. *J. Comp. Neurol.* **197,** 207–216 (1981).
204. Lichtman, J. W., Purves, D. & Yip, J. W. On the purpose of selective innervation of guinea-pig superior cervical ganglion cells. *J. Physiol. (Lond.)* **292,** 69–84 (1979).
205. Njå, A. & Purves, D. Specific innervation of guinea-pig superior cervical ganglion cells by preganglionic fibres arising from different levels of the spinal cord. *J. Physiol. (Lond.)* **264,** 565–583 (1977).
206. Easton, R. M., Deckwerth, T. L., Parsadanian, A. S. & Johnson, E. M. Analysis of the mechanism of loss of trophic factor dependence associated with neuronal maturation: a phenotype indistinguishable from Bax deletion. *J. Neurosci.* **17,** 9656–9666 (1997).
207. Ruit, K. G., Osborne, P. A., Schmidt, R. E., Johnson, E. M. & Snider, W. D. Nerve growth factor regulates sympathetic ganglion cell morphology and survival in the adult mouse. *J. Neurosci.* **10,** 2412–2419 (1990).
208. Nigri, J. *et al.* CD9 mediates the uptake of extracellular vesicles from cancer-associated fibroblasts that promote pancreatic cancer cell aggressiveness. *Sci.*

Signal. **15,** eabg8191 (2022).

209. Yuan, Q.-L., Zhang, Y.-G. & Chen, Q. Mesenchymal Stem Cell (MSC)-Derived Extracellular Vesicles: Potential Therapeutics as MSC Trophic Mediators in Regenerative Medicine. *Anat Rec (Hoboken)* **303,** 1735–1742 (2020).
210. Asai, H. *et al.* Depletion of microglia and inhibition of exosome synthesis halt tau propagation. *Nat. Neurosci.* **18,** 1584–1593 (2015).
211. Polanco, J. C., Hand, G. R., Briner, A., Li, C. & Götz, J. Exosomes induce endolysosomal permeabilization as a gateway by which exosomal tau seeds escape into the cytosol. *Acta Neuropathol.* **141,** 235–256 (2021).
212. Patel, M. R. & Weaver, A. M. Astrocyte-derived small extracellular vesicles promote synapse formation via fibulin-2-mediated TGF-β signaling. *Cell Rep.* **34,** 108829 (2021).
213. Cline, H. & Haas, K. The regulation of dendritic arbor development and plasticity by glutamatergic synaptic input: a review of the synaptotrophic hypothesis. *J. Physiol. (Lond.)* **586,** 1509–1517 (2008).
214. Couch, Y. *et al.* A brief history of nearly EV-erything - The rise and rise of extracellular vesicles. *J Extracell Vesicles* **10,** e12144 (2021).
215. Pedrioli, G. & Paganetti, P. Hijacking endocytosis and autophagy in extracellular vesicle communication: where the inside meets the outside. *Front. Cell Dev. Biol.* **8,** 595515 (2020).
216. Hyenne, V. *et al.* Studying the fate of tumor extracellular vesicles at high spatiotemporal resolution using the zebrafish embryo. *Dev. Cell* **48,** 554–572.e7 (2019).

217. Verweij, F. J. *et al.* Live Tracking of Inter-organ Communication by Endogenous Exosomes In Vivo. *Dev. Cell* **48,** 573–589.e4 (2019).
218. Ghoroghi, S. *et al.* Ral GTPases promote breast cancer metastasis by controlling biogenesis and organ targeting of exosomes. *Elife* **10,** (2021).
219. Williams, C. *et al.* Assessing the role of surface glycans of extracellular vesicles on cellular uptake. *Sci. Rep.* **9,** 11920 (2019).
220. Shimoda, A., Tahara, Y., Sawada, S.-I., Sasaki, Y. & Akiyoshi, K. Glycan profiling analysis using evanescent-field fluorescence-assisted lectin array: Importance of sugar recognition for cellular uptake of exosomes from mesenchymal stem cells. *Biochem. Biophys. Res. Commun.* **491,** 701–707 (2017).
221. Crescitelli, R., Lässer, C. & Lötvall, J. Isolation and characterization of extracellular vesicle subpopulations from tissues. *Nat. Protoc.* **16,** 1548–1580 (2021).
222. Andreassi, C. *et al.* An NGF-responsive element targets myo-inositol monophosphatase-1 mRNA to sympathetic neuron axons. *Nat. Neurosci.* **13,** 291–301 (2010).
223. Riccio, A., Pierchala, B. A., Ciarallo, C. L. & Ginty, D. D. An NGF-TrkA-mediated retrograde signal to transcription factor CREB in sympathetic neurons. *Science* **277,** 1097–1100 (1997).
224. Kaplan, D. R. & Stephens, R. M. Neurotrophin signal transduction by the Trk receptor. *J. Neurobiol.* **25,** 1404–1417 (1994).
225. Michaelidis, T. M. *et al.* Inactivation of bcl-2 results in progressive degeneration of motoneurons, sympathetic and sensory neurons during early postnatal development. *Neuron* **17,** 75–89 (1996).

226. Scott-Solomon, E., Boehm, E. & Kuruvilla, R. The sympathetic nervous system in development and disease. *Nat. Rev. Neurosci.* **22,** 685–702 (2021).

227. Moiseev, K. Y., Romanova, I. V., Masliukov, A. P. & Masliukov, P. M. Development of nNOS-positive preganglionic sympathetic neurons in the rat thoracic spinal cord. *Cell Tissue Res.* **375,** 345–357 (2019).

228. Winckler, B. & Mellman, I. Trafficking guidance receptors. *Cold Spring Harb. Perspect. Biol.* **2,** a001826 (2010).

229. Davies, A. M. The neurotrophic hypothesis: where does it stand? *Philos. Trans. R. Soc. Lond. B, Biol. Sci.* **351,** 389–394 (1996).

230. Chong, Y. & Cooper, E. Converging preganglionic axons refine without synaptic transmission when targets downstream of sympathetic nerves are active. *BioRxiv* (2020). doi:10.1101/2020.10.21.349142

231. Alkaslasi, M. R. *et al.* Single nucleus RNA-sequencing defines unexpected diversity of cholinergic neuron types in the adult mouse spinal cord. *Nat. Commun.* **12,** 2471 (2021).

232. Russ, D. E. *et al.* A harmonized atlas of mouse spinal cord cell types and their spatial organization. *Nat. Commun.* **12,** 5722 (2021).

233. Gargano, N., Levi, A. & Alema, S. Modulation of nerve growth factor internalization by direct interaction between p75 and TrkA receptors. *J. Neurosci. Res.* **50,** 1–12 (1997).

234. Franco, M. L. *et al.* Neurotrophin signaling is modulated by specific transmembrane domain interactions. *BioRxiv* (2021). doi:10.1101/2021.05.24.445441

235. Morelli, A. E. *et al.* Endocytosis, intracellular sorting, and processing of exosomes by dendritic cells. *Blood* **104,** 3257–3266 (2004).

236. Barrès, C. *et al.* Galectin-5 is bound onto the surface of rat reticulocyte exosomes and modulates vesicle uptake by macrophages. *Blood* **115,** 696–705 (2010).

237. Feng, D. *et al.* Cellular internalization of exosomes occurs through phagocytosis. *Traffic* **11,** 675–687 (2010).

238. Svensson, K. J. *et al.* Exosome uptake depends on ERK1/2-heat shock protein 27 signaling and lipid Raft-mediated endocytosis negatively regulated by caveolin-1. *J. Biol. Chem.* **288,** 17713–17724 (2013).

239. Nanbo, A., Kawanishi, E., Yoshida, R. & Yoshiyama, H. Exosomes derived from Epstein-Barr virus-infected cells are internalized via caveola-dependent endocytosis and promote phenotypic modulation in target cells. *J. Virol.* **87,** 10334–10347 (2013).

240. Montecalvo, A. *et al.* Mechanism of transfer of functional microRNAs between mouse dendritic cells via exosomes. *Blood* **119,** 756–766 (2012).

241. Hao, S. *et al.* Mature dendritic cells pulsed with exosomes stimulate efficient cytotoxic T-lymphocyte responses and antitumour immunity. *Immunology* **120,** 90–102 (2007).

242. Tian, T., Wang, Y., Wang, H., Zhu, Z. & Xiao, Z. Visualizing of the cellular uptake and intracellular trafficking of exosomes by live-cell microscopy. *J. Cell Biochem.* **111,** 488–496 (2010).

243. Perez-Hernandez, D. *et al.* The intracellular interactome of tetraspanin-enriched microdomains reveals their function as sorting machineries toward exosomes. *J.*

Biol. Chem. **288,** 11649–11661 (2013).

244. Christianson, H. C., Svensson, K. J., van Kuppevelt, T. H., Li, J.-P. & Belting, M. Cancer cell exosomes depend on cell-surface heparan sulfate proteoglycans for their internalization and functional activity. *Proc. Natl. Acad. Sci. USA* **110,** 17380–17385 (2013).
245. Franzen, C. A. *et al.* Characterization of uptake and internalization of exosomes by bladder cancer cells. *Biomed Res. Int.* **2014,** 619829 (2014).
246. Escrevente, C., Keller, S., Altevogt, P. & Costa, J. Interaction and uptake of exosomes by ovarian cancer cells. *BMC Cancer* **11,** 108 (2011).
247. Bermejo-Jambrina, M. *et al.* C-Type Lectin Receptors in Antiviral Immunity and Viral Escape. *Front. Immunol.* **9,** 590 (2018).
248. Bozzuto, G. & Molinari, A. Liposomes as nanomedical devices. *Int. J. Nanomedicine* **10,** 975–999 (2015).
249. Yap, C. C., Digilio, L., McMahon, L. & Winckler, B. The endosomal neuronal proteins Nsg1/NEEP21 and Nsg2/P19 are itinerant, not resident proteins of dendritic endosomes. *Sci. Rep.* **7,** 10481 (2017).
250. Enes, J. *et al.* Satellite glial cells modulate cholinergic transmission between sympathetic neurons. *PLoS One* **15,** e0218643 (2020).
251. Mapps, A. A. *et al.* Satellite glia modulate sympathetic neuron survival, activity, and autonomic function. *Elife* **11,** (2022).
252. Hanani, M. Satellite glial cells in sympathetic and parasympathetic ganglia: in search of function. *Brain Res. Rev.* **64,** 304–327 (2010).
253. Avraham, O. *et al.* Satellite glial cells promote regenerative growth in sensory

neurons. *Nat. Commun.* **11,** 4891 (2020).

254. Hanani, M. & Spray, D. C. Emerging importance of satellite glia in nervous system function and dysfunction. *Nat. Rev. Neurosci.* **21,** 485–498 (2020).

255. Mapps, A. A. *et al.* Diversity of satellite glia in sympathetic and sensory ganglia. *Cell Rep.* **38,** 110328 (2022).

Appendix I. Inhibition of MEK Does not Affect EV Secretion in Sympathetic Cell Cultures

Introduction

When NGF binds to TrkA, the receptor becomes activated and can recruit different effectors to initiate kinase cascades such as the Ras/MAPK pathway[19,32–35]. Activation of different downstream pathways of TrkA has been shown to affect the trafficking and functional output of the $TrkA^+$ SE. Since we have shown that $TrkA^+$ SE can be a source of TrkA that is secreted on extracellular vesicles, we asked whether inhibiting the Ras/MAPK would interfere with the secretion of $TrkA^+$ EVs. Here I show using compartmentalized SCG neurons that addition of the MEK inhibitor, PD98059 to the cell bodies of neurons does not impact TrkA inclusion or secretion in EVs. Furthermore, there is no change in overall EV secretion by sympathetic cultures.

Material and Methods

Compartmentalized Anti-FLAG antibody feeding assay

Sympathetic neurons from *TrkA*$^{FLAG/FLAG}$ animals were dissected and plated at 14,000 cells per microfluidic device as previously described[36,37]. At 6 DIV, 150 µL of complete media was added to the CB chamber and 100 µL of anti-FLAG-AF488 antibody (1:200) in complete media was added to the DA chamber. Conditioned media was collected from the CB chamber 15 hours after the addition of the anti-FLAG-AF488 antibody and EVs were isolated. For inhibitor treatment, 100 µL of complete media containing PD98059 (50µM) or 0.1% v/v DMSO was added to the CB chamber and 150 µL of anti-FLAG-AF488 antibody (1:200) in complete media was added the DA chamber. Conditioned media was collected from the CB chamber 15 hours after the addition of

the anti-FLAG-AF488 and inhibitors and EVs were isolated. Fluorescent NTA analysis was conducted as described in the material and methods section of Chapter III.

Immunocytochemistry

Cells were fixed in 4% PFA for 20 minutes at room temperature in the MFDs. Cells were washed 3 times with 1X PBS and then blocked and permeabilized in 5% normal donkey serum and 0.2% TritonX-100 for 20 minutes. Primary antibodies were diluted in 1% BSA and applied overnight at 4 °C. Secondary antibodies were diluted in 1% BSA and added for 30 mins at room temperature. MFDs were washed 3x with 1x PBS and imaged on an inverted Zeiss 980 microscope with an Airyscan detector using a 40X oil objective (NA 1.3).

REAGENT or RESOURCE	SOURCE	IDENTIFIER
Sheep Anti- Tyrosine Hydroxylase	Millipore	Cat # AB1542 **RRID: AB_90755**
Rabbit Anti-BLBP	Abcam	**Cat # ab279649; RRID:AB**
Chicken Anti-MAP2	EnCor Biotechnology	Cat # CPCA-MAP2 RRID: AB_2138173
Anti- FLAG DYKDDDDK tag (D6W5B) Rabbit mAb Alexa R 488	Cell Signaling Technology	Cat # 15008S Lot 2 and 3 RRID: N/A

Statistics and Measurements.

Statistical analyses were performed using Prism 9 software. All values are shown as mean ± SEM. Differences between samples were determined using unpaired, two-tailed t-tests. Statistical significance is a p-value < 0.05. The p-values are denoted on top of each bracket pair.

Results

Inhibition of MEK does not change the number of TrkA EVs or total EVs secreted from sympathetic cells.

The ligand-bound activated TrkA receptor transduces its signal via several canonical downstream pathways such as phosphatidylinositol-3-kinase (PI3K) and phospholipase-C-ɣ (PLC-ɣ) and mitogen-activated protein kinase kinase (MEK). We tested whether activation of the MAPK/MEK pathway is important for $TrkA^+$ EV release. Inhibition of MEK using the chemical inhibitor, PD98059, did not change the total number of particles secreted (Fig. 1A), nor did it cause a significant decrease in the number of fluorescent TrkA particles detected in the P100 fraction (Fig. 1B) compared to a DMSO control. To ensure that the inhibitor treatment did not cause any morphological alterations to the cells, we fixed and stained the cultures and did not detect any appreciable difference between the PD98059 treated cells and control (Fig. 1C).

Figures

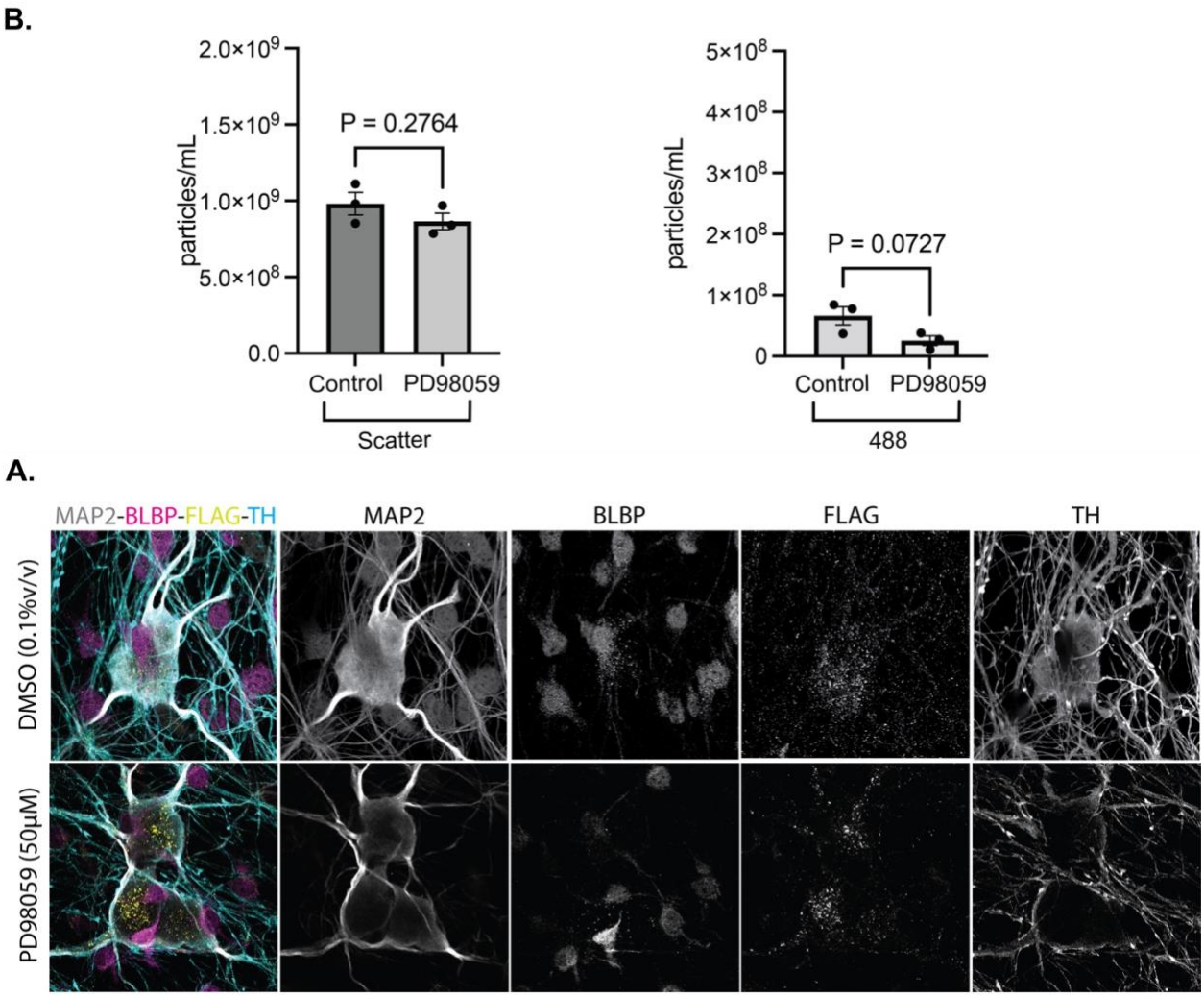

Figure 1. Inhibition of TrkA-dependent signaling pathways, MEK does not change EV release

A. Quantification of the total number of scatter particles detected after anti-FLAG-AF488 antibody addition to the DA chamber of MFDs containing *TrkA*$^{FLAG/FLAG}$ SCG neurons treated with the MEK inhibitor, PD98059. **B.** Quantification of the total number of fluorescent (Anti-FLAG-AF488^{+}) particles detected after anti-FLAG-AF488 antibody addition to the DA chamber of MFDs containing *TrkA*$^{FLAG/FLAG}$ SCG neurons treated with the MEK inhibitor, PD98059. **C.** Images of the cell bodies of compartmentalized SCG neurons treated with DMSO (control) or inhibitor PD98059 in the cell body chamber and

anti-FLAG-AF488 antibody in the distal axon chamber for 15 hours. Staining against MAP2 (somatodendritic domain), BLBP (satellite glia), anti-FLAG-AF488, and TH (SCG neuron). Scale bar is 30 μm.

Appendix II. Uptake of Lipid-labeled EVs *In Vitro*

Introduction

How does an EV get internalized by its recipient cell? While this question is not as pertinent to researchers using EVs as biomarkers for pathology it is especially relevant to researcher using EVs as drug targeting tools and to those looking to EVs as a mode of intercellular communication. Despite this high importance, EV targeting and uptake remains one of the least characterized mechanisms in the field. Characterizing EV uptake has been one of the more difficult mechanisms to answer as their small size and lack of a specific marker makes it difficult to track and visualize EVs both *in vivo* and *in vitro*. Additionally, the propensity to internalize EVs appears to be cell type specific as phagocytic cells take up EVs more readily than non-phagocytic cells. Lastly, given that all cells produce EVs there is vast heterogeneity in EV cargoes and surfaces proteins which might influence the targeting and mechanism of uptake by the recipient cell. Here using a lipophilic dye, MemGlow, I show that EVs derived from sympathetic cells can also be internalized by sympathetic cells. Furthermore, I show that the lectin, WGA, can be injected into the salivary glands of mice and be detected in the SCG and Spinal Cord 12-72 hours post injection.

Material and Methods

MemGlow labeling of isolated sympathetic EVs

Conditioned media (CM) was collected 48 hours after a media change from 7 DIV donor sympathetic cultures. Naïve sympathetic cultures were grown for 7 DIVs as recipient cells. Donor CM was then incubated with 100nM MemGlow (Cytoskeleton) for 1 hour at RT in the dark. The CM was then spun at 10,000 x g for 15 mins. The supernatant was

then transferred to a qEV1/ 70nm SEC column (Izon) and fractions 1-4 and 5-8 were collected and pooled. EVs were then recovered using Amicon 100kDa centrifugal filters (Millipore sigma) and EVs from fractions 5-8 were confirmed by Western blot against CD81 (Cell Signaling). EVs were then added to naïve recipient cells for 30 mins, 90 mins or 24 hours before imaging. Undyed EVs were used as a control.

Salivary gland injection

Postnatal day 3 wildtype mouse pups were anesthetized on ice for 5 mins. A Hamilton syringe was used to inject 4 µL WGA-488 into the salivary glands of mice pups. Pups were then returned to their mother and sent to recover in the vivarium. Pups were sacrificed at 12-, 24-, 48-, and 72-hours post injection and tissue were collected, fixed in 4% PFA for 8 hours, dehydrated in 30% sucrose for 3 days, embedded in O.C.T compound and rapidly frozen on dry ice. Tissue was then sectioned on a cryostat in 30 µm thick sections and subsequently imaged for WGA-488 signal.

Results

EV uptake in the SCG can be visualized *in vitro*

Incubation of MemGlow labeled EVs with naïve recipient cells results in EV uptake. At 30 mins, MemGlow labeling is mostly seen on plasma membrane (Fig. 1A). By 90 mins to 24 hours incubation, the MemGlow label is largely detected as aggregated puncta in the cell body, possibly in late endosomal compartments (Fig. 1A). Live imaging at 30 mins showed small endosomal like compartments labeled by MemGlow migrating through the neurites of the recipient cell (data not shown). These data suggest that EVs are internalized are rapidly transported to the soma, but further experiments will need to be conducted. Importantly, MemGlow labeled EVs are fixable

and compatible with immunocytochemistry procedures, thus enabling this technique to be used to identify specific cell types that internalize EVs in the SCG (Fig. 1B). Importantly, no signal was detected by fluorescence microscopy when unlabeled EVs were added to naïve cultures (Fig. 1B). Lastly, only labeled EVs from fractions 5-8 were added to naïve cells. EVs could not be recovered from fractions 1-4 or 5-8 using centrifugal filters with molecular weight cutoffs below 100 kDa (Fig. 2B).

WGA is retrogradely trafficked throughout neurons and traverses' synapses *in vivo*

Based on published data showing WGA-488 labels sympathetic EVs *in vitro*, I wanted to determine if WGA-488 could be trans-synaptically transferred *in vivo.* Analysis of SCG and spinal cords 12, 24, 48, and 72 hours after salivary injection show robust labeling of the SCG and some labeling along the ventral horn and medial columns of the spinal cord (Fig. 2A, top). Importantly, WGA-488 was not detected on the SCG on the contralateral side from the injection, thus serving as an important control (Fig. 2A, middle). Total counts of all WGA-488 signal in both the spinal cord and SCG is quantified in Table 3.

Figures

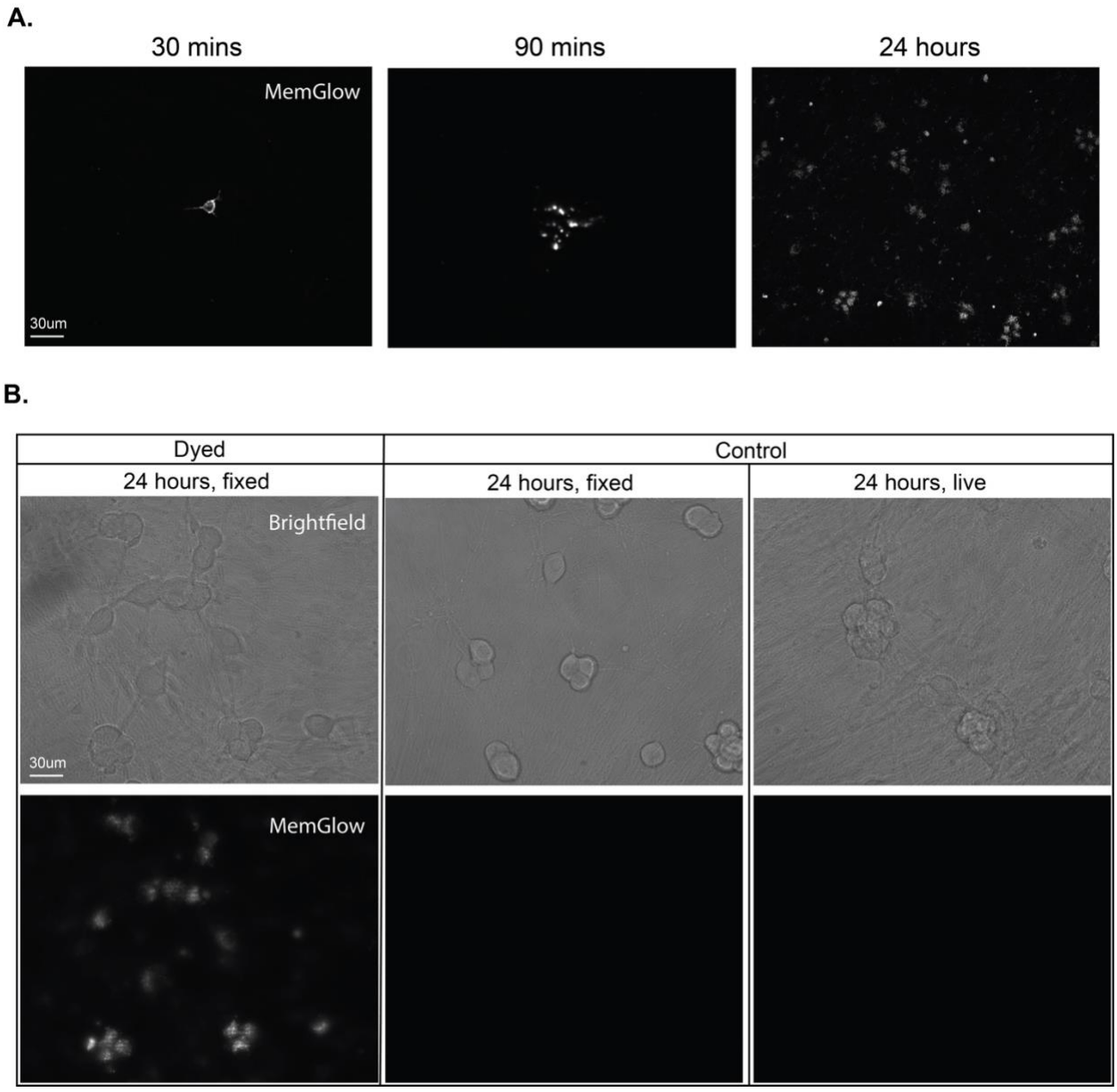

Figure 1. MemGlow labeled EVs are internalized by SCG cells

A. MemGlow signal detected on the plasma membrane of neurons (30 mins) and inside neurons (90 mins & 24 hours) after MemGlow labeled EV incubation on naïve cells. **B.** Incubated MemGlow EVs can be fixed. Un-labeled (No MemGlow) EVs do not show fluorescent signal by microscopy. Scale bar is 30 μm for all images.

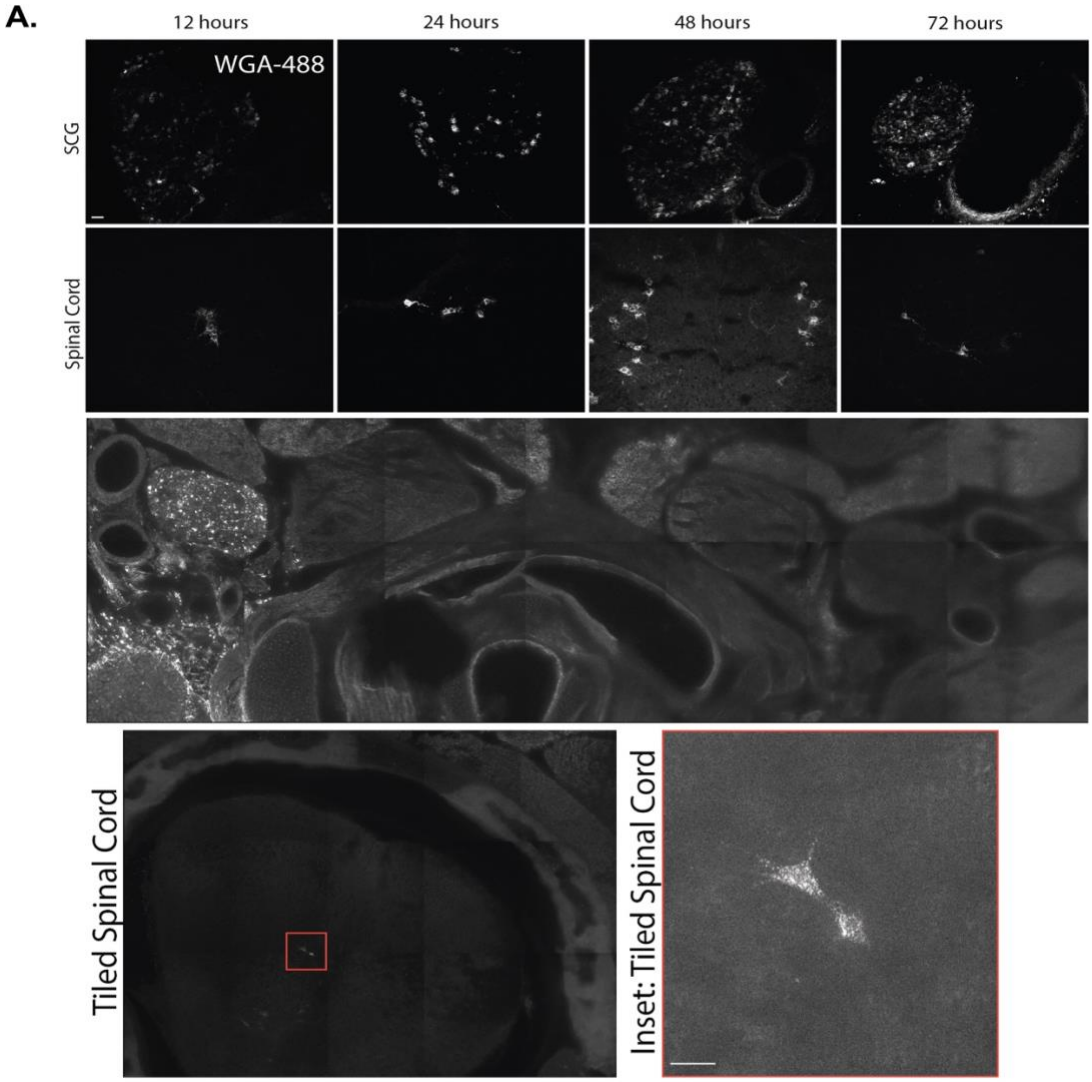
A.
12 hours
24 hours
48 hours
72 hours
WGA-488
SCG
Spinal Cord
Tiled Spinal Cord
Inset: Tiled Spinal Cord

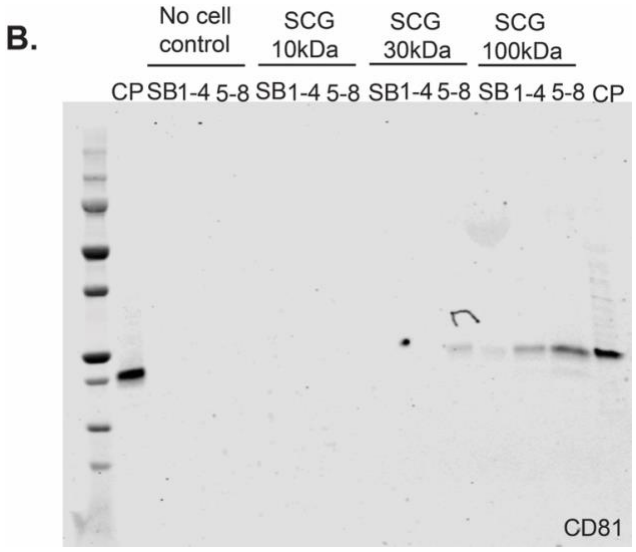
B.
No cell control
SCG 10kDa
SCG 30kDa
SCG 100kDa
CP SB1-4 5-8 SB1-4 5-8 SB1-4 5-8 SB 1-4 5-8 CP
CD81

Figure 2. WGA labeling of SCG and spinal cord *in vivo*

A. SCG and spinal cord labeling by WGA-488 at 12, 24, 48, and 72 hours post salivary gland injection. **B.** Immunoblot against CD81 showing robust EVs marker staining from SEC fractions 1-4 and 5-8 after recovery using a 100kDA centrifugal filter. CP: cell pellet, SB: sample buffer.

Table 3. Quantification of WGA-488 trafficking *in vivo*

Total # of slides counted	259
Total # of sections counted	1554
Total # of spinal cord sections with WGA-488 detected	128
Total # of SCG sections with WGA-488 detected	102

Discussion

Visualizing EV uptake in vitro and in vivo is challenging due to a lack of tools, no universal marker and their small size. Here I discuss the current literature on EV uptake and challenges to this research. Most studies report the same experimental paradigm for visualizing uptake. First, they label their EVs of interest with a fluorescent dye either PKH67, a fluorescent lipid intercalator, or DiD which is a fluorescent dye for cell membranes. They then incubate the labeled EVs with the intended recipient cell for a duration between 2-8 hours followed by imaging. Next, they perturb uptake by screening different compounds that are known to inhibit different uptake pathways.

Clathrin-Mediated Endocytosis and Caveolin dependent endocytosis

Clathrin-mediated endocytosis (CME) relies on the formation of clathrin coated pits that deform the plasma membrane and then pinch off into coated vesicles with the

help of the GTPase, dynamin. In contrast, caveolin-dependent endocytosis relies on the internalization of plasma membrane pits or invaginations formed by the integral membrane protein, caveolin, which is enriched in lipid rafts. Dendritic cells, PC12 cells and rat reticulocytes were shown to reduce EV uptake in the presence of dynamin inhibitors, such as the pharmacological compound, dynasore or through expression of dominant-negative dynamin 2[235–237]. However, these results are somewhat contradictory because in another type of phagocytic recipient cell, inhibition of clathrin-coated pit assembly did not decrease EV internalization suggesting CME may not be the primary mechanism of EV internalization for macrophages[237]. This finding was corroborated in human umbilical vein endothelial cells (HUVEC) when an 80% knockdown of the clathrin heavy chain did not decrease EV uptake[238]. Instead, inhibition of caveolin dependent endocytosis by the inhibitor filipin III resulted in decreased uptake indicating a caveolin-dependent mechanism[238]. Other studies have indeed shown knockdown of caveolin-1 resulted in reduced EV uptake in lymphocytes[239].

Phagocytosis

Phagocytosis is the process by which larger molecules such as apoptotic cells or pathogens get internalized by specialized cells. This engulfment process relies on actin remodeling to deform the membrane around the material. Inhibition of this actin polymerization using cytochalasin B or D results in decreased EV uptake in dendritic cells, rat reticulocytes, and PC12 cells[235,236,240–242].Furthermore, incubation of labeled EVs with the recipient cells at 4°C resulted in reduced uptake suggesting that internalization occurs by an active process. Lastly, in some phagocytic cells, inhibition of

micropinocytosis or internalization of fluid and small membranes with 5-ethyl-N-isopropyl amiloride (EIPA), an inhibitor of macropinocytosis that blocks Na+/H+ exchange, did not affect exosome uptake[237].

Tetraspanins, Proteoglycans, Lectins and lipids

Tetraspanins form microdomains (TEM) on the plasma membrane that can regulate the selection and sorting of cargos and receptors[243]. Tetraspanins are highly enriched in EVs and the tetraspanins CD63, CD81 and CD9 are used as EV markers. Blocking of the tetraspanins CD9 and CD81 reduced EV internalization in dendritic cells; however, blocking of CD63 did not interfere with uptake [235,238]. Proteoglycans, especially heparin sulfate proteoglycans such as syndecan are known to sequester ligands and serve as coreceptors mediating internalization[244]. A dependence on glycoproteins for EV uptake was shown as exogenous application of heparin was able to reduce EV uptake in bladder cancer cells, whereas application of chondroitin sulfate had no effect [244–246]. Lectins, specifically C-type lectin receptors (CLRs) are a type of pattern recognition receptor that recognize carbohydrates of invading pathogens allowing dendritic cells to internalize them and present them as an antigen[247]. Blocking DEC-205, a C-lectin, with antibodies prevented uptake of EVs in dendritic cells [241]. Furthermore, saturation of the receptor with excess galectin-5, another lectin, reduced EV uptake[236]. Lastly, as mentioned previously, lipids and lipid rafts serve as potential zones for uptake. Depletion of cholesterol, a core component of lipid rafts through drugs such as methyl B cyclodextrin or simvastatin reduced EV uptake in HUVEC cells[238].

Membrane fusion

Membrane fusion, similar to secretion, involves the close apposition and then subsequent SNARE mediated fusion of the plasma membrane and the EV membrane. To visualize this process, a fluorogenic dequenching assay system is used whereby a lipophilic dye is incorporated at a high density into the EV membrane. Upon fusion, the density of the dye in the EV outer leaflet is reduced resulting in dequenching of the fluorophore and thus detection of fluorescence. Montecalvo et al. used this assay system to show that EV membranes fuse with the plasma membrane of dendritic cells[240]. This fluorescent signal is not apparent in paraformaldehyde fixed cells and is subsequently abolished after treatment of the EVs with triton, a membrane permeabilizer[240]. To test whether EVs release their cargo in full fusion or hemi fusion events they loaded the EVs with uncaged Luciferin and added them to cells transfected with luciferase. When luciferin encounters luciferase it will be oxidized and thus emit fluorescence. After an 8-minute incubation with luciferin loaded EVs, light emission above background was detected indicating a rapid time-scale of uptake and the sufficient transfer of cargo[240]. While it was not specifically addressed, this reporter assay could indicate hemi fusion or full fusion events as the pore formed through hemi fusion might be large enough for luciferin to cross into the cell.

While all these studies provide initial clues towards the mechanisms of EV uptake the results should be taken with some caveats. 1) The use of dyes to label EVs can be problematic due to non-specific staining and leakage of the dyes onto the membrane of the recipient cell in the absence of a fusion event. Secondly, labeling EVs after they have been excreted from the cell does not give any insight into the diverse

pools of physiologically secreted EVs. Instead using a fluorophore conjugated to your protein of interest or to a known EV marker might serve as a more physiologically relevant paradigm. Although if a highly secretory cell type is not used for production, fluorescent EV yield might be low. 2) Incubation of EVs with their recipient cells and subsequent imaging without an acid wash off step or trypsinization to remove surface bound EVs might erroneously result in counting EVs stuck to the surface as internalized. While some papers do provide adequate washes after EV incubation, the use of acid or trypsin is necessary to eliminate any doubt that these highly sticky and lipophilic EVs don't remain stuck to the membrane. However, cell surface or juxtacrine signaling might be the mechanism by which these EV communicate and therefore internalization would not be required. 3) There are very few instances of recorded live imaging uptake events. Some papers have been able to capture membrane ruffle formation around fluorescent EVs, but overall, there is a lack of uptake being shown either live with TIRF microscopy or through EM analysis. 4) The use of broad-spectrum non-specific inhibitors makes it difficult to ascertain the precise mechanisms of uptake as shutting down normal uptake for a cell could potentially have deleterious effects that might cause non-physiological responses of uptake or cell membrane leakiness. Additionally, blocking one pathway might result in compensation by another pathway making it difficult to parse apart which pathway contributes more to internalization. 5) As mentioned previously, one can only track EV uptake *in vitro* but not *in vivo*. The ability to barcode and track individual EV uptake *in vivo* would open the field to discovering how these tiny particles traverse great distances to affect their downstream target cell. However, how an EV targets and tracks to its specific recipient cell is unknown. EVs

might rely on passive diffusion across a small space or through bulk fluid flow through the bloodstream until it can bind with high affinity to its cell of choice based on the cell surface receptors it expresses. Lastly, it is important to note that these mechanisms are not EV specific as a subset of these mechanisms of uptake apply to the internalization of small artificial liposomes. An excellent review on liposomes as drug delivery vesicles covers mechanisms of uptake by cells via endocytosis, membrane fusion, and coating proteins added to the EV to aid in target recognition[248].

Appendix III. Analysis of EVs Isolated from Different Donor Cells

Introduction

Recently, the field of extracellular vesicles has grown tremendously; however, research regarding EVs derived from sympathetic neurons remains sparse. Additionally, there are a variety of techniques to assess EV concentration and sizing and a few studies comparing different assays. Here I analyze EVs derived from four different cell types: NGF-differentiated PC12 cells, Rat SCG neurons, and tissue extracted EVs from whole mouse SCGs. I also utilize two different concentration and sizing instruments to compare and contrast their effectiveness in characterizing EVs.

Material and Methods

PC12 cell culture

PC12 cells were seeding onto 10 cm PDK and laminin coated dishes at a density of 2.2 x 10^6 cells and grown to confluency for 2 DIV. At 2 DIVs, 45 ng/mL of NGF was added to the cells to trigger differentiation for 5 days. At 7 DIVs, 48 hours after the last media change the CM was collected for EV isolation.

Rat sympathetic neuron culture

SCGs were dissected from P1 rat pups, dissociated, and plated in 24- well plates. Cells were grown for 1, 2, 5, or 6 weeks in complete media (as described in Chapter III) before CM collection and EV isolation.

Tissue extraction of EVs from mouse SCGs

SCGs were dissected from CO2 euthanized 2-month-old male C57bl/6J mice and enzymatically dissociated as previously described in Chapter III. SCGs were then transferred to 1X dPBS and triturated using a fire-polished Pasteur pipette. The cells were then passed through a 45 um and then 20um filter, sequentially. EVs were then isolated by differential centrifugation as described in Chapter III.

EV analysis by nanoparticle tracking analysis (ZetaView) and tunable resistive pulse sensing (qNano)

EV analysis using ZetaView NTA was performed as described in Chapter III. TRSP measurements were conducted using a qNano gold instrument (Izon Ltd) using a NP100 (50-330 nm) polyurethane membrane. PBS containing 0.03% (v/v) Tween-20 filtered with a 0.1 μm syringe filter (Sartorius) was used as the buffer solution.

Results

EVs derived from NGF – differentiated PC12 cells and analyzed by ZetaView decrease in concentration (compare P20 to P100, or SN 5k to SN 100k) at higher centrifugation spins as expected (Fig. 1A). The size of particles in the supernatants are similar in size (149 nm vs. 142 nm) than the size of particles between the P20 (162 nm) and P100 (149 nm) fractions (Fig. 1A). Rat sympathetic EV concentration and particle size remains relatively unchanged as time in culture increases (Fig. 2A, Fig. 3A-C). Analysis of Rat SCG EVs by qNano shows higher particle counts in the P100 and early supernatant fractions (Fig. 3A,B). Importantly, particle recovery comparing starting supernatant (SN4.6) to final pellet (P100) is greater (44.4%) using the ZetaView than qNano (Fig. 5A and Table 4). Lastly, I analyzed tissue derived EVs from adult mouse

SCGs and found that particles can be detected by ZetaView analysis in the P20 and P100 fraction compared to mock (negative control) P20 and P100 fractions (Fig. 6A,B). Size histogram analysis shows a peak at 120 nm for the P100 fraction with a peak in the P20 fraction at 150 nm. The concentration of the P20 fraction was higher than the P100 and particle-depleted supernatant fraction (SN100).

Figures

A.

PC 12 cells

Supernatant 5,000 x g

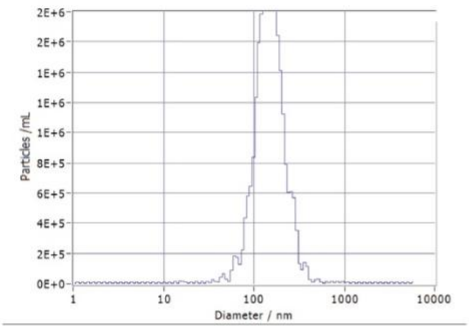

Concentration: 2.7E+9 particles/mL

Peak size: 149 nm

Supernatant 100,000 x g

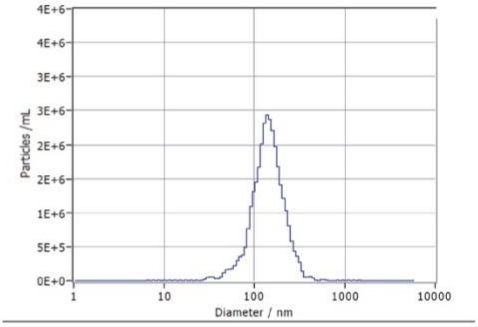

Concentration: 3.0E+7 particles/mL

Peak size: 142 nm

P20

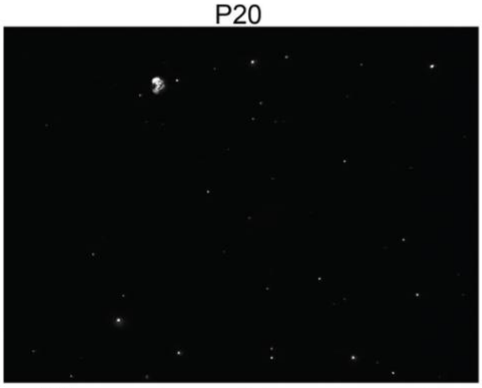

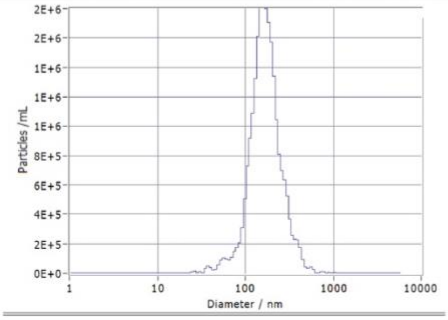

Concentration: 4.6E+10 particles/mL

Peak size: 162 nm

P100

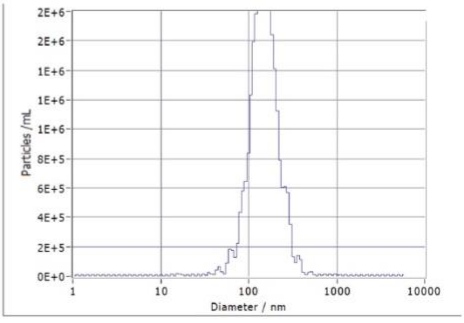

Concentration: 2.7E+9 particles/mL

Peak size: 149 nm

Figure 1. NGF differentiated PC12 cells secrete EVs

A. Still images captured from ZetaView videos at t = 30secs (top) from the following fractions: supernatant 5,000 x g, supernatant 100,000 x g, P20 and P100. Concentration (particles/ mL) versus size (nm) plot from ZetaView NTA (bottom).

A.

Rat SCG Neurons P100

Week 1

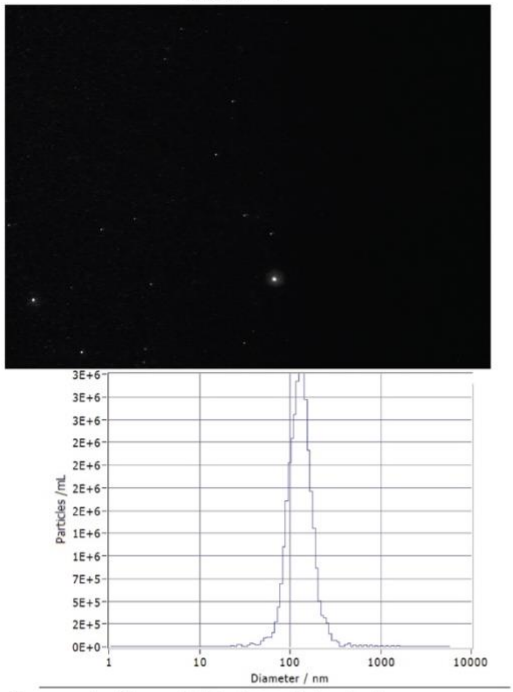

Concentration: 4.7E+9 particles/mL

Peak size: 130 nm

Week 2

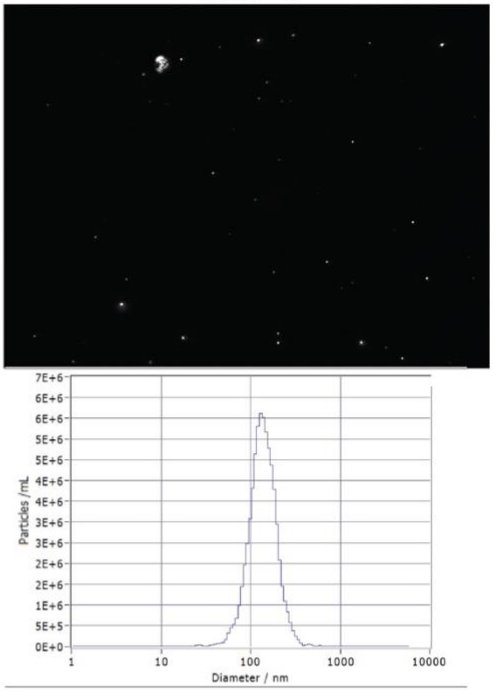

Concentration: 6.5E+9 particles/mL

Peak size: 135 nm

Week 5

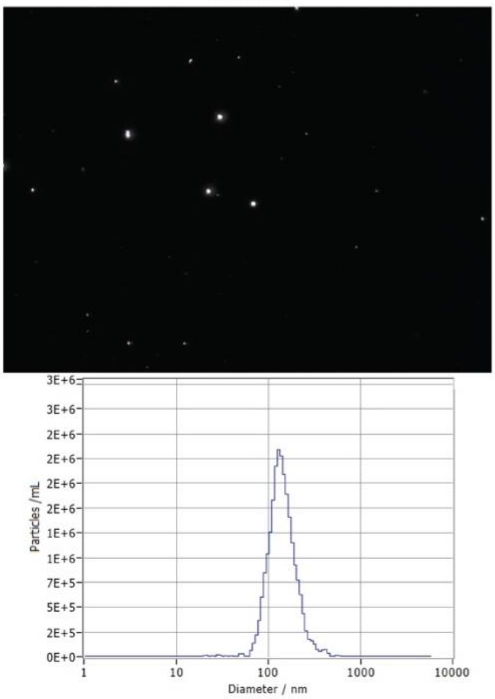

Concentration: 5.5E+9 particles/mL

Peak size: 133 nm

Week 6

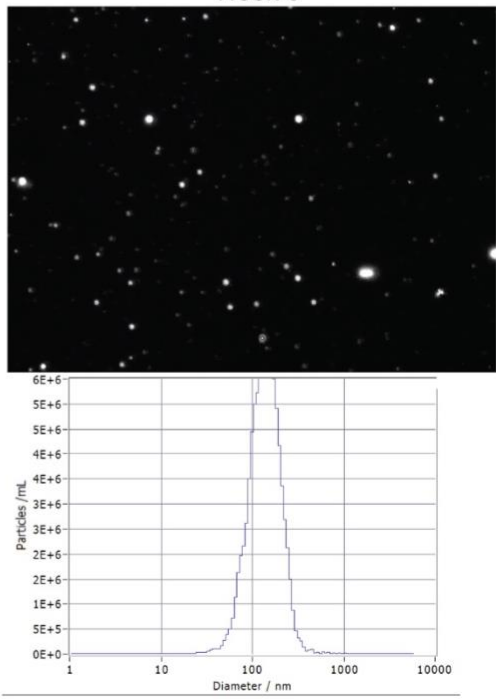

Concentration: 1.8E+10 particles/mL

Peak size: 141 nm

!!

Figure 2. Rat SCG cells secrete EVs

A. Still images captured from ZetaView videos at t = 30secs (top) from the P100 fraction isolated from SCG cells at either 1, 2, 5, or 6 weeks. Concentration (particles/ mL) versus size (nm) plot from ZetaView NTA (bottom).

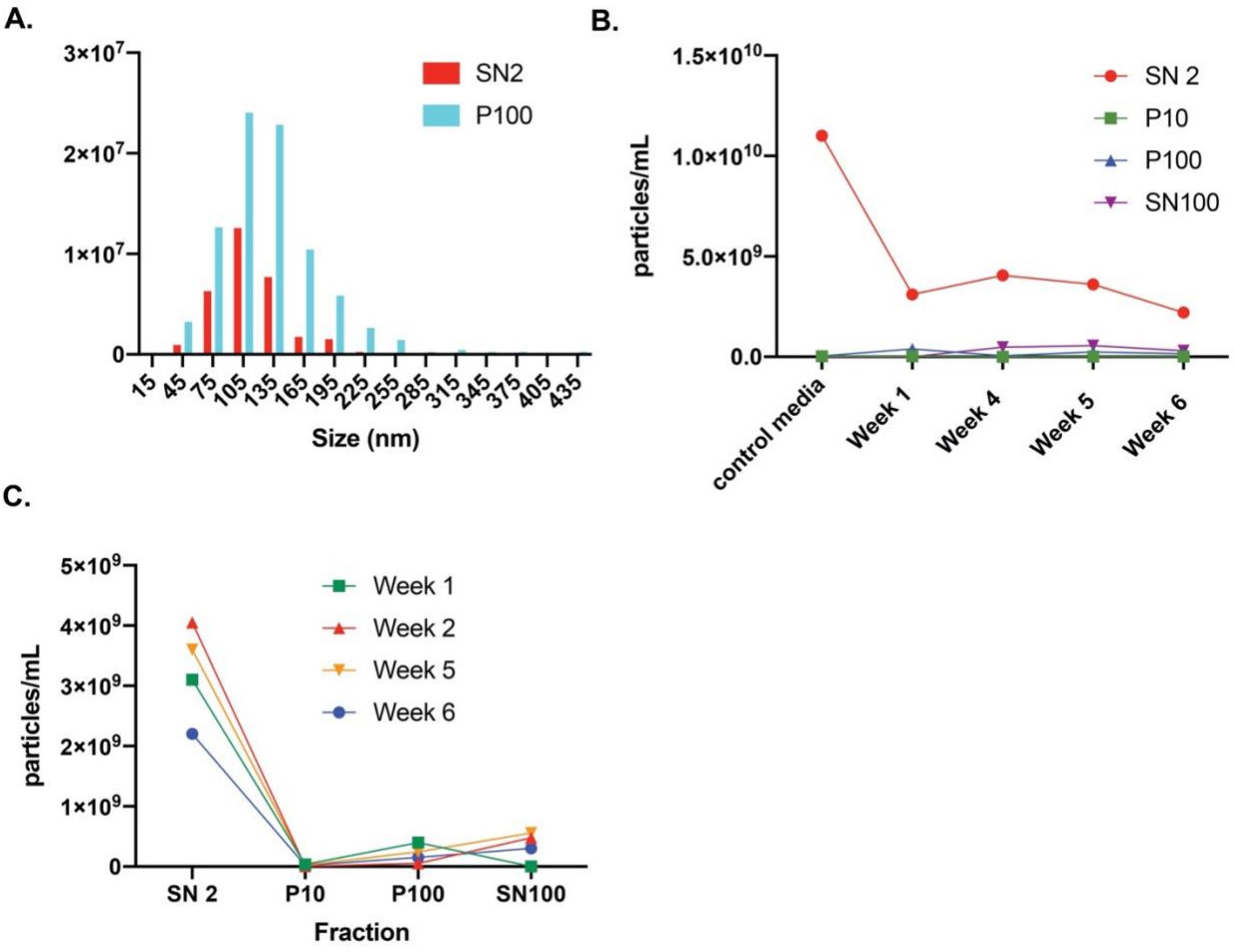

Figure 3. Rat SCG - derived EVs compared over time in culture

A. Histogram comparing the P100 versus SN2 fractions. **B.** Particle concentration change over time by fraction. **C.** Particle concentration by fraction for each time point.

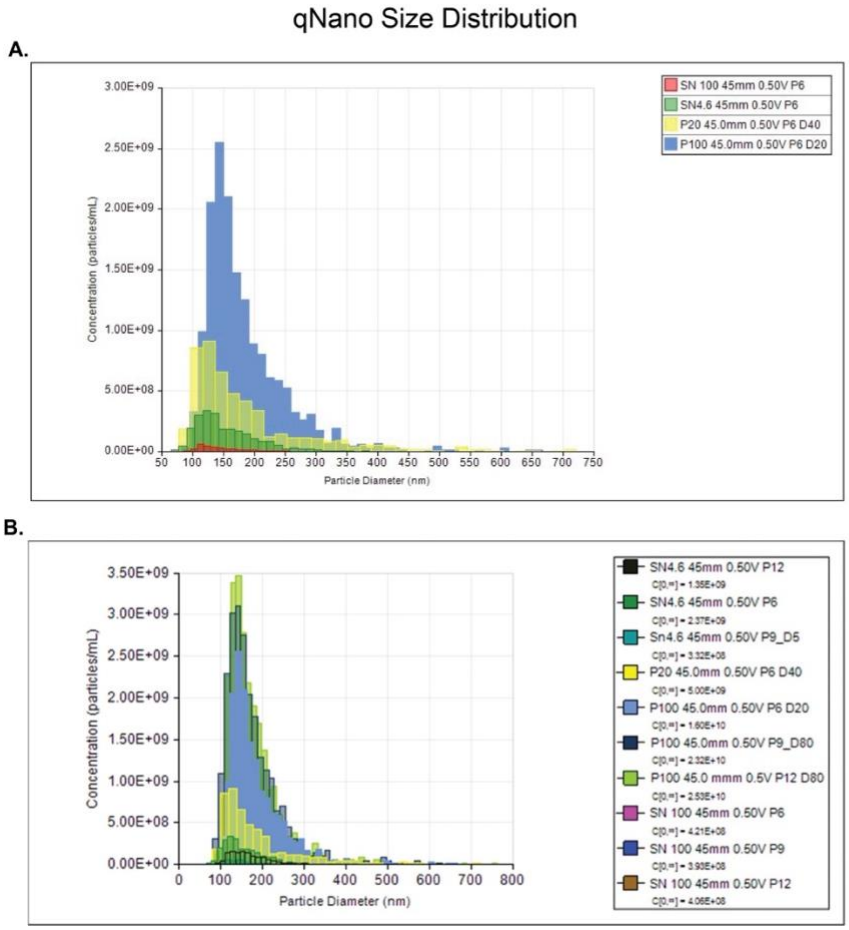

Figure 4. Mouse SCG - derived EVs analyzed by qNano

A. Histogram comparing the supernatants to the P20 and P100 fractions by qNano. **B.** Histogram of the concentration and size of different fractions when vary dilution and pressure changes on the qNano.

Table 4. Recovery comparing qNano (TRPS) to ZetaView (NTA)

	Starting volume	volume fraction	raw particles/ml	Number of particles	particles/ml
SN4.6	50	50	1.86E+09	9.30E+10	1.86E+09
P20	12.5	0.05	5.00E+09	1.00E+09	2.00E+07
P100	12.5	0.05	2.15E+10	4.30E+09	8.60E+07
SN100_HFDa	50	2.5	4.06E+08	1.02E+09	2.03E+07
				6.32E+09	1.26E+08

6.8% recovery from SN4.6 to P100

	Starting volume	volume fraction	raw particles/ml	Number of particles	particles/ml
SN4.6	50	50	2.04E+09	1.02E+11	2.04E+09
P20	12.5	0.05	4.65E+10	9.30E+09	1.86E+08
P100	12.5	0.05	1.75E+11	3.50E+10	7.00E+08
SN100_HFDa	50	2.5	3.75E+08	9.38E+08	1.88E+07
				4.52E+10	9.05E+08

44.4% recovery from SN4.6 to P100

A.

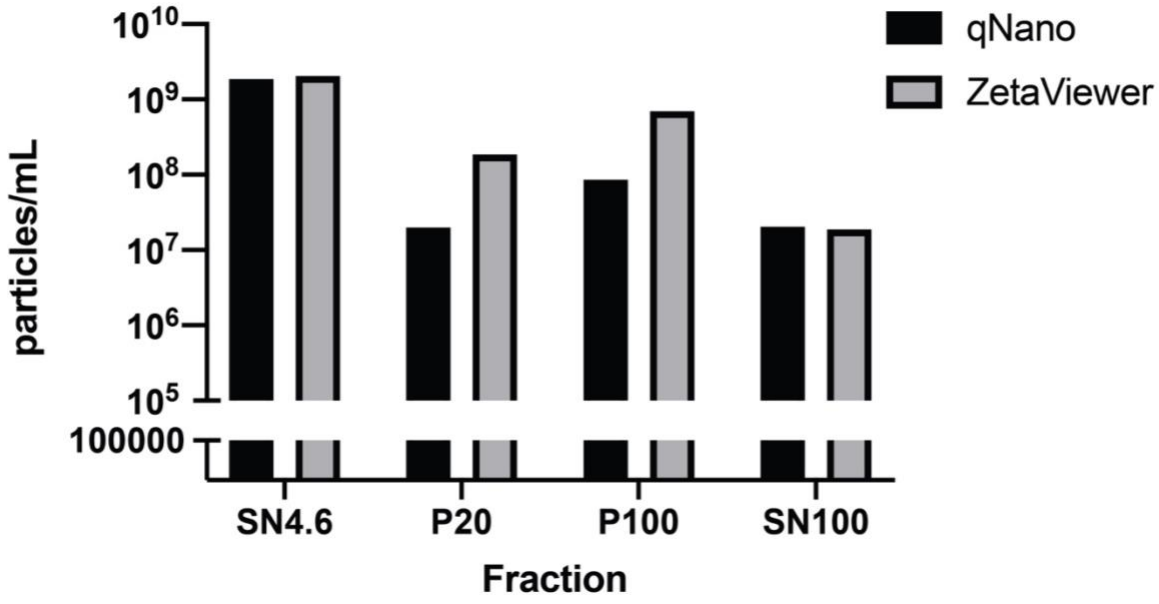

Figure 5. Comparison of EV concentration by analysis method

A. Graph comparing EV concentration by fraction between different analysis methods either the qNano or ZetaView.

Tissue Extracted EVs (TEEV)

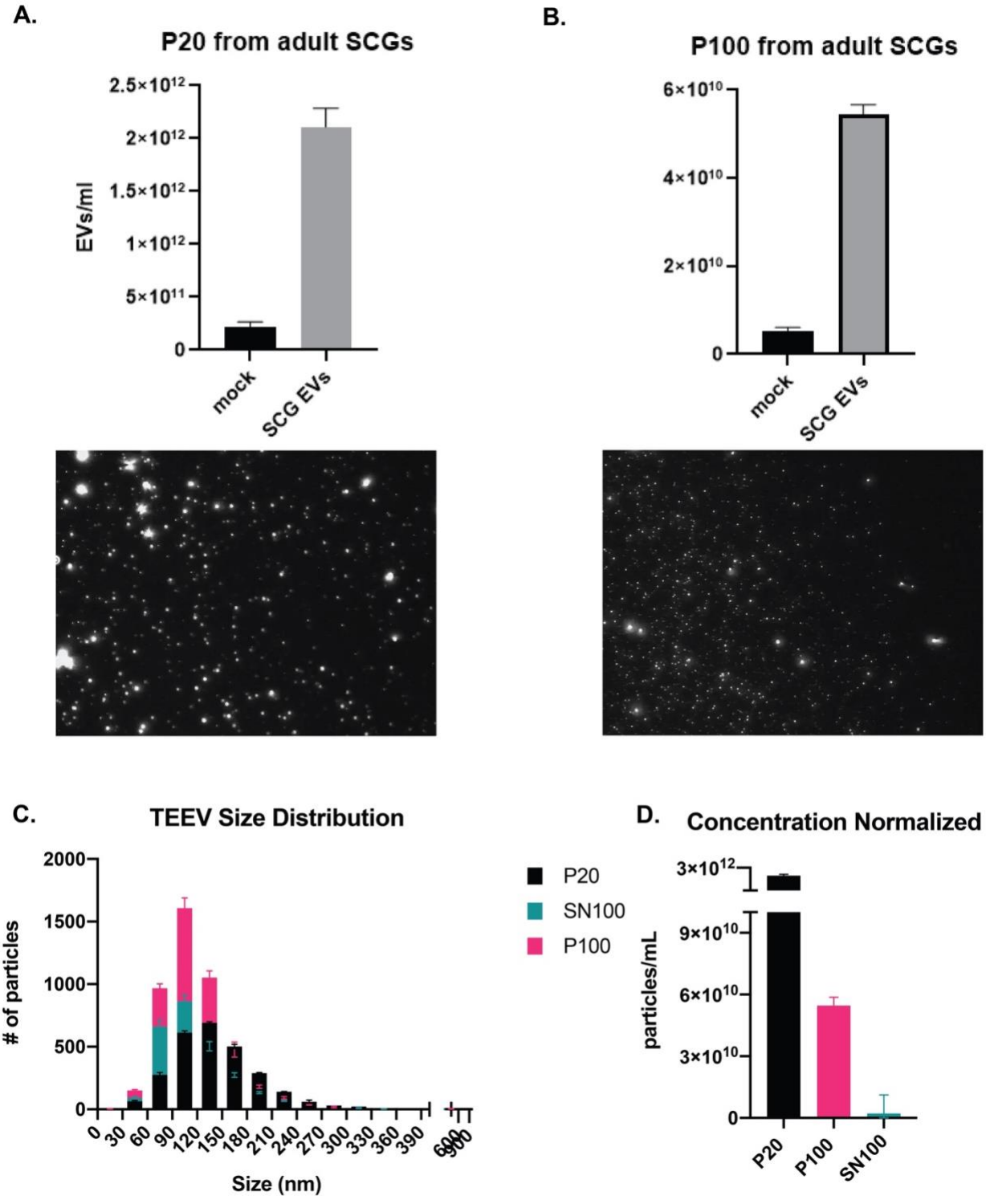

Figure 6. EVs can be extracted from mouse SCG tissue

A. Concentration of P20 EVs derived from SCGs or a “no tissue” mock control by ZetaView. **B.** Concentration of P100 EVs derived from SCGs or a “no tissue” mock control by ZetaView. **C.** Size distribution histogram comparing tissue extracted P20 or P100 EV fractions to the supernatant. **D.** Concentration of EVs by fraction from SCG tissue.

Appendix IV. Preliminary Characterization of CD63 and TrkA Colocalization in SCG Neurons

Introduction

My work provides the foundation of assessing EV release from sympathetic neurons that contain TrkA; however, there are many remaining questions regarding the biogenesis TrkA EVs. Here I investigate the trafficking of the canonical EV marker, CD63 with TrkA. First, I preliminarily characterize CD63 localization in SCG neurons using a transgenic mouse model. Second, I live image CD63 and TrkA and assess their colocalization.

Material and Methods

Neuronal cell culture and staining

Neuronal cultures were prepared as previously described[249]. Briefly, cultures were prepared from E18 rat hippocampi and plated on 35 mm glass-bottom dishes (MatTek). After 4 h, the plating medium was removed and replaced with serum-free medium supplemented with B27 (Thermo Fisher Scientific), and neurons were cultured for 7 DIV Transfections were conducted using Lipofectamine 2000 (Invitrogen). Neurons were transfected with Cre recombinase construct for 36 hours. Cells were washed with PBS and fixed with 4% PFA at room temperature for 15 mins. Cells were then permeabilized at blocked with 1% BSA and 0.2% Triton-X for 20 mins at room temperature. Primary and secondary antibodies were diluted in 1% BSA and applied for 1 hour. Antibodies used included MAP2 (RRID AB_399947) and LAMP1 (RRID AB_2629474). Fixed cells were imaged on Zeiss AxioZoom Oberserver.Z1 with Apotome 2.1 structured illumination and captured with a 40X objective.

Anti-FLAG feeding assay and live imaging

Sympathetic neurons from a triple transgenic mouse line *CD63emGFP^{loxPSTOPloxP};DBH^{Cre};TrkA$^{FLAG/FLAG}$* were dissected and plated in microfluidic devices as described in Chapter III. This mouse line expresses CD63 emeraldGFP that is driven by a DBH^{cre} thereby only expressing CD63 in the adrenergic SCG neurons. This line also expresses a FLAG-tagged TrkA receptor allowing for the tracking of CD63 and TrkA simultaneously. At 7 DIV, 100 µL of complete media (described in Chapter III) containing anti-FLAG-Cy3 antibody (1:200) (RRID AB_439700) and 100nM MemGlow 590 (Cytoskeleton) was added to the DA chamber. After 20 mins, cell bodies were imaged live on an inverted Zeiss 980 microscope with an Airyscan detector using a 40X oil objective (NA 1.3). Line scan analysis was computed in ImageJ.

Results

To assess the association between the canonical EV marker, CD63, and TrkA in neurons I first wanted to characterize CD63-GFP expression in neurons. Transfecting *CD63emGFP^{loxPSTOPloxP}* cortical neurons with a Cre-recombinase allowed sparse expression of CD63 in the cultures. Immunocytochemical analysis showed that CD63 appeared in puncta primarily in the somatodendritic domain of neurons (Fig. 1A). Additionally, CD63 expression colocalized with the late endosome/ lysosomal marker LAMP1 in the proximal dendrites and soma. This is expected as CD63 enriches on late endosomal/ multivesicular bodies that are primarily destined for degradation after fusion with lysosomes. In these cultures, several issues arose. First not all neurons expressed

CD63. Secondly, the CD63 was often overexpressed resulting in large aggregates in the proximal dendrites. Lastly, other cell types besides neurons were also transfected with Cre recombinase and thus turned-on expression of CD63. To circumvent these issues, I utilized the triple transgenic *CD63emGFP*^{loxPSTOPloxP}*;DBH*^{Cre};*TrkA*$^{FLAG/FLAG}$ mouse line to selectively turn on CD63-GFP expression in SCG neurons. Using this line, I first imaged CD63-GFP live in the somatodendritic domain and saw robust puncta representing endosomes cluster in the cell body (Fig. 1B). Additionally, video analysis showed smaller CD63-GFP+ endosomes moving retrogradely towards the cell body in the neurites (video not shown). Next, I wanted to assess CD63 colocalization with TrkA. To do this, I feed M2-Cy3 (anti-FLAG) antibody to the distal axon chamber of the microfluidic devices along with a lipophilic membrane probe, MemGlow, to label the plasma membrane. I found that 20 mins after distal feeding of FLAG antibody to the axons there was robust labeling of CD63-GFP;FLAG-TrkA double positive endosomes in the cell body. Line scan analysis showed extensive colocalization between CD63 and TrkA in the soma of SCG neurons (Fig. 1C).

Figures

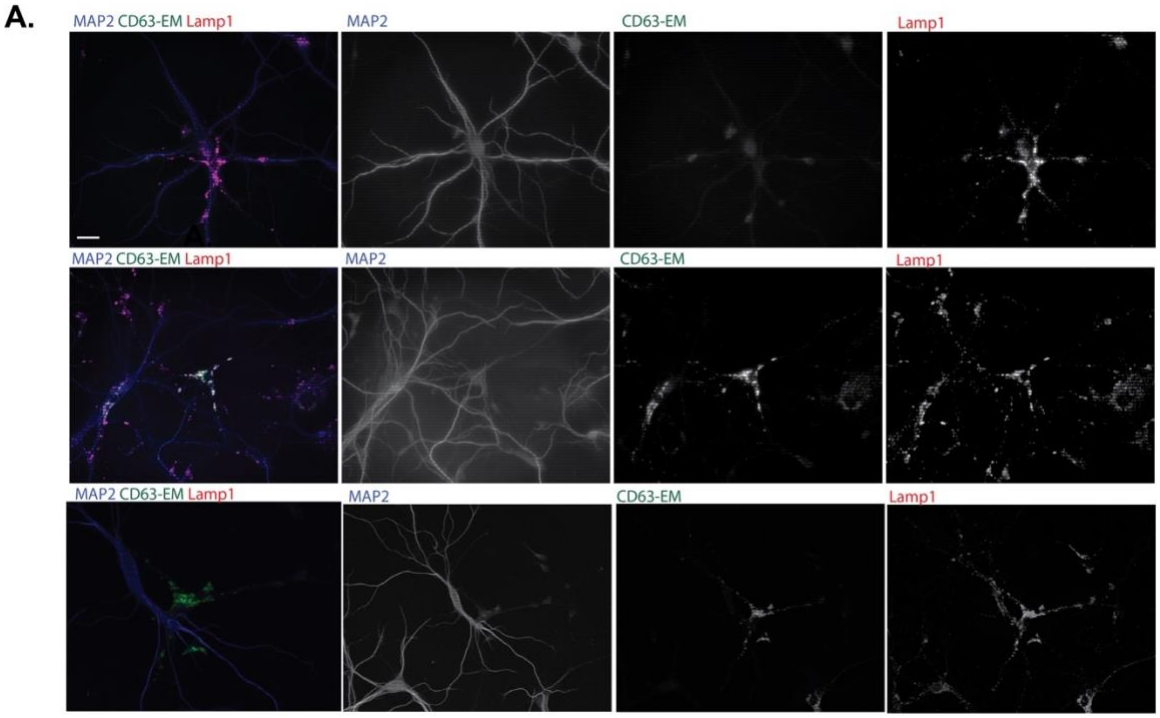
A.
MAP2 CD63-EM Lamp1
MAP2
CD63-EM
Lamp1
MAP2 CD63-EM Lamp1
MAP2
CD63-EM
Lamp1
MAP2 CD63-EM Lamp1
MAP2
CD63-EM
Lamp1

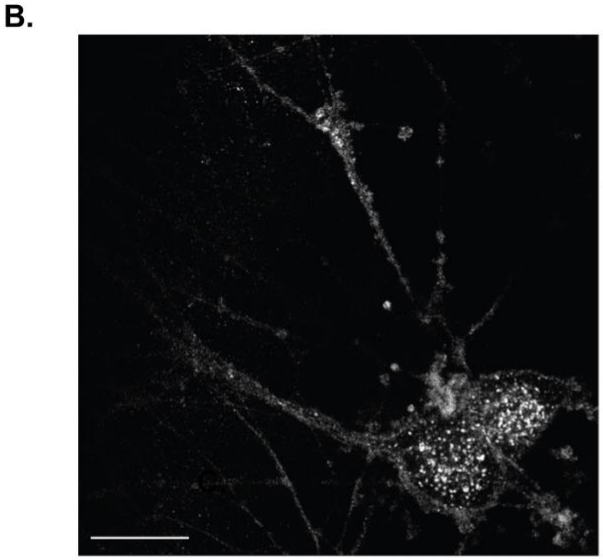
B.

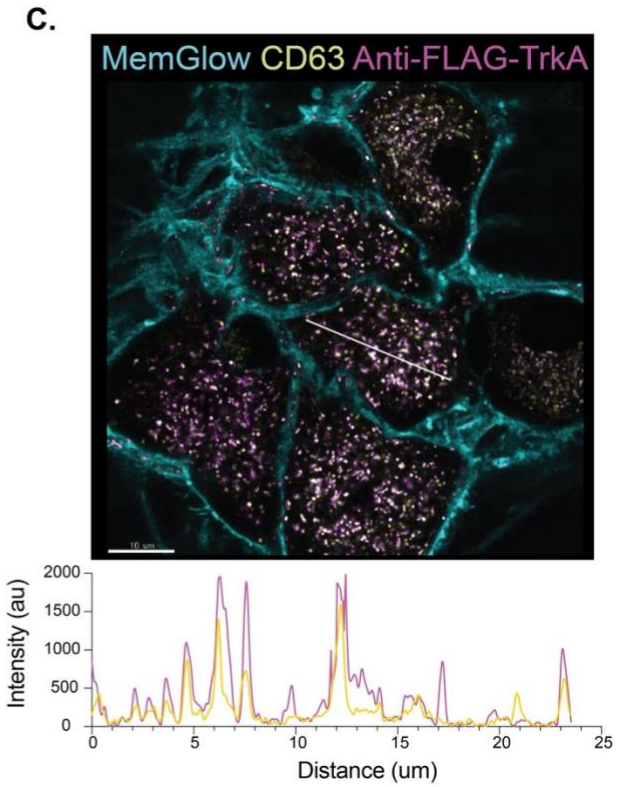
C.
MemGlow CD63 Anti-FLAG-TrkA
Intensity (au)
2000
1500
1000
500
0
0
5
10
15
20
25
Distance (um)

Figure 1. CD63 colocalizes with TrkA in the somatodendritic domain of SCG neurons.

A. CD63 shows robust expression in cortical neurons after Cre recombinase transfection and colocalizes with LAMP1 in the somatodendritic domain if cortical neurons. **B.** Still image from a *CD63emGFP^{loxPSTOPloxP};DBH^{Cre};TrkA$^{FLAG/FLAG}$* mouse sympathetic neuron showing CD63-GFP puncta in the soma. **C.** Still image and line scan showing robust colocalization of CD63 and TrkA in the soma of SCG neurons 20 mins after distal feeding of Anti-FLAG antibody. Scale bar is 30 µm for all images.

Appendix V. Immunocytochemical Antibody Validation of an Improved Satellite Glial Cell Marker *In Vitro*

Introduction

One of the open questions from my work is what cell types internalize TrkA$^+$ EVs? Physiologically, TrkA is retrogradely trafficked up the SCG neurons where it gets incorporated into and released as EVs. *In vivo*, SCG neurons are unsheathed by satellite glia cells which support critical functions of the neurons[250,251]. Satellite glia are so intimately wrapped around the SCG neuron that there is only a space of about 10 nm between the neuronal plasma membrane and the glial plasma membrane[250,252–254]. Therefore, I purported that satellite glia cells might serve as an intermediary or a final destination for SCG secreted TrkA$^+$ EVs. In order to test this hypothesis, I needed a good protein marker to label satellite glia. My initial work showed that GFAP, a common glial marker, was not sufficient for detecting satellite glia in culture. Thus, I turned to work of Dr. Aurelia Mapps to identify BLBP as a strong marker for satellite glia cells; however, BLBP had not been tested on cultures[255]. Here I test a BLBP antibody on SCG cultures that were intentionally dissociated in clumps. Using confocal Z-stacks and Imaris software, I show that satellite glia cells are closely apposed to SCG neurons in vitro.

Material and Methods

Sympathetic cell culture and immunocytochemistry

Sympathetic neurons from C57Bl/6J mice were dissected and plated on PDK and laminin coated coverslips as previously described[36,37]. Importantly, SCG were not fully dissociated and triturate to maintain clumps of closely associated satellite glia and SCG neurons. At 7 DIV, cells were fixed in 4% PFA for 20 minutes at room temperature. Cells were then washed 3 times with 1X PBS and then blocked and permeabilized in 5%

normal donkey serum and 0.2% TritonX-100 for 20 minutes. Primary antibodies were diluted in 1% BSA and incubated for an hour at room temperature. Secondary antibodies were diluted in 1% BSA and added for 30 mins at room temperature. Coverslips were washed with 1x PBS, mounted with fluorogold media mount onto glass slides and imaged as Z-stacks on an inverted Zeiss 980 microscope with an Airyscan detector using a 40X oil objective (NA 1.3).

REAGENT or RESOURCE	SOURCE	IDENTIFIER
Rabbit Anti-GFAP	Cell Signaling Technology	Cat # 80788 **RRID: AB_2799963**
Rabbit Anti-BLBP	Abcam	**Cat # ab279649;** **RRID: N/A**
Chicken Anti-MAP2	EnCor Biotechnology	Cat # CPCA-MAP2 RRID: AB_2138173
Mouse Anti-tau	In House, Deppmann lab	
Guinea Pig Anti-NeuN	Millipore Sigma	Cat # ABN90 RRID: AB_11205592

Results

Initially, I wanted to assess glia markers we had inventory of and therefore I tested GFAP on my clusters of SCG cells. I did not detect any GFAP signal in my cultures, except for on one coverslip. The GFAP+ cells did not fully wrap around the SCG neurons although their processes appeared to be somewhat ramified (Fig. 1A). In contrast, staining sympathetic cultures with BLBP showed robust labeling of satellite glia cells forming both a confluent mesh-layer adherent to the coverslip and wrapping around and in between SCG neurons labeled by NeuN (Fig. 1B,C). Further analysis of Z-stacks in Imaris using cross hairs shows the satellite glia surround neuronal cell body

cluster and even interpose between adjacent neurons with a thin sheet of plasma membrane (Fig. 1B,C).

Figures

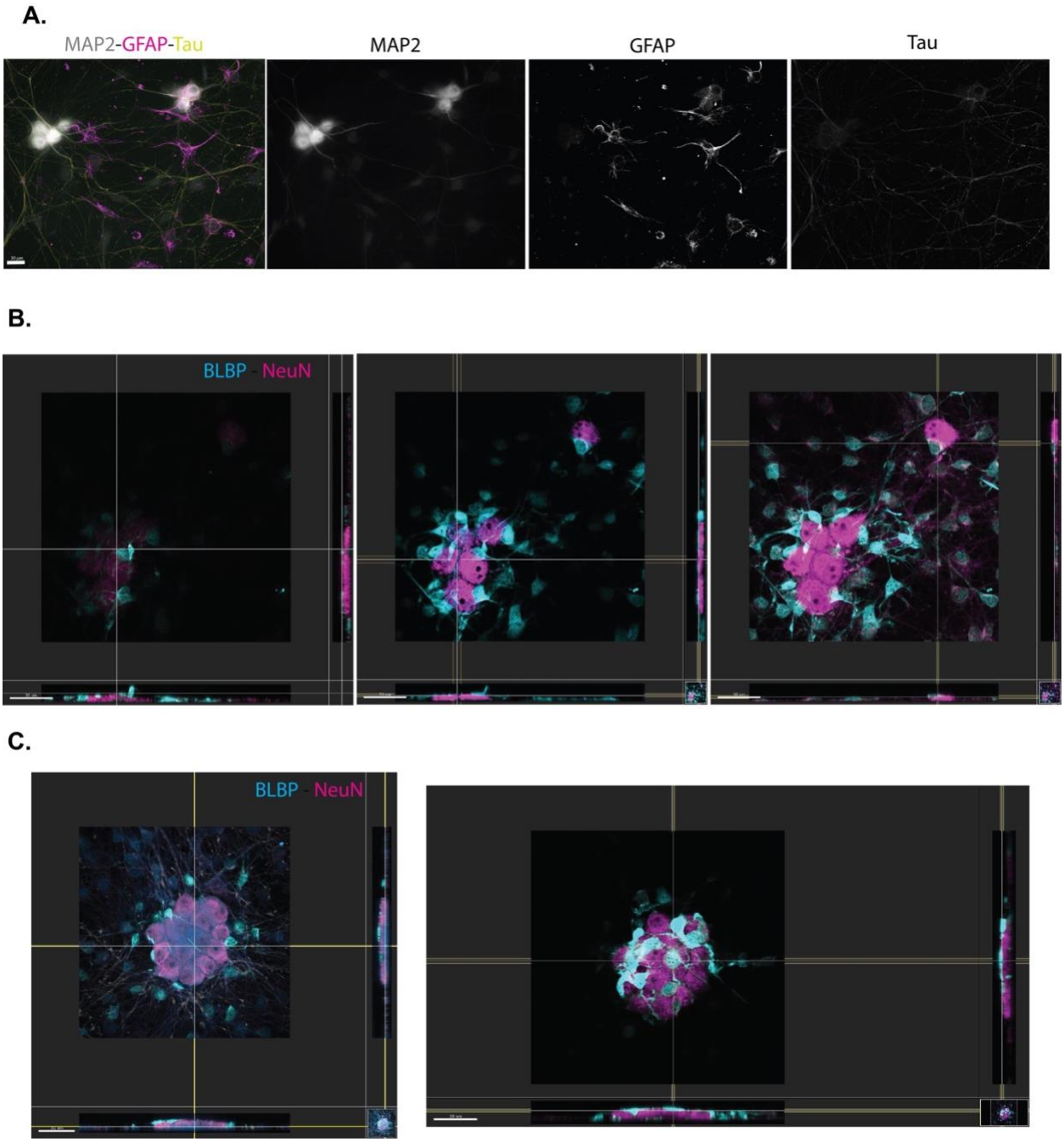

Figure 1. BLBP is a robust marker for satellite glia in sympathetic cell cultures.

A. Images of sympathetic cells grown for 7 DIV and stained with MAP2 (somatodendritic domain), GFAP (glia), and tau (axons). Scale bar is 30 μm. **B.** Cross-hair analysis of Z-Stacks moving up the Z-plane starting from the bottom of the coverslip (left) to the top of the neuronal cluster (right). Staining against NeuN (neuron cell body) and BLBP (satellite glia). **C.** Cross-hair analysis of Z-Stacks moving up the Z-plane starting from the middle of the neuronal cluster (left) to the top of the neuronal cluster (right). Staining against NeuN (neuron cell body) and BLBP (satellite glia).